Working fluid selection for a diesel engine waste heat recovery ORC module

Integral optimization of an ORC system

L.M. Vonk

Technische Universiteit Delft

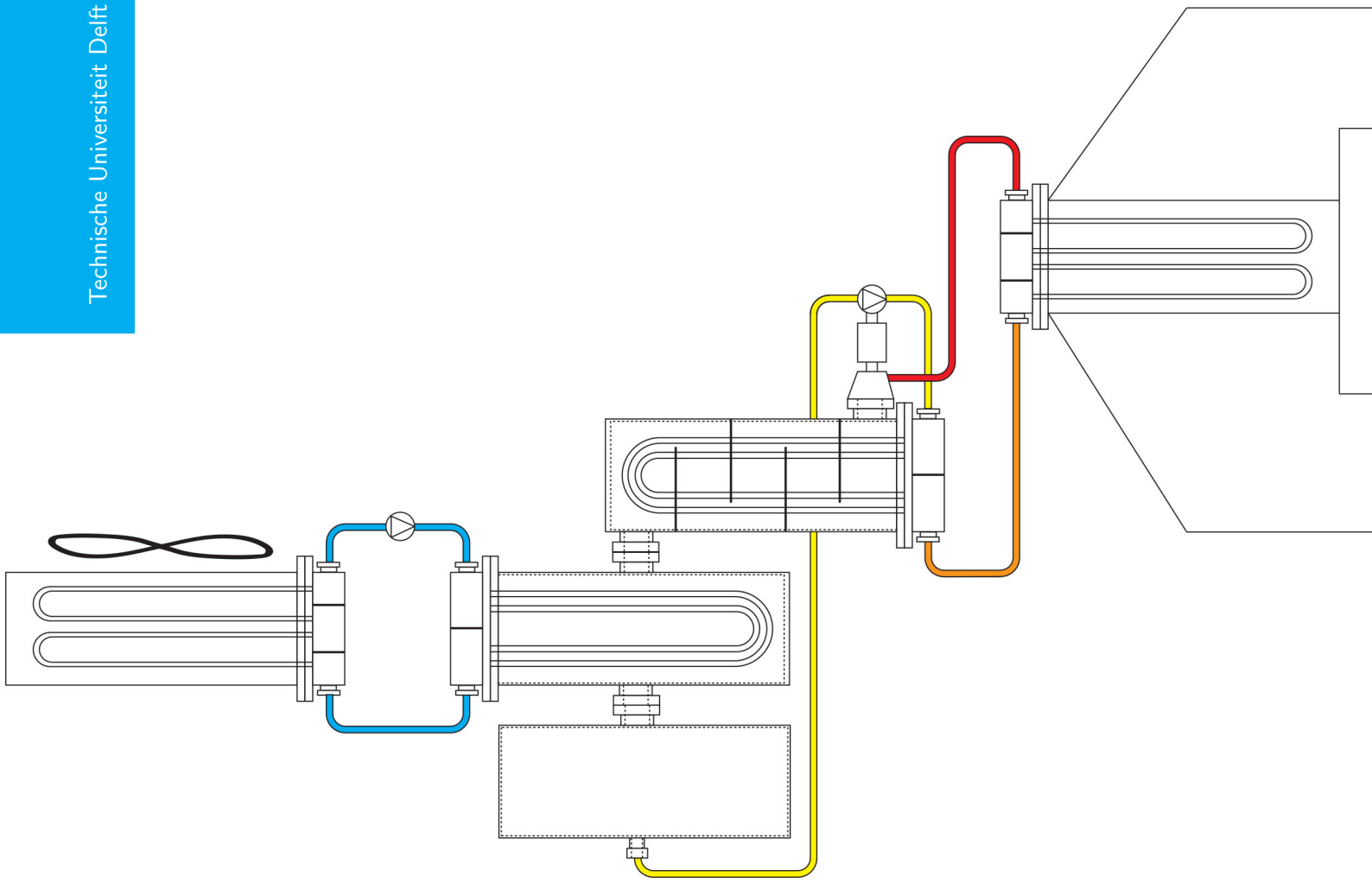

TU Delft Delft University of Technology

TRIOGEN

Challenge the future

Power from heat

WORKING FLUID SELECTION FOR A DIESEL ENGINE WASTE HEAT RECOVERY ORC MODULE

INTEGRAL OPTIMIZATION OF AN ORC SYSTEM

by

L.M. Vonk

to obtain the degree of Master of Science
at the Delft University of Technology,
to be defended publicly on Thursday June 9, 2016 at 3:30 PM.

Student number:	4013255	
Report number:	P& E-2744	
Project duration:	September 1, 2016 – June 9, 2016	
Thesis committee:	Prof. dr. ir. T. J. H. Vlugt,	TU Delft, chairman
	Dr. ir. C. A. Infante Ferreira,	TU Delft, supervisor
	Dr. R. Pecnik	TU Delft
	Prof. ir. J. P. van Buijtenen,	Triogen

This thesis is confidential and cannot be made public until May 31, 2019.

An electronic version of this thesis is available at http://repository.tudelft.nl/.

TU Delft

PREFACE

You are about to start reading a report on the selection of working fluid and process parameters for an ORC, to be designed for the recovery of waste heat from diesel generator exhaust gases. Selection of a working fluid can be compared to selection of a material to build a chair from. Whether you select wood, stainless steel or a plastic does not influence the possibility to build the chair. It does limit though, the applicable production techniques, the possible shapes, visual qualities, cost and durability of the chair. Therefore when selecting a material, considerations of application, target market, production and shape must be taken into account, although the detailing can only be done when a material is selected. Likewise, the selection of a working fluid influences and should be influenced by the application, design and performance of the ORC system and its components.

In this work I tried to identify the aspects relevant when selecting a working fluid and process parameters. And fitted these aspects in a model in order to be able to evaluate these aspects and take them into consideration when selecting a working fluid. The model does not provide a full system design, it gives a starting point for further development of a new module design.

And what may be a starting point for Triogen, is for me the end of almost seven years of study in Delft. Seven years of studying Industrial Design Engineering and later Energy Technology of which this thesis is the final bit.

I would like to thank Jos van Buijtenen for the opportunity to do this thesis project for Triogen. Also I would like to thank Quirijn Eppinga for his supervision, confidence and encouragement, as well as Stefano Ganassin for his critical attitude and enthusiasm.

Next I want to thank Carlos Infante Ferreira for his supervision, his focus on planning and progress and his great eye for detail. Thanks also to the rest of the thesis committee.

As there is a large distance between Delft and Goor (Triogen), I also want to thank Tjark Post for his hospitality and the possibility to stay at his house in Enschede once a week. In addition I would like to thank Geertjan Roks for the good time and conversations, when carpooling from Delft to Goor and back.

Last I want to thank my mother for her love and support during graduation and the rest of my study.

L.M. Vonk
Delft, May 2016

ABSTRACT

The Organic Rankine Cycle (ORC) is a thermodynamic cycle for the conversion of heat into electricity. ORC technology is applied to waste heat, biomass and natural heat sources, there is currently over 2000 MW installed capacity worldwide. Triogen is a Dutch company producing standardized ORC modules for the application with gaseous (waste) heat sources with at least 1 MW heat available, at a temperature of ca. 450°C. In this work the application of ORC technology for efficiency enhancement of modern diesel generators (flue gas: 350°C, 5 kg/s) is studied. It is pursued to identify all relevant phenomena possibly influencing the system performance and cost and to assess the significance of their influence on system performance. This is done in order to decide whether or not a phenomenon should be taken into account when selecting a fluid. A steady state off design model is developed for the optimization of a sub-critical ORC system for minimal specific cost. Turbine isentropic efficiency is estimated based on in and outflow conditions using efficiency charts by Astolfi and Macchi. Pressure drop, effectivity and cost of evaporator, recuperator and condenser are evaluated using the Triogen evaporator design model and a shell and tube heat exchanger recuperator and condenser model respectively. The influence of ambient temperature, water temperature and water mass flow on the cooling system cost and power consumption is estimated based on supplier figures. In addition limitations on the diesel engine back-pressure and limitations related to flue-gas condensation are taken into account. A genetic algorithm is applied to optimize the process parameters and heat exchanger geometry for minimum specific costs. From the simulations acetone appears to be the optimal working fluid, which can be explained by its good thermodynamic behaviour and good heat transfer properties in recuperator and condenser due to the relatively high condensation pressure. Turbine inlet pressure appears to be relatively low due to the negative effect of high pressure ratios on turbine efficiency. Ambient temperature as well as evaporator wall- and flue-gas temperature limitations appear to have a diverging influence on the specific cost per working fluid, proving the necessity to evaluate these phenomena properly when selecting a working fluid for a specific application.

NOMENCLATURE

Symbol	Unit	
A	$[m^2]$	Area
A_f	$[m^2]$	Cross sectional area
$A_{o,sb}$	$[m^2]$	Leakage area between baffle and shell
$A_{o,tb}$	$[m^2]$	Leakage area between baffle and tubes
a	$[-]$	Ratio X_t/d_o
b	$[-]$	Ratio X_l/d_o
C	[€]	Cost
C_{min}	$[kJ/s/K]$	Minimum heat capacity rate
c_p	$[kJ/kg/K]$	Isobaric heat capacity
C_r	[-]	Heat capacity ratio
C_{spec}	$[€/kW]$	Specific cost
D	$[D]$	Diameter
d_h	$[m]$	Hydraulic diameter
d_i	$[m]$	Inner tube diameter
d_o	$[m]$	Outer tube diameter
e	$[m]$	Shortest distance between two adjacent pipes
ex	$[kJ/kg]$	Exergy
f_A	$[-]$	Correction factor for staggering of tubes
f_G	$[-]$	Heat transfer correction factor for geometry
f_L	$[-]$	Heat transfer correction factor for leakage through baffle
f_P	$[-]$	Correction factor for fluid properties at tube wall
f_{N_r}	$[-]$	Condensation heat transfer correction factor for inundation
F	$[-]$	Fraction of tubes/ LMTD correction factor for number of tube passes
$\dot{G}$	$[kg/m^2 s]$	Mass flux
g	$[m/s^2]$	Gravitational constant
h	$[kJ/kg]$	Enthalpy
h_{fg}	$[kJ/kg]$	Enthalpy of vaporization
J_L	$[-]$	Pressure drop correction factor for leakage
L	$[m]$	Length
$L_{b,c}$	$[m]$	Baffle spacing
l_c	$[m]$	Baffle cut
$\dot{m}$	$[kg/s]$	Mass flow
m	$[-]$	Correction factor for condensate inundation

Symbol	Unit	
n_{mr}	$[-]$	Number of main resistances
n_p	$[-]$	Exponent for determining fluid property correction factor
N_t	$[-]$	Number of tubes
N_r	$[-]$	Number of rows
Nu	$[-]$	Nusselt number
p	$[bar]$	Pressure
Pr	$[-]$	Prandtl number
P_t	$[m]$	Tube pitch
Q	$[J/s]$	Heat flow
q	$[-]$	Vapor quality
$\dot{q}$	$[W/m^2]$	Heat flux
Re	$[-]$	Reynolds number
SP	$[-]$	Size parameter
T	$[°C]$	Temperature
U	$[W/m^2/K]$	Overall heat transfer coefficient
$\dot{V}$	$[m^3/s]$	Volume flow rate
V_r	[-]	Volumetric ratio
W	$[kW]$	Power/work
w	$[m/s]$	Velocity
X_l	$[m]$	Longitudinal tube pitch
X_t	$[m]$	Transverse tube pitch
x	$[m]$	Length of (section of) heat exchanger

Symbol	Unit	
α	$[W/m^2K]$	Heat transfer coefficient
γ	[-]	Heat capacity ratio
Δp	$[bar]$	Pressure drop
$\delta p/m$	$[bar]$	Pressure drop per meter
δ_{tw}	$[m]$	Tube wall thickness
ΔT	$[K]$	Temperature difference
ΔT_{wo}	$[K]$	Temperature difference between wall and saturated state
ϵ_{rec}	$[-]$	Recuperator effectiveness
η	$[-]$	Efficiency
θ_b	$[rad]$	Baffle cut angle
λ	$[W/mK]$	Thermal conductivity
μ	$[Pa*s]$	Viscosity
ξ	$[-]$	Moody friction factor
ρ	$[kg/m^3]$	Density
ψ_t	$[-]$	Correction factor for number of passes

subscript

av	Average
$air-cooler$	Air-cooler
amb	Ambient conditions
aq	Water
b	Bulk
c	In crossflow section/ critical
$cold$	Cold side
$cond$	Condenser
ctl	Center tube limit
eff	Effective
eq	Equivalent
$evap$	Evaporator
fan	Fan for cooling air-cooler
fg	Flue-gas
gen	Generator
ha	Heat available
hot	Hot side
II	Second law
in	At inflow
is	Isentropic
l	Liquid state
lam	Laminar
$mech$	Mechanical
N	Nozzle
Nu	Nusselt
net	Net (power output)
otl	Outer tube limit
out	At outflow
$pinch$	Pinch (temperature difference)
$pump$	Pump
rec	Recuperator
s	At shell side / shell
sec	Of one section
sat	Saturated condition
sub	Sub-cool
sup	Superheat
t	At tube side
th	Thermal
tot	Total
$turb$	Turbulent
$turbine$	Turbine
v	Vapor state
w	In window section
wf	Working fluid

Abbreviations

BWR	Back work ratio
CAMD	Computer aide molecular design
GWP	Global warming potential
LMTD	Logarithmic mean temperature difference
NFPA	National fire protection association
NTU	Number of transfer units
ODP	Ozone depletion potential
OHST	Optimal heat source temperature
ORC	Organic Rankine Cycle
SP	Size parameter
TEMA	Tubular exchanger manufacturers association

CONTENTS

1

INTRODUCTION

1.1. ORC TECHNOLOGY

Over the last decades the Organic Rankine Cycle (ORC) has gained interest and currently worldwide over 2.000 MW electric power is installed [1]. This increase of interest is related to the phenomenon of global warming, and the urge to reduce emissions and fossil fuel usage. This urge is discussed again recently at the COP21 climate conference in Paris 2016, where goals have been set to reduce future greenhouse gas emissions and limit the global temperature increase to 1.5 °C. The awareness of global warming has caused increased interest in all sorts of alternative energy, of which wind turbines and solar cells are best known. ORC technology is one of these technologies contributing to the reduction of the use of fossil fuels and harmful emissions. This is possible due to the ability of ORC technology to convert low grade thermal energy into mechanical energy and eventually electricity. The technology is applicable in the generation of electricity from biomass, industrial waste heat, solar and geothermal heat sources.

1.2. TRIOGEN AND APPLICATION

Triogen is a company based in Goor, the Netherlands, currently producing standardized 170 kW ORC modules for the European market (figure 1.1). These modules are designed for the conversion of heat in gaseous (waste) heat streams with temperatures ranging from 350 to 500 °C and use toluene as working fluid. Currently these ORC engines are applied for the generation of electricity from heat from landfill and biomass burners and from the exhaust gas of (bio)gas engines. For the design of a new module Triogen is now looking for a new working fluid and system design for temperatures of 300 to 400 °C. This new module should be designed to work with modern diesel engines, which have exhaust gases at these temperatures, this module though, could as well be applied with alternative heat sources.

1.3. FLUID SELECTION STUDIES

The working fluid selection in most of the cases is based on an optimization of a Cycle to an objective function. In case of waste heat recovery this is most often maximum output power or second law efficiency, because the remaining heat will not be used again. This was pointed out by Liu et al. [2], they claim thermal efficiency as objective or an assumed constant heat source temperature, may result in considerable deviation for system design compared to the varying temperature conditions of actual waste heat recovery. In applications where the heat source is reheated, for example in solar applications, thermal efficiency is the best objective to optimize for. In addition objectives such as minimum heat exchanger area and cost per kW can be observed. Shu et al.[3] for example use the sizing parameter and volume flow ratio to take into account expander considerations in this stage of

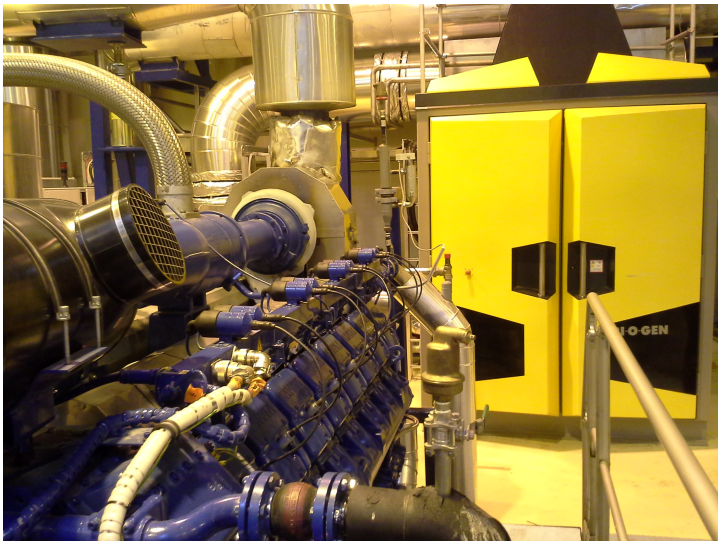

Figure 1.1: Triogen module in Finland, powered by sewage gas engine (waste) heat

the cycle design. In addition to these objectives it has been proposed to use alternative or multiple criteria. Xi et al. [4] for example propose a graphical criterion based on exergy efficiency and annual cash flow, and plots for all the candidate working fluids a pareto front in this domain, to enable a simultaneous consideration of the two objectives. Another proposed method for the selection of working fluids is by reverse engineering the working fluid. Papadopoulos et al. [5] propose the use of computer aided molecular design (CAMD) in combination with a thermodynamic optimization model, for the design of fictitious working fluids from a set of molecular building blocks. The thermodynamic properties are predicted and used for the simulation of a simple thermodynamic model, which predicts only the thermodynamic efficiencies. Lampe et al. [6] propose a similar method for the holistic design of working fluid and cycle, and optimize for a maximum work output. The drawback of the CAMD method is that the working fluids which these methods come up with are often rare or unused fluids and will therefore be very expensive. In addition this method has not been applied yet in combination with a thermo-economic or component specific analyzes, although secondary fluid properties, which are necessary for these calculations, can be predicted as well.

Most of the former mentioned analyzes are rather superficial, and neglect fluid-component interactions which in reality are non-negligible. Colonna et al.[1] argue that the selection of the working fluid should be part of the integrated and iterative design of the process, because the choice of working fluid affects the design choices on component level and viceversa. Mondejar et al. [7] for example point out that some working fluids may be considered advantageous from a thermodynamic point of view, while they have unfavorable impact on the turbine efficiency. Ahlgren et al. [8] took this into account and modelled a heat recovery system for marine application aiming at the selection of working fluids with focus on turbine performance. The performance of other components has an influence on cycle performance and cost as well, and may be necessary to be taken into account as well. Xu et al. [9] optimized an ORC using R134a as working fluid for industrial waste heat recovery, with a focus on the heat exchanger design. The system was optimized for maximum heat exchanger performance, maximum system performance and specific investment cost. Great impact is shown, of the heat exchanger design on the performance and economics of the cycle and vice versa. Even the pump efficiency can have a diverging effect according to Maraver et al. [10]. They point out the difference in necessary pump power for transcritical and sub-critical cycles causes the subcritical cycle to be preferred when low pump efficiencies are reached, while for higher pump efficiencies transcritical cycles are preferred.

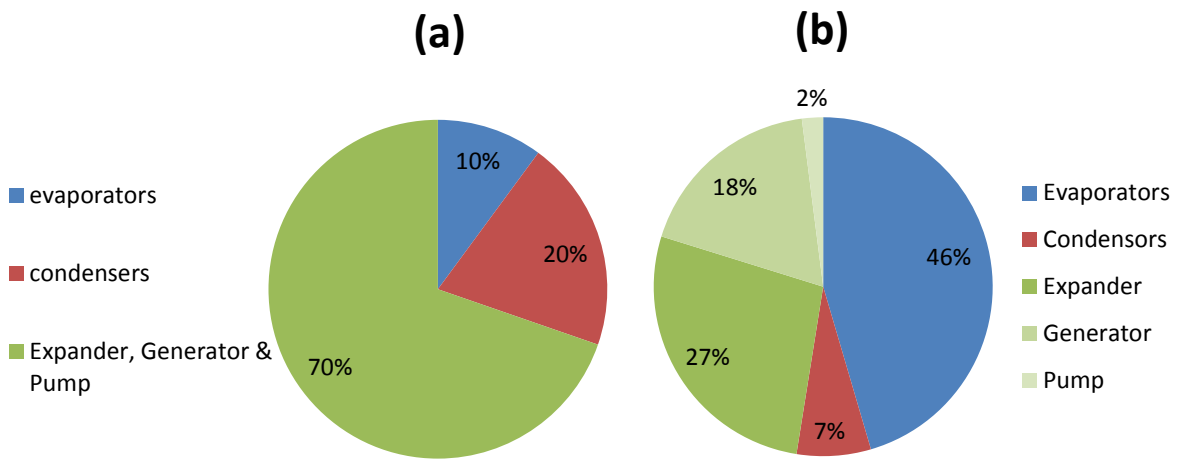

Figure 1.2: Real(a) and estimated(b) purchased equipment cost [11]

The detailing of a model used for the selection of working fluids though, is limited by some practical constraints such as computational time and applicability of correlations, and is always preferred to be executed in a manner that is just precise enough to draw the desired conclusions. When estimating and optimizing for the cost as well as for thermodynamic performance, the precision of these cost estimation needs to be taken into account as well. This was pointed by Lemmens [11], who observed that cost estimations are often given as a number without the uncertainty. For example figure 1.2 shows the relative discrepancy between the estimated and the real equipment cost of a project. This could possibly influence the fluid selection, and will certainly influence the process parameters. This raises the question what conclusions need to be drawn when doing a working fluid selection. It can for example be desired to have the economically best performing working fluid with some level of certainty, another demand can be that the selected working fluid is compatible with some type of component. This research focuses on the composition of a model which reaches desired accuracy without adding unnecessary complexity.

1.4. OBJECTIVE AND FOCUS

The objective of this work is the design and optimization of a new ORC system for Triogen, for application with modern diesel generators. A working fluid and process parameters will be selected with focus on the design of the heat exchangers and especially the recuperator and condenser. In short the objective could be formulated as: Integral optimization of an ORC, considering working fluid, process parameters and hardware geometry, using a gaseous heat source with a temperature of 350°C and a mass flow of 5 kg/s.

This objective is split up in the following sub-questions:

1. What is the optimal type of working fluid and Organic Rankine Cycle, for the generation of electricity from diesel generator exhaust gas waste heat, apparent from previous research?

2. What type of model is suitable for the selection of a working fluid and process parameters for an ORC applied with diesel generator exhaust gas waste heat?

3. In what level of detail should the cycle and its components be modeled in order to reach sufficient accuracy?

4. How can the performance and cost of the main components of an ORC system be modeled?

5. What are the optimal working fluid, process parameters and component geometry for this application?

In chapter 2 first an introduction is given of the ORC and its main components. Then based on literature types of cycles and the properties of working fluids are analyzed in order to answer sub-question 1. Sub-question 2 and 3 are also treated in chapter 2 where these questions are discussed based on literature. Sub-question 2 and 3 are also leading in chapter 3, but now more on a practical level. First the structure of the model is discussed, then using a simple model the sensitivity of the power output for important component performance parameters is tested as a supplementary answer on question 3. In chapter 4 the model framework is completed with sub-models for the main components, based on the demanded accuracy from question 3. Both design and modelling method are discussed, answering sub-question 4. In chapter 5 question 5 is answered. The model is used to simulate a number of cases, based on which the working fluid and process parameters can be selected. Some additional cases are used to raise discussion on modeling and the influence of some external parameters.

2

LITERATURE AND BACKGROUND

In this chapter background is given. First a description is given of the ORC system, explaining the function of each component, as well as different measures for the cycle efficiency. Thereafter a description is given of the possible cycle types. Then the main components of the ORC system are described in the context of former ORC fluid selection literature. After which an overview is given of the important fluid properties. Last a description of the boundaries and boundary conditions is given.

2.1. SYSTEM DESCRIPTION

In this section the system nomenclature is introduced, as well as the functionality of the main components. Also different measures of efficiency are introduced here.

2.1.1. ORGANIC RANKINE CYCLE DESCRIPTION

The purpose of the Organic Rankine Cycle is the conversion of heat into mechanical energy. This mechanical energy is most often converted to electrical energy using a generator, which is therefore mostly considered as part of the cycle. The cycle consists of four main components namely the evaporator, turbine, condenser and pump and a set of auxiliary components. In figures 2.1 and 2.2 an overview is given of the cycle, also the states are numbered in both figures. Each main component basically changes the state of the working fluid. In this subsection all components and their phase changes are introduced. In figure 2.2 an indication of the temperature slopes of the hot and cold source is given as well.

PUMP (1-2)

The pump raises the pressure of the condensed working fluid to the higher pressure level. In the TS diagram, this is only a small step as the amount of energy added to the cycle in this stage is only small.

EVAPORATOR (3-4)

The evaporator is a heat exchanger with a heat source on the hot side and the working fluid on the cold side. The working fluid is first preheated, then evaporated and last super-heated, the liquid typically enters the evaporator as sub-cooled liquid and leaves it as super-heated vapor. The heat source can be either a liquid or gaseous stream, Triogen uses only gaseous (waste) heat streams. In this work the evaporator design as normally used by Triogen is used. This evaporator design is based on the design of a flue-gas cooler with plain tubes to prevent excessive fouling. The working fluid is situated on the tube side.

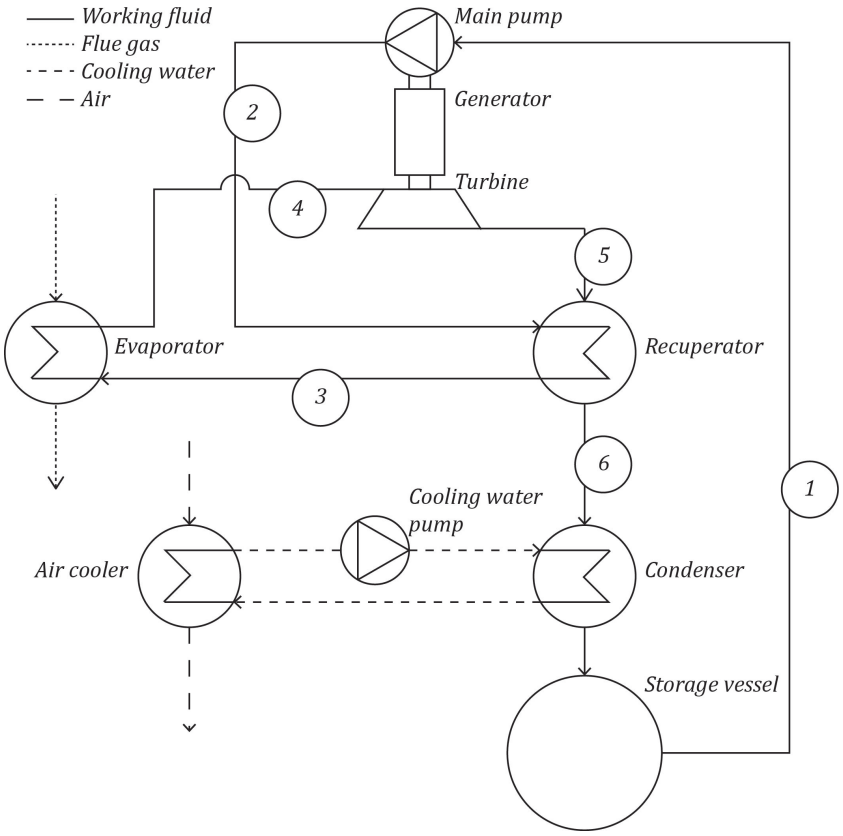

Figure 2.1: Schematic overview of the Triogen ORC system

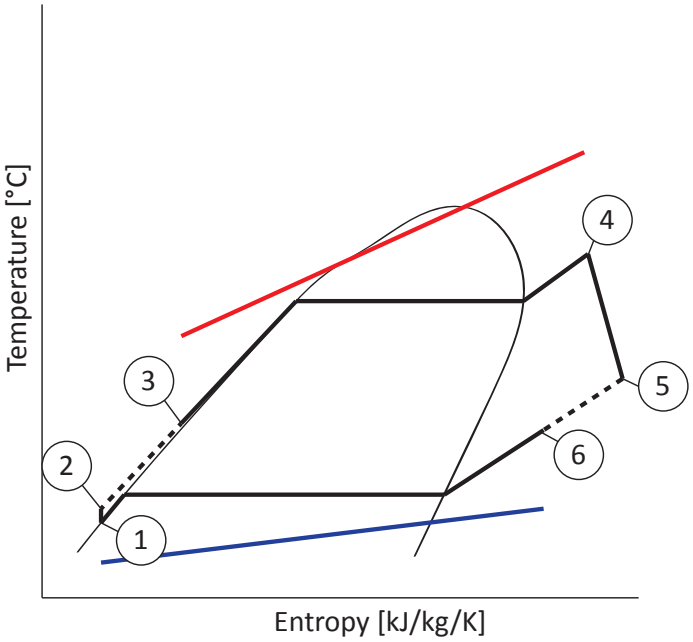

Figure 2.2: TS diagram of a sub critical ORC cycle

EXPANDER (4-5)

The expander is the component where thermal energy is converted to mechanical energy. For larger systems (100 kW+) a turbine is preferred as expander, for smaller systems positive displacement

expanders are preferred. Formation of vapor in the turbine must normally be prevented in order to prevent erosion of the turbine blades. This can be accounted for by limiting the vapor saturation at the outlet of the turbine to be 1 or higher. To enable saturation at the turbine outlet, superheat at the entrance of the turbine may be necessary, depending on the shape of the vapor saturation curve in the T,S diagram. Three types of these saturation curves are distinguished in figure 2.3 the vapor curve of a wet, isentropic and dry fluid are shown. For the purpose of preventing blade erosion, superheat is only necessary in cycles using a wet fluid.

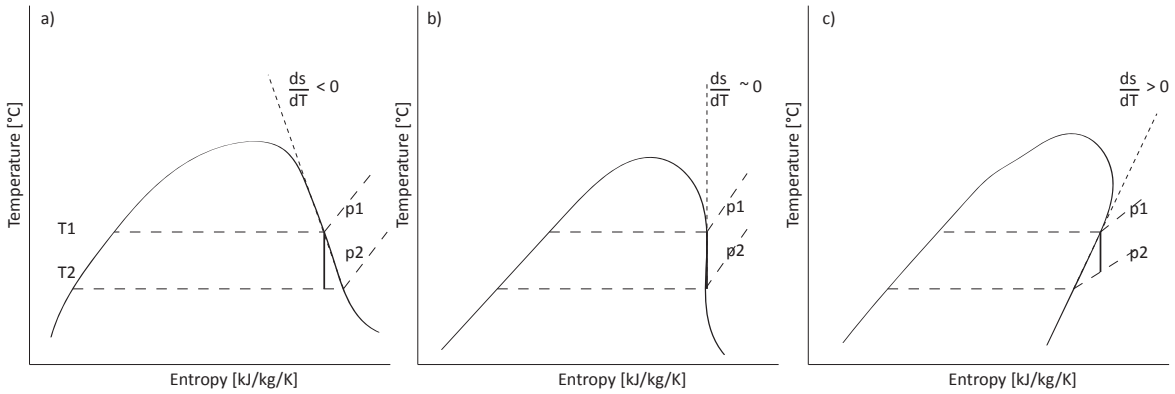

Figure 2.3: T-s diagram for fluids (a) wet, (b) isentropic and (c) dry

CONDENSER (6-1)

In the condenser the working fluid is first desuperheated and then condensed and slightly sub-cooled, a cold source is used to cool down the working fluid. This cold source in most cases is water or air. In case of air-cooled systems an intermediate cycle may be applied in order to reduce the size of the condenser to reduce cost. In this work an intermediate loop with air-cooler is used for the cooling, the design of the condenser will be discussed later more elaborately.

RECUPERATOR (2-3 AND 5-6)

The recuperator transfers heat from the vapor flow coming from the turbine, to the liquid flow to preheat this flow before it enters the evaporator. As both desuperheating of the vapor (5-6) and preheating of the liquid (2-3) are also done by the condenser and evaporator respectively, the application of a recuperator is optional. It is used to reduce the total heat input and output of the system and therefore raise the efficiency, in addition it can be used to increase the temperatures at the inlet of the evaporator to prevent condensation of flue-gases.

2.1.2. SYSTEM EFFICIENCY

In literature multiple definitions are given in order to measure the quality or performance of the cycle. Here the most common efficiencies are given, as well as the measures for system performance as used in this work.

First there is the first law or thermal efficiency.

$$\eta_{th} = \frac{W_{turbine} - W_{pumps}}{Q_{evap,in}} \tag{2.1}$$

This efficiency compares the total work output to the total heat input.

Then there is the second law or exergy efficiency, which takes into account the quality of the energy called exergy. The total work output is for this efficiency compared with the work output

of an ideal Carnot cycle. The Carnot cycle gives the maximum theoretical work for a certain heat source temperature and cold source temperature.

$$\eta_{II} = \frac{W_{turbine} - W_{pumps}}{W_{carnot}} \tag{2.2}$$

The Carnot work can be calculated using equation 2.3. Alternatively the exergy present in the cooling medium can be neglected.

$$W_{carnot} = \dot{m}_{fg} * (ex_{fg,in} - ex_{fg,out}) + \dot{m}_{aq} * (ex_{aq,in} - ex_{aq,out}) \tag{2.3}$$

Next is the available heat efficiency, which compares the total work output to the total heat available instead of the heat transferred in the evaporator.

$$\eta_{ha} = \frac{W_{turbine} - W_{pumps}}{Q_{available}} \tag{2.4}$$

Mainly in waste heat recovery this definition is useful as it is after all preferred to convert as much energy as possible from a given heat source. This definition of efficiency is therefore used in this work by giving only the total work as the heat source is maintained constant.

Last is the cost efficiency, or specific cost. Here the heat source is not taken into account as reference, although an economic value could be given to it, this value can be neglected as the ORC is applied with waste heat streams. Instead the system cost are compared to the total power output:

$$C_{spec} = \frac{C_{total}}{W_{turbine} - W_{pumps}} \tag{2.5}$$

The specific cost is in ORC applications much more relevant compared to the thermal efficiency as natural and waste heat sources are widely available. The challenge is to convert this energy in a cost effective way.

2.2. CYCLE TYPES

In this section the two main types of Organic Rankine Cycles are discussed. Also the application of working fluid mixtures in a sub-critical cycle is discussed here. This is chosen, because the type of considerations fit better in this section compared to the next section where fluid properties are discussed. The TS-diagrams for all cycle types discussed in this section are given in figure 2.4

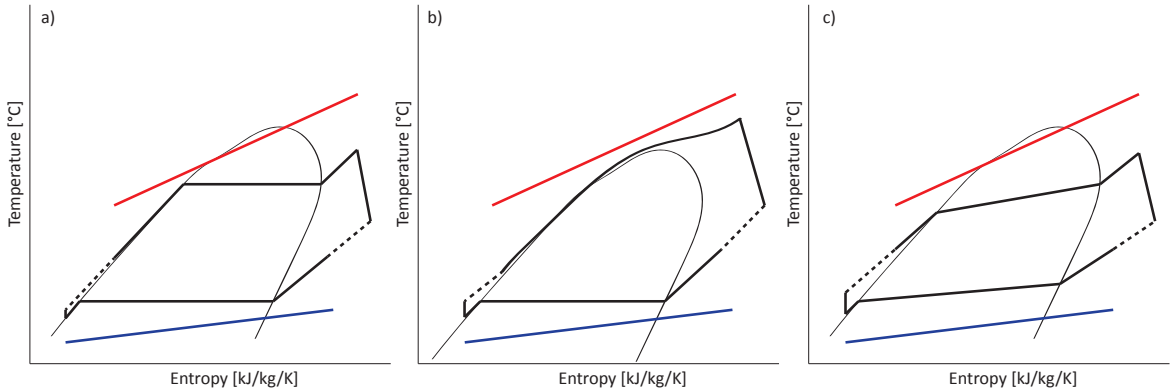

Figure 2.4: TS diagram of a) sub-critical cycle, b) Transcritical cycle, c) sub-critical cycle with a mixture as working fluid

2.2.1. SUB-CRITICAL CYCLE

The subcritical cycle is the most common type because of its moderate process parameters and simple design. The main disadvantage of this cycle type is the constant evaporation temperature which causes large temperature differences and thus exergy losses in the evaporator. This might be reduced by using fluids with evaporation pressures relatively close to the critical pressure (reducing the latent heat of evaporation) [12]. Also a bit of superheat may decrease the exergy loss in the evaporator, and thus increase cycle efficiency, though it may cause losses at other points. In case of a dry working fluid, the working fluid leaves the turbine often highly superheated, and the application of a recuperator may be beneficial. This is an apparatus that transfers the heat in the superheated vapor leaving the turbine, to the sub-cooled liquid coming from the pump. The recuperator increases the thermal efficiency because part of the energy needed to heat the working fluid is reused, and is therefore often marked as beneficial. The use of a recuperator though, is not in all cases beneficial. Only in applications where the hot flow may not be cooled further then a specific point (e.g. condensing flue-gases), or where the hot flow is reheated (e.g. solar applications), the use of a recuperator gives significant benefits.

2.2.2. TRANSCRITICAL CYCLE

The transcritical cycle can be applied when the critical temperature of a working fluid is much lower than the heat source temperature. The benefits of a transcritical cycle are improved second law efficiency, due to the temperature profile for evaporation, and secondly the downsizing of cycle components due to the higher densities at high pressures. The disadvantages though are increased volume ratio's which may require multiple stages in expansion and the relatively high pressures. Also the transcritical cycle requires an efficient pump because of the high pressure differences. Maraver et al. [10] point out lower pump efficiencies for small systems may discourage the use of a transcritical cycle.

The relative performance of the transcritical cycle compared to the subcritical cycle also depends on the pinch temperature difference[12], using the transcritical cycle decreases the exergy loss in the evaporator due to the approximately linear temperature slope in the Th domain. When a higher pinch temperature is assumed, the reduction in exergy destruction achieved is relatively lower. Therefore the total efficiency increase compared to a sub-critical cycle will be lower. Lecompte et al. [13] compared the second law efficiency of the subcritical partial evaporation and transcritical cycle for heat source temperatures ranging from 150 to 350°C. One of the conclusions is that the application of alternative cycle designs mainly increases the second law efficiency for low heat source temperatures. At higher temperatures the efficiency gain due to the use of a transcritical cycle decreases.

2.2.3. MIXTURES

Chys et al. [14] compared the performance of a subcritical cycle using pure fluids and mixtures as working fluids. Two cases were researched and it was concluded that for low temperature heat sources (150°C) a work output increase of 16% was reached by using a mixture instead of a pure fluid. For higher temperatures (250°C) this increase was much lower (6%). Similar results are reported by Lampe et al.[15] who researched the integrated design of working fluid mixtures and Organic Rankine Cycles for a heat source temperature of 270°C. They conclude that the increase of net power output when using an optimal mixture of fictitious working fluids is just 3% compared to when using a pure fluid. This increase in power output is low, when taking into account the extra cost due to larger heat exchangers and added complexity are not taken into account. Lampe et al. also conclude that the increase of efficiency depends largely on the slope of the cooling temperature, when a constant cooling temperature is assumed, pure fluids gave best results while for larger temperature slopes the mixtures performed better. The increase of heat exchanger area is caused by the decrease

of average temperature difference and the heat transfer properties of mixtures. Radermacher [16] concluded heat transfer decreases when using mixtures due to a decreased thermal conductivity and increased viscosity as well as to a diffusion-controlled phase change process. Andreasen et al. [17] researched for a heat source temperature of 90 °C the maximum power output and minimum cost per kW for R32, R134a and a mixture of the two. They conclude an increase of maximum power of 13.8 % is possible when using a mixture instead of a pure fluid. When considering the specific cost though, a decrease of around 3% is reachable. For the reason of limited impact of mixtures on the total cycle performance, as well as the problem of increased complexity of cycle design and modelling, it is in this research chosen to only use pure working fluids.

2.3. MAIN COMPONENTS

2.3.1. PUMP

The pump is often thought to have a very small influence on the total system efficiency and cost. Its power consumption for sub-critical cycles accounts for only a few percent of the total power production, while for trans-critical cycles it easily reaches power consumptions of around 10% of the total power production due to the higher pressures that are reached. The pump is most often modeled as adiabatic with a fixed isentropic efficiency, which is given in equation 2.6. The design and process conditions can highly influence this isentropic efficiency and at the same time this isentropic efficiency might influence the choice for cycle design and working fluid according to Maraver et al. [10]. Figure 2.5 shows the influence of pump efficiency on the second law efficiency of some cycle with a 300°C heat source temperature. In this research toluene and MDM are modeled as sub-critical cycles, and the other fluids as trans-critical cycles, it is seen that the pump efficiency has great influence on the trans-critical cycle, while the sub-critical cycle is almost unaffected. Quoilin et al. [18] show something similar for sub-critical cycles, they relate the Back Work Ratio (BWR, equation 2.7) to the evaporation temperature of different fluids, and show a relation between the critical temperature and the BWR. In figure 2.6 it is shown that the BWR increases significantly when the cycle is operated close to the critical temperature, also it is shown that for higher critical temperatures lower BWR is reached, so pump efficiency will have less influence on cycle performance for these fluids.

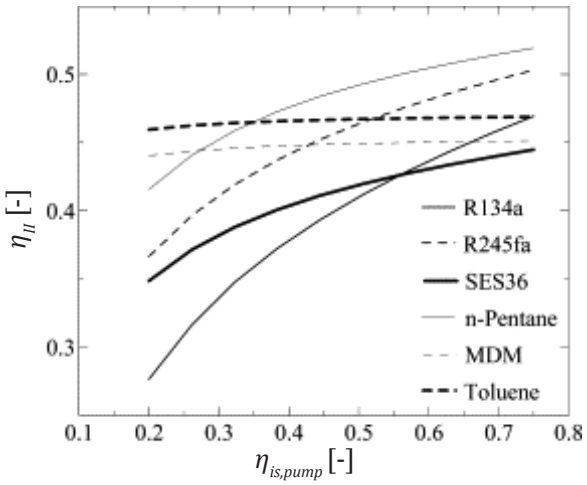

Figure 2.5: Influence of pump isentropic efficiency on cycle second law efficiency, for a heat source of 300 °C, by Maraver et al. [10]

Because there is a difference in influence of the pump efficiency on cycle performance a realistic efficiency has to be chosen, which is close to the reachable efficiency for trans-critical cycles of this size. Quoilin et al. [18] report the isentropic efficiencies for pumps in +- 1kW systems to be around

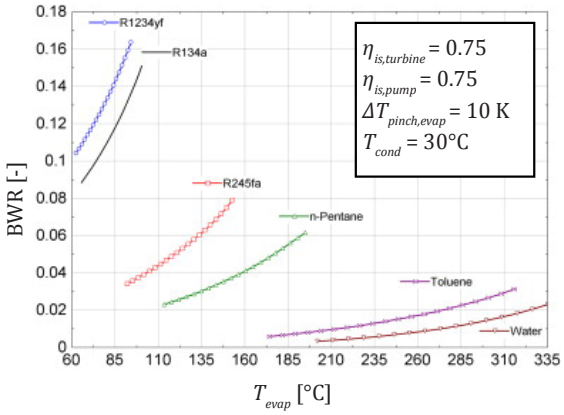

Figure 2.6: Influence of evaporation temperature on back work ratio [18]

20% and adds that efficiencies for larger systems are not available in literature, though manufacturers data says centrifugal pumps are able to reach efficiencies higher than 60% and diaphragm pumps should reach over 40-50% isentropic efficiency. A design study conducted by Fu et al. [19] for a 250 kW system using R245fa as working fluid reports a reached pump efficiency of 68.1%. Also it needs to be mentioned, although not taken into account at this stage of the research, there is a possibility of cavitation at the pump inlet due to the net pressure suction head.

$$\eta_{is,pump} = \frac{h_{2,is} - h_1}{h_2 - h_1} \tag{2.6}$$

$$BWR = \frac{W_{pump}}{W_{turbine}} \tag{2.7}$$

2.3.2. EVAPORATOR

The evaporator is the module where heat coming from some heat source is transferred to the working fluid. For subcritical cycles the evaporator consists of three regimes: preheat, evaporation, and superheat. In transcritical cycles there is no difference between the regimes. In literature, the evaporator is most commonly modeled using a pinch temperature difference, and a degree of superheat or turbine inlet temperature. Also the pressure drop and the heat transfer coefficient could be considered, which are mostly fixed for simple models. If the evaporator is modeled in more detail, correlations are used to calculate the pressure drop and the heat transfer coefficient.

In order to reduce exergy destruction in the evaporator it is preferred to have the temperature glide of the evaporating fluid to match the temperature glide of the heat source, enabling a constant temperature difference in the evaporator. Because evaporation of pure fluids occurs at constant temperature, the exergy destruction in the evaporator is normally relatively large for sub-critical cycles. Transcritical cycles and cycles using mixtures normally have better matching temperature glides. Liu et al. [2] wrote on the effectiveness of heat recovery, up to then in most fluid selection studies the heat source temperature was assumed constant while in most practical cases the hot flow is cooled down significantly in the evaporator. Therefore it is necessary to have a temperature profile of the evaporating working fluid matching to the temperature profile of the flue-gas. Because of the thermal stability of some working fluids it may in some cases be necessary to have an intermediate cycle, which transfers the heat to the cycle at a lower temperature. This intermediate cycle causes an exergy loss but prevents the working fluid temperature from being locally above the temperature at which the working fluid decomposes.

Although, not for all fluids readily available, the thermal stability point is an important parameter (section 2.4.1). If heat source temperatures are above the thermal stability point of the working fluid, the application of an intermediate loop or the precooling or dilution of the flue-gas might be necessary. In the first analysis the thermal stability is not taken into account, due to the lack of data.

2.3.3. TURBINE

In fluid selection studies, the turbine is often modeled as an adiabatic component with an isentropic efficiency. The efficiency relates the pressures, and enthalpies as seen in equation 2.8. The isentropic enthalpy is calculated from the outflow pressure and the inflow entropy. In most fluid selection studies the isentropic efficiency is assumed fixed. This efficiency though is highly dependent on the working fluid properties, the process parameters and the design of the turbine. Also the turbine efficiency relates directly to the efficiency or output power of the cycle, and is therefore a decisive parameter. Mondejar et al. [7] take a relation for the estimation of the turbine efficiency into account and argument that for fluid selection, the isentropic efficiency should be calculated from the process conditions. Correlations for estimating turbine efficiency have been constituted for different types and applications of turbines, which will be studied later in the process.

$$\eta_{is,turbine} = \frac{h_4 - h_5}{h_4 - h_{5,is}} \tag{2.8}$$

2.3.4. GENERATOR AND BEARINGS

Also the bearings and generator are a cause of losses. For low frequencies these losses are often small. For smaller system sizes though, high frequencies are necessary and significant losses are expected in the generator and bearings.

2.3.5. CONDENSER

The condenser is the component where the working fluid is cooled and condensed at a low pressure. This will probably be done by using an intermediate loop with a water glycol mixture as coolant which is cooled using air coolers. These auxiliaries are not taken into account at this stage. Later in this work it needs to be evaluated if indeed this is the most cost effective way of cooling. In this work pure water is used as coolant.

2.3.6. RECUPERATOR

The recuperator is often associated with increased efficiency of the cycle. When analyzing the thermal efficiency this is in almost all cases true, as the heat intake may be reduced with constant power output for waste heat sources, or the power output increases for constant heat input with for example solar heat sources. Power output on the other hand does not necessarily increase. Zhu et al. [20] for example conclude that the recuperator for a sub-critical ORC cycle with a heat source of 200 °C improves the thermal and exergy efficiency, though will never affect the total power output. They claim that only when an outlet temperature restriction is used for the flue-gas, the recuperator will improve the total power output. Also Maraver et al. [10] concludes for a large range of heat source temperatures, that the recuperator only promotes power output in case of a limitation of the outlet temperature.

On the other hand when the pinch point is at the working fluid entrance of the evaporator, the total mass flow of working fluid could be increased by adding a recuperator. This only happens when the working fluid has a low critical temperature. Another often not mentioned effect of the recuperator is that it combines the cooling of vapor and the heating of liquid in one heat exchanger, which would half the total heat exchanger surface, in case the product of temperature difference and heat transfer coefficient would have the same magnitude. In other words, it might be possible

to reduce total cost, by reducing the cost of evaporator, condenser and cooling circuit and adding a recuperator.

Walraven et al. [21] for example simulated for a 120°C heat source the application of shell and tube and on the other hand plate heat exchangers for condenser, evaporator and recuperator. They limited the total surface area and conclude best exergy efficiency is reached when no recuperator is used. Again only in case of a restriction on the outlet temperature the recuperator increased performance.

The recuperator transfers heat from the low pressure hot process flow coming from the turbine to the high pressure cold process flow before it enters the evaporator. In literature the recuperator is usually described using a minimum temperature difference, the log mean temperature difference, a degree of superheat in the cooled stream after the recuperator or a recuperator effectiveness, additionally a pressure drop and a heat transfer coefficient can be used. In this first model it is assumed there is no heat transfer to the environment.

The effectiveness is defined as the heat transfer divided by the maximum possible heat transfer. The maximum possible heat transfer is defined as the minimum heat capacity rate times the temperature difference between the hot and cold inflow temperature, or by using the corresponding enthalpies as seen in equation 2.9.

$$\dot{q}_{max} = \dot{m}_{hot} * (h_{hot,in} - h_{hot,out}) \tag{2.9}$$

This means that maximum effectiveness is reached only when the outflow temperature of one of the flows is equal to the inflow temperature of the other flow. effectiveness of 1 is thus only reached in infinitely large pure counter flow heat exchangers or infinitely large heat exchangers in which one of the flows has a constant temperature (evaporation and condensation of pure fluids). For real heat exchanger designs the effectiveness will never reach 1, as the area of the heat exchanger is limited for economic and fluid dynamic reasons. A measure for the size of an heat exchanger is the NTU (number of transfer units), which is defined from the overall heat transfer coefficient (U), the heat transfer area (A), and the minimum heat capacity rate (Cmin, equation 2.10) as in equation 2.11.

$$C_{min} = c_{p,hot} * \dot{m}_{hot} \tag{2.10}$$

$$NTU = (U * A)/C_{min} \tag{2.11}$$

The effectiveness of any heat exchanger for flows with constant heat capacity rate is a function of the NTU and the heat capacity ratio, $Cr = Cmin/Cmax$. The maximum effectiveness of a shell and tube heat exchanger with a preselected number of shell and tube passes can be calculated by inserting an infinitely large NTU in the effectiveness function for shell and tube heat exchangers (equation 2.12). The total heat transfer in the recuperator is calculated using equation 2.13

$$\epsilon_{rec} = f(NTU, C_{min}/C_{max}) \tag{2.12}$$

$$\dot{q} = \epsilon_{rec} * \dot{q}_{max} \tag{2.13}$$

Another often used parameter is the pressure drop. For simple simulations it may be an assumed fixed value or the pressure drop may be neglected. In more detailed models, often empirical correlations are used to estimate the pressure drop. The pressure drop on the hot (vapor) side of the recuperator will have the greatest impact because the pressure drop has a relatively large impact at low pressures compared to high pressures. In addition it can be desired to calculate the total heat exchanger area in order to calculate the cost or the total heat exchanger surface per kW output power as a measure of cost. To calculate the area the heat transfer coefficient must be calculated, or as often happens for simpler models a heat transfer coefficient can be assumed.

2.4. WORKING FLUIDS

The working fluid in an Organic Rankine Cycle largely determines the performance and design of such a system. In this section an overview is given of the important fluid properties and their influence on system performance and design according to literature. Some of these fluid properties will be used for preselection of the working fluids.

Table 2.1: Table of considered working fluids, and main thermophysical properties

Fluid name	Critical temperature [°C]	Critical pressure [bar]	Maximum temperature [°C]	Boiling temperature [°C]
Toluene	318.6	41.3	426.9	110.1
Benzene	288.9	49.1	451.9	79.6
Cyclohexane	280.5	40.8	426.9	80.3
Heptane	267.0	27.4	326.9	97.9
MM	245.5	19.4	399.9	99.8
Ethanol	241.6	62.7	376.9	78.1
Methanol	240.2	82.2	346.9	64.1
Acetone	235.0	47.0	276.9	55.7
Hexane	234.7	30.3	326.9	68.3
Isohexane	224.6	30.4	276.9	59.8
R113	214.1	33.9	251.9	47.2
R141b	204.4	42.1	226.9	31.7
R11	198.0	44.1	351.9	23.3
Pentane	196.6	33.7	326.9	35.7

2.4.1. THERMOPHYSICAL PROPERTIES

The thermodynamic performance of a cycle is highly enhanced by only a few fluid characteristics. Quoilin et al. [18] say on thermodynamic performance: "*The efficiency and/or output power should be as high as possible for given heat source and heat sink temperatures. This performance depends on a number of interdependent thermodynamic properties of the working fluid: critical point, acentric factor, specific heat, density, etc. It is not straightforward to establish an optimum for each specific thermodynamic property independently. The most common approach consists in simulating the cycle with a thermodynamic model while benchmarking different candidate working fluids.*" The critical temperature is often claimed to relate to the thermodynamic performance strongly and will be treated here in more detail. Also the shape of the dew curve in the TS diagram has a significant influence on the cycle parameters and performance as mentioned in section 2.1.1. Besides the critical temperature also properties such as density, viscosity, thermal conductivity and the fluid's state at ambient conditions are discussed.

CRITICAL TEMPERATURE

Vivian et al. [12] relate the efficiency of the cycle to the difference between the critical temperature of the working fluid and the inflow temperature of the hot source. They concluded that for sub-critical cycles the critical temperature should be around 35 °C lower compared to the heat source temperature. They concluded this for heat sources ranging from 120 to 180 °C, with in all heat exchangers a pinch of 10 K, a condensation temperature of 35 °C and no minimum outflow temperature for the hot source. The cycle efficiency and the critical temperature were also researched by Aljundi [22]. He assumed a constant evaporation temperature of 90 °C as well as a constant condensation temperature of 30 °C and found increasing efficiencies for increasing critical temperatures (figure

2.7). This results can be explained by the relation between critical temperature and latent heat of evaporation. As for constant temperature heat sources and sinks best efficiency is reached when an as large as possible fraction of the energy is added during vaporization. In case of non-constant heat source temperature this relation is not applicable due to the large gradient in the heat source temperature.

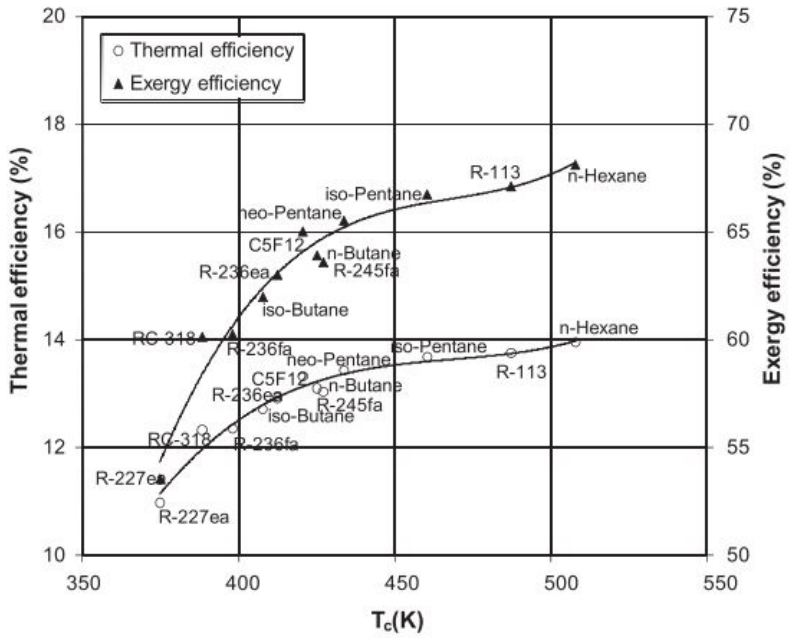

Figure 2.7: Thermal and exergy efficiencies as a function of the fluid's critical temperature, for cycles with an evaporation temperature of 90°C and a condensation temperature of 30°C [22]

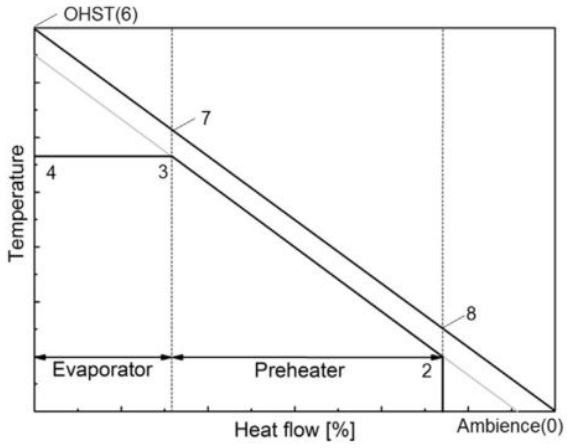

Figure 2.8: Graphical representation of the optimal heat source temperature theory (OHST), showing that the optimal heat source temperature (point 6) is a function of the working fluid heat capacity (2-3), the pinch temperature difference in the evaporator (3-7) and heat of vaporization (3-4). [23]

Liu et al. [23] predict the optimal heat source temperature (OHST) for sub-critical cycles using the heat of vaporization, the liquid heat capacity, the evaporation temperature and the pinch temperature difference (equation 2.14). They base their theory on the optimization of cycles for optimum available heat efficiency and exergy efficiency. Using this theory, a range of heat source temperatures can be estimated for which the working fluid performs relatively good compared to

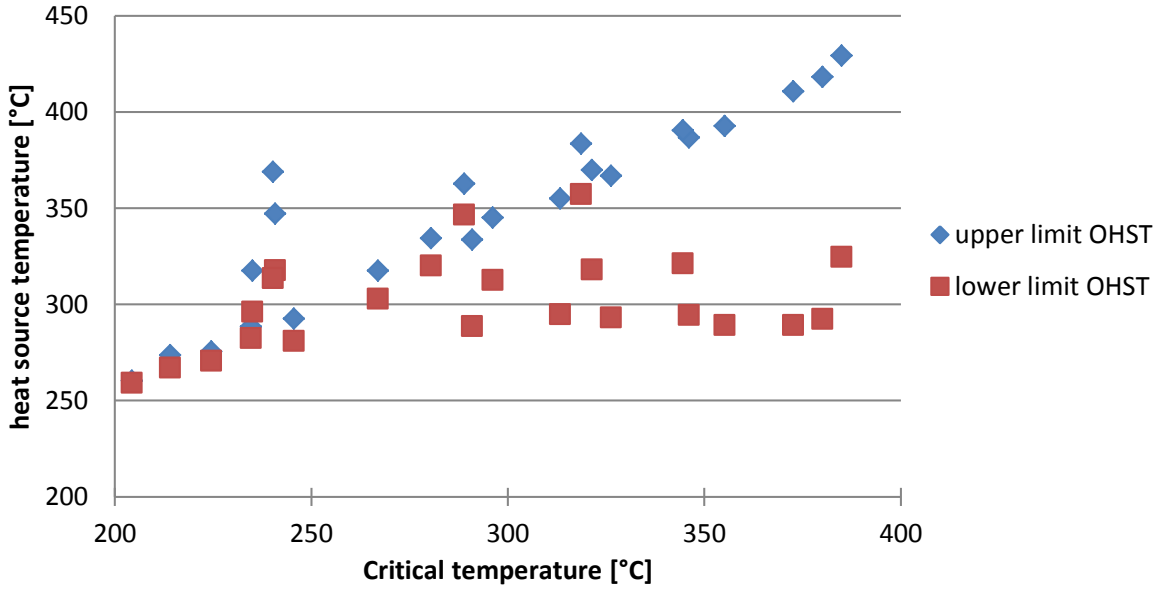

Figure 2.9: Optimal heat source temperature constructed using the optimal heat source temperature theory (OHST) [23], for fluids with critical temperatures ranging from 200 to 400°C.

other working fluids. The theory is based on the assumption that best performance is reached when the slope of the preheat section in the TQ diagram is parallel to the slope of the heat source temperature (figure 2.8). Although this theory is designed for heat sources without a minimum stack temperature, such as geothermal heat, the method gives interesting results for waste heat recovery as well. Figure 2.9 shows the relation between the optimal heat source temperature and the critical temperature. This figure is plotted using the OHST theory, assuming the evaporation temperature is between 200°C and the critical temperature. The c_p is estimated by dividing the enthalpy difference by the temperature difference, assuming fluid is preheated from 160°C to the evaporation temperature. Apart from a few outliers, namely water, the aromatic hydrocarbons and the alcohols a clear relation is shown between the critical temperature and the optimal heat source temperature.

$$OHST = \Delta h_{evap} / \bar{c}_{p,preheat,wf} + T_{sat} + \Delta T_{pinch,evap} \tag{2.14}$$

DENSITY

The density closely relates to the volumetric flowrate and therefore it relates also to the design of the system components. Lower densities yield higher volumetric flowrates, larger pressure drops and larger component sizes. The density in the vapor phase is highly determined by the pressure, thus low condensation pressures often relate to expensive equipment. Also the turbine efficiency is dependent on the volumetric ratio over the turbine, as well as the total volume flow through the turbine.

VISCOSITY

The viscosity relates to the pressure drop and the heat transfer coefficient. Low viscosities are preferred because it leads to lower pressure drops in the heat exchangers and other equipment. Viscosity is also an important property when the working fluid is used as lubrication for the bearings. Bearing lubrication is not within the scope of this work.

THERMAL CONDUCTIVITY

Thermal conductivities should be high, in order to achieve high heat transfer coefficients in all heat exchangers.

EVAPORATING PRESSURE

The evaporating pressure depends highly on the process conditions, and has an important impact on the system design and cost. Higher pressures need larger wall thicknesses, which will raise the cost. At higher pressures shell and tube heat exchangers become more preferable compared to plate heat exchangers because of the good pressure resistance of the tubes and the limited pressure resistance of plates. In some works an upper limit of the evaporation pressure is assumed.

CONDENSING PRESSURE

Some papers report ambient pressure as a lower limit for the condensing pressure[18]. Below ambient pressure leaks in the system will result in contamination of the working fluid with air and water. In most commercial applications though, condensing pressures are below ambient pressure, and in some cases a device is installed to clean the working fluid from these contaminants. When condensation pressure is above ambient pressure, leakage of working fluid to the environment might occur. This will demand safety systems for monitoring and cleaning of the air. Higher condensation pressures in almost all cases lead to increased heat transfer in both the recuperator and condenser due to increased density and thermal conductivity. At the same time pressure drop in these components has less influence, therefore smaller heat exchangers can be used when condensing pressures are higher.

THERMAL STABILITY POINT

The thermal stability point temperature of the working fluid is an important parameter for the selection of working fluid and the design of the cycle. Above this temperature the fluid starts decomposing at a measurable rate, which will influence the cycle performance in the long term, and might lead to breakdown. Cycle temperatures above this temperature must be prevented, therefore an intermediate cycle might be applied when heat source temperature is too high to prevent the working fluid temperature from rising above the thermal stability point locally. Not much research has been done though into the thermal stability of working fluids, also the thermal stability point depends on a multitude of parameters. Not only temperature, but also pressure, containing materials and contaminants in the working fluid may function as catalyst and enhance the decomposition of the working fluid. Due to the large amount of influencing parameters and the variety of definitions of what is still thermally stable and what is not, thermal stability data are available for few working fluids only. According to Calderazzi and Colonna [24] no evident degradation of R141b with stainless steel as containing material occurs at temperatures up to 90°C, which eliminates the R141b as candidate fluid as the working conditions are far above 90°C. Fabuss et al. [25] estimated the decomposition temperatures of pure hydrocarbons with a relatively high decomposition temperature as result, as they measured the decomposition temperature by gradually increasing the temperature and keeping it constant for 15 minutes, the temperature at which measurable pressure change would occur first, was called the decomposition temperature. They concluded a thermal stability point for decane of 371°C, and the thermal stability of a large amount of other hydrocarbons which are not in the scope of this research. Johns et al. [26] did a similar research and came -among others- up with a thermal stability point of 565°C for toluene. The thermal stability points of isopentane and butane, 290°C and 310°C respectively, where found by Pasetti et al. [27].

MELTING POINT TEMPERATURE

The melting point temperature must be below the cooling temperatures, this is necessary to prevent the working fluid from solidifying, and to ensure it will stay a liquid. Also it has to be taken into

account, that if ambient temperatures may decrease below the melting point temperature of the cycle, the working fluid might solidify during standby.

STATE AT AMBIENT CONDITIONS

The boiling point at ambient pressure is often reported. The fluid is desired to be in the liquid state because this increases the ease of filling an ORC. It is not strictly necessary though to have a high boiling point at ambient pressures, as alternative filling methods are widely available.

2.4.2. ENVIRONMENTAL PROPERTIES

Next to thermophysical properties there is a second category of fluid properties, influencing the selection of working fluids. These properties, which relate to the environment and safety, are described here. The influence of working fluids on the environment is described using the Global Warming Potential (GWP) and the Ozone Depletion Potential (ODP). In relation to safety toxicity and flammability are the two greatest risks. In table 2.2 the environmental properties are listed for all considered fluids.

Table 2.2: Environmental properties for all considered fluids, ODP relative to R11, GWP relative to carbon dioxide

Fluid name	ODP	GWP	Toxicity	Flamability	Reactivity
Toluene	N/A	N/A	2.0	3.0	0
Benzene	N/A	N/A	2.0	3.0	0
Cyclohexane	N/A	N/A	1.0	3.0	0
Heptane	N/A	N/A	1.0	3.0	0
MM	N/A	N/A	0.0	3.0	0
Ethanol	N/A	N/A	1.0	3.0	0
Methanol	N/A	N/A	1.0	3.0	0
Acetone	N/A	N/A	1.0	3.0	0
Hexane	N/A	N/A	2.0	3.0	0
Isohexane	N/A	N/A	2.0	3.0	0
R113	0.80	4800	0.0	1.0	0
R141b	0.12	725	2.0	1.0	0
R11	1.00	4000	1.0	0.0	0
Pentane	N/A	N/A	1.0	4.0	0

GLOBAL WARMING POTENTIAL

The GWP is an index which relates the potential contribution of the fluid to global warming in relation to the global warming potential of CO_2. As these molecules are broken down by nature at different time scales, a standard timescale of 100 years is commonly use for comparing the impact of different media

OZONE DEPLETION POTENTIAL

The ODP is an index that determines the relative ability of chemical substances to destroy ozone molecules in the stratosphere. Working fluids with low or zero ODP are preferred, fluids with very high ODP are banned. Ozone depletion is caused by reaction of hydroxyl radicals [OH], nitric oxide radicals [NO], chlorine atoms [Cl] and bromine atoms [Br]. The chlorine atom is the most important (man-made) cause of ozone depletion. The presence of chlorine in the stratosphere is amongst others, caused by the leakage and spilling of working fluids for refrigeration and power cycles. The ozone depletion potential is defined relative to the depletion potential of R11. Multiple working fluids are nowadays banned because of their ozone depletion potential. Among the higher temperature working fluids, there is no or few chlorine in the molecules.

FLAMMABILITY AND TOXICITY

When selecting a working fluid also the flamability of the working fluid must be assessed, the flammability of a medium is defined as the ability of a medium to burn or ignite. Also the toxicity must be assessed. Best known method for the rating of fluid flammability, toxicity and reactivity is the NFPA diamond (figure 2.10). In this diamond a rating is given for the possible hazards and necessary precautions. The working fluids used in Organic Rankine Cycles are mostly moderately toxic and highly flammable, and precautions must be taken in the design and maintenance of an ORC based on the used working fluid. The reactivity must be low as only a stable fluid will have the desired properties for multiple years.

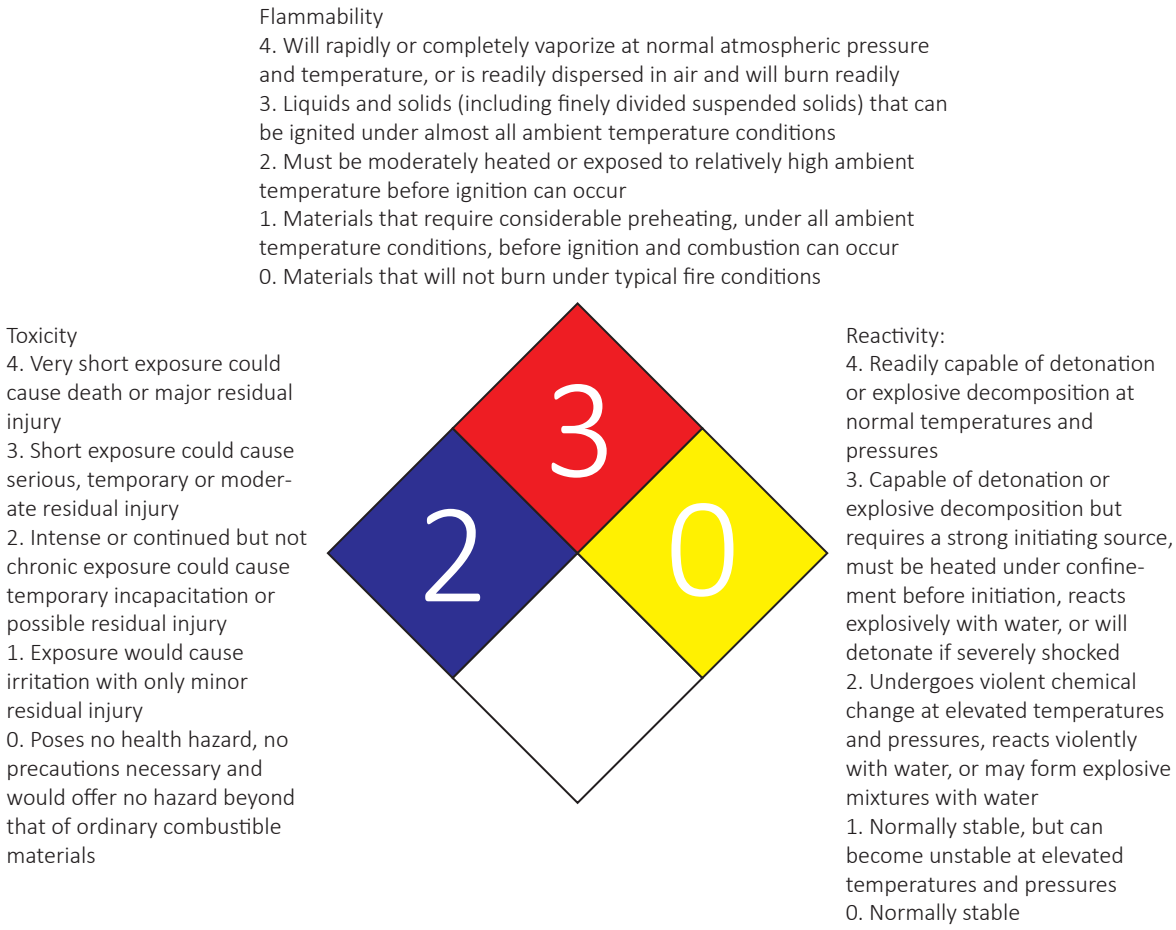

Figure 2.10: NFPA diamond, used for the hazard risk assessment for chemicals

2.5. APPLICATION AND BOUNDARIES

2.5.1. DIESEL GENERATORS

The new module is to be used with large modern diesel generators. A full market analysis of these engines is outside the scope of this research. It is nevertheless relevant to know what the exhaust gas temperatures are expected to be, and in which regions these generators are used, in order to estimate the ambient temperature. Due to the good availability of grid connection throughout Europe only few diesel generators are used there as base load energy supply. In health-care and industry diesel generators are used as backup power supply, for the application of ORC technology though, a constant heat flow is necessary. Due to the reliability of diesel engine technology, diesel generators

are also often used for local medium scale electricity production in rural areas, where no grid connection is available. This application is most used in parts of Africa and Asia. Ambient temperature is expected to have a large impact on optimal system design as it is closely related to the condensation temperature of the ORC, in this work a reference ambient temperature of 25°C is assumed, also the sensitivity for variation of the ambient temperature will be assessed.

Due to ongoing development of diesel engine technology, the efficiency of these engines is increasing and exhaust gas temperature is slightly decreasing, It is expected for modern diesel engines to have an exhaust gas temperature of around 350 °C. For example the modern Wartsila generators have exhaust gas temperatures ranging from around 320 to 380 °C. In order to be able to produce around 150 kW with an inlet temperature of around 350 °C a flue-gas massflow of around 5 kg/s is needed. When comparing this to the Wartsila engine specifications, it is expected a minimum engine capacity of 2.5 MW is needed to power this module, and a total power output increase of maximum 6% can be reached.

In table 2.3 the flue-gas specifications are listed for a range of Wartsila and Catterpilar Diesel engines based on generator set specifications. It shows that the flue-gas temperatures leaving the Wartsila engines is around 350°C while the Catterpilar flue-gases have temperatures around 500°C. The last important thing to mention regarding the flue-gases is the maximum back-pressure of the diesel engines. This is an important parameter for the design of the evaporator because it limits the pressure drop at the flue-gas side. In the back-pressure the pressure drop over the flue-gas piping, filter and the evaporator is included. In this work a rather conservative pressure drop of 1 kPa is assumed as maximum pressure drop over the evaporator.

Table 2.3: Flue-gas mass flows and temperatures for multiple diesel engines

Engine type	**Output power [kW]**	**Load factor [%]**	**Temperature [°C]**	**Mass flow [kg/s]**	**Max. back pressure [kPa]**
Wartsila 2400W8L26	2513	100	347	4.9	3.0
60 Hz IMO Tier 2		85	349	4.2	3.0
Wartsila 2700W9L26	2827	100	347	5.5	3.0
60 Hz IMO Tier 2		85	349	4.8	3.0
Wartsila 2400W6L32	2520	100	331	4.89	4.0
60 Hz IMO Tier 2		85	329	4.43	4.0
Wartsila 2750W6L32	2880	100	380	5.13	4.0
60 Hz IMO Tier 2		85	328	4.88	4.0
Caterpillar continuous 3516B 60 Hz low fuel consumption	1640	100	406	3.45	6.7
Caterpillar continuous C175-16 60 Hz low fuel consumption	2500	100	446	5.15	6.7

2.5.2. EXHAUST GASES

As the ORC is designed for use with diesel engines, the fuel is expected to contain some amount of sulfur. The presence of sulfur is associated with corrosion due to the formation of sulfuric acid. “When cooling combustion flue-gas for heat recovery and efficiency gain, the temperature must not be allowed to drop below the sulfur trioxide dew point. Below the SO_3 dew point, very corrosive sulfuric acid forms and leads to operational hazards on metal surfaces.” [28]. The sulfur present in the fuel reacts in the engine and becomes sulfur-dioxide and sulfur-trioxide. The sulfur-dioxide may react with oxygen and form sulfur-trioxide. The equilibrium of this reaction favors the formation of sulfur-trioxide as the flue-gas temperature decreases.

$2SO_2 + O_2 \longrightarrow 2SO_3$

Sulfur-trioxide may react with water and form sulfuric acid (H_2SO_4) which may condense at the evaporator walls, which causes corrosion.

$SO_3 + H_2O \longrightarrow H_2SO_4$

To prevent this sulfuric acid condensation the wall temperature needs to be above the acid dew temperature, which is for fuels with a weight percentage of 3 % sulfur content in the fuel around 135°C. For a lower sulfur content of around 0.5% the dew temperature is around 120°C. For common diesel exhaust gases the acid dew temperature ranges from 60 °C to around 150°C. The sulfuric acid will condense at the evaporator walls when wall temperatures are below the acid dew point.

Mosburger et al. [29] studied for a cooled exhaust gas re-circulation system the effect of the condensation of sulphuric acid on the walls of the cooler. They concluded for a cooler temperature of 87°C, when using high-sulfur fuel, no sulfuric acid was detected in the coolers. This lack of sulfuric acid was explained by the reaction kinetics of the reaction from sulfur-dioxide to sulfur-trioxide which has a large timescale compared to the time the flue-gas stays in the system.

When the flue-gas is cooled further to below the saturated water temperature of the flue-gas, which is typically around 50°C for diesel flue-gases, condensate forms at the walls. Now sulfur-dioxide may react directly with the water droplets and form sulfurous acid (H_2SO_3).

$SO_2 + H_2O \longrightarrow H_2SO_3$

To fully prevent corrosion due to condensation of these acids, a minimum wall temperature of at least the acid dew point temperature must be taken into account. As the acid dew point may vary per application the sensitivity of the system for the minimum wall temperature in the evaporator will be tested later. Alternatively the water condensation temperature may be taken as a limit, which will be for this system in all cases below the working fluid condensation temperature, and will therefore be no limiting factor for the system. The wall temperature in a well designed evaporator is normally close to the working fluid temperature, because pressure drop and therefore heat transfer are limited at the flue-gas side.

2.5.3. AMBIENT TEMPERATURE

For the design and cost estimation of the cooling system, the ambient temperature has to be known. In order to give an estimate of this temperature, several parameters need to be taken into account. First there is the location at which the system will be placed. As most generator sets are used in remote regions with limited access to the electricity grid, main market will probably be Africa and Asia. As these continents cover climates in which temperatures barely reach 0°C as well as climates with average temperatures far above 30°C cooling systems will need to be adjusted to these regions and also the cycle optimum will be different for the two temperatures. An other consideration is the variation of temperature over day and year. For the sizing of the cooling system for example the maximum or average temperature might be used. In this work a constant ambient temperature of 25°C is assumed.

2.5.4. FOULING OF HEAT EXCHANGER SURFACES

In addition to corrosion due to condensation of sulfuric and sulfurous acid, fouling will occur on heat exchanger walls. The type and severity of fouling will differ per heat exchanger surface and will therefore be discussed here briefly for the different surfaces. Fouling can be divided in roughly 5 categories. First there is Crystallization Fouling, which happens with fluids in which salts are dissolved such as in cooling water and which may become supersaturated at the working conditions. Second there is particulate fouling, which might occur at the working fluid side as due to wear in bearings small particles might be suspended in the working fluid and deposited later, also in the evaporator soot present in the flue-gas might foul at the surface. Then there is chemical reaction fouling in which the surface material itself does not participate. This might happen for example in the evap-

orator when working fluid temperatures are too high and the working fluid decomposes, and for example carbon particles might form. Fourth there is corrosion fouling, this type of fouling might happen in the evaporator due to condensation of acids, in the condenser it might happen as well at the cooling water side. Stainless steel might be necessary to prevent corrosion here. Last there is biological fouling, this type of fouling is only expected on the cooling water side of the condenser.

The heat transfer resistance of fouling is dependent on the working conditions, time and the flow regime. For example fouling will be more severe at lower velocities and fouling of soot on the evaporator surface will depend on the composition of the flue-gas, also the resistance will increase with time as fouling increases over time. TEMA has composed a list of rough guideline values for the fouling in shell and tube heat exchangers for typical fluids in 1949. Instead of using these values as an estimate of the fouling resistance it is probably more useful to take into account the conditions at which the fouling may be minimized. Therefore all fouling is neglected in this work.

At the working fluid side of the heat exchangers the fouling is neglected. This is legitimate as for now it is assumed a pure working fluid is used, which is also applied as lubricant. When fluid decomposition and severe wear don't happen only negligible fouling will take place at the working fluid side. In the water loop fouling can be minimized by using stainless steel to reduce corrosion fouling, using a water velocity of 2 to 3 m/s and a high water quality will also reduce the effect of biological and particulate fouling. The water velocity must be taken into account in designing the condenser, and will determine the number of tube passes.

3

MODEL DESCRIPTION

In this work a model of the ORC system is used for the selection of working fluid and process parameters. In this chapter the framework of the model is presented. In addition, all components are modeled simply in order to test the cycle performance sensitivity for some important component performance parameters. At the end of the chapter also a cost analysis is presented, showing the share of each component in the total cost of the system. These sensitivities and the cost composition are used in the next chapter where the components are elaborated in more detail.

3.1. MODEL FRAMEWORK

The model is fully programmed in Excel VBA and uses excel as interface. All components are programmed as individual functions and communicate the process parameters according to the scheme in figure 3.1, represented in excel as in figure 3.2. The turbine inlet pressure and condenser outlet pressure are given as inputs. The turbine inlet enthalpy is derived from the turbine inlet pressure and the degree of superheat. All parameters of the hot source are given as input, the cold source is also fully defined. The model is steady state, and all components are isolated from the surroundings, apart from the generator and bearings which dispose all their heat to the surroundings. These assumptions take away much of the complexity as well as the need for a model framework communicating all process parameters to components and pipes. This framework will also be the basis for the later model in which relations will be included for pressure drop in heat exchanging equipment.

3.2. OBJECTIVES

As already mentioned in section 1.3 multiple options are available as optimization objective for the system. In this chapter the cycle is optimized for maximum available heat efficiency. Because the heat source is assumed constant optimizing for maximum available heat efficiency is equal to optimizing for maximum power output. It is chosen because it takes into account both the heat recovery by the evaporator and the efficiency of the cycle, while the first law efficiency does not. For the optimization using the detailed model, the objective is cost per kW. This is chosen based on the assumption that the heat source has no value in contrast with conventional power production using fossil fuels. It is therefore more relevant to create a standardized, low specific cost module instead of a more expensive module efficiently converting all the heat available. For a relatively small module producing around 150 kW this will probably result in a system with almost as high as possible power output, while at the same time taking into account high enough pinch temperature differences.

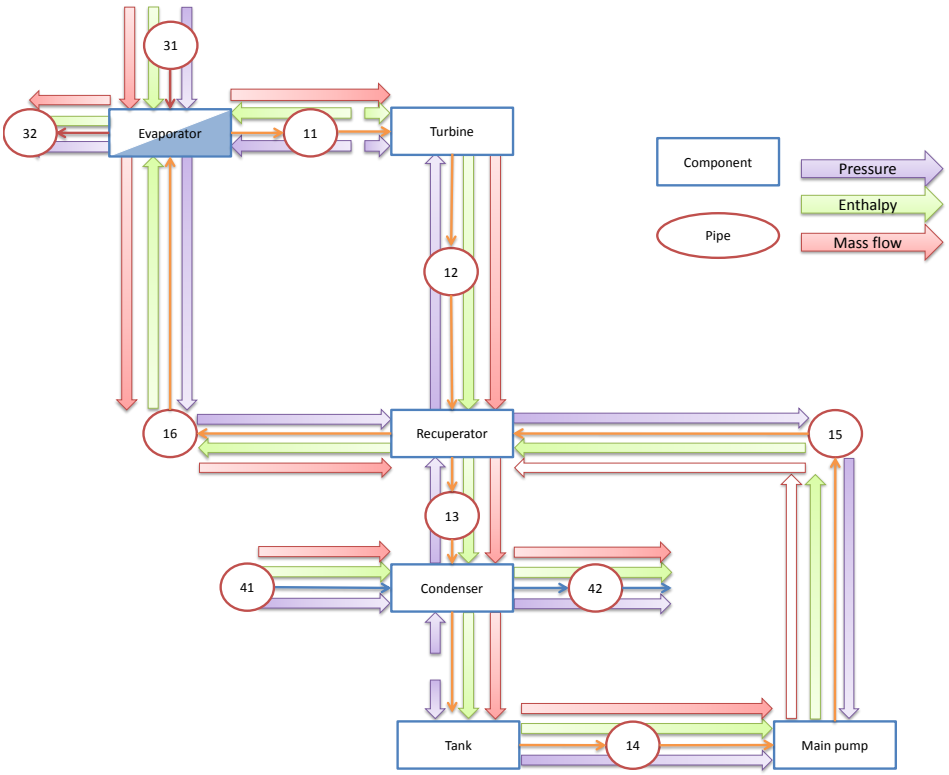

Figure 3.1: schematic overview of the model, in which the slim arrows indicate the flow direction, red = flue-gas, orange = working fluid, blue = cooling water. The thicker arrows indicate the information flows for communication between the components, purple = pressure, green = enthalpy, red = mass flow. Turbine inlet pressure and temperature are given in pipe 11, condensation pressure is given in pipe 14.

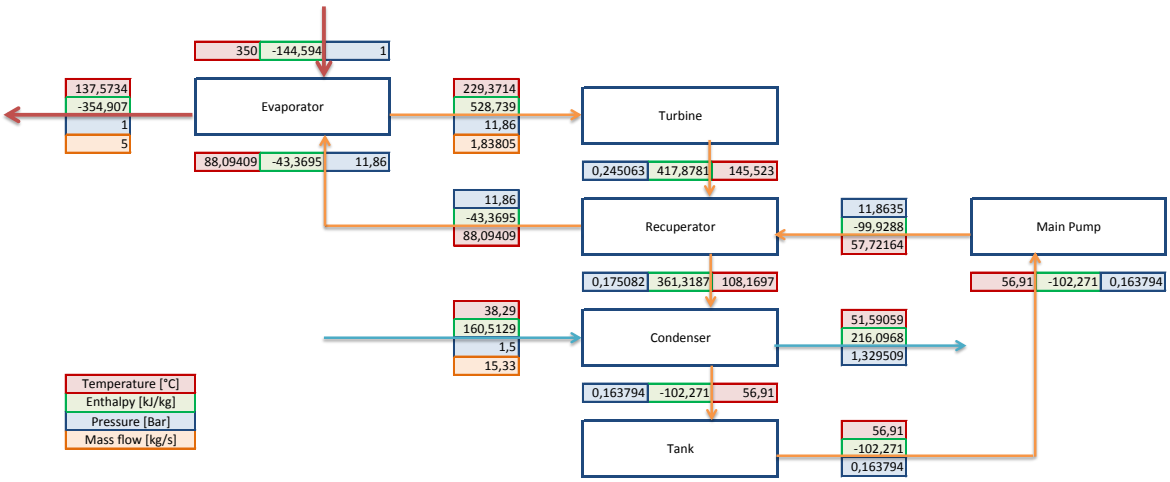

Figure 3.2: Implementation of the scheme in figure 3.1 in excel

3.3. RELATIONS, INPUTS AND OUTPUTS

The description of the relations implemented in the first model are given here. First there is the pump of which the performance is defined using the isentropic efficiency (equation 2.6).

Then there is the evaporator in which the mass flow of the working fluid is determined based on the pinch temperature difference, the flue-gas definition and the inflow, outflow and saturated conditions of the working fluid. The pinch can be situated either at the working fluid inflow or at

the saturated liquid point. In addition the pressure drop over the evaporator is modeled using a pressure drop at the inlet and outlet of the evaporator.

The turbine is again defined using an isentropic turbine efficiency (equation 2.8). The total turbine work is reduced by mechanical losses in the bearings and losses in the generator which are defined using the mechanical and generator efficiency. Also the saturation of the vapor leaving the turbine is checked in order to make sure there is no liquid in the vapor stream.

For the condenser a fixed condensing temperature of 55°C is assumed, also a small degree of sub-cooling of 0.1 K is used to ensure saturation at the outlet of the condenser. In addition a pressure drop is applied at the inlet of the condenser. The recuperator is described using an effectiveness, which is defined as a fraction of the total possible heat transfer when one of the flows would be heated, or cooled down to the inlet temperature of the other flow. In addition a pressure drop is applied at both the hot and cold side of the recuperator.

Table 3.1: Inputs for the model

Variable	**Unit**	**Value**
Working fluid	[-]	var
Turbine inlet pressure	[bar]	var
dT superheat	[K]	var
Condensation temperature	[°C]	55
dT subcool	[K]	0.1
Flue-gas	[-]	air
Flue-gas massflow	[kg/s]	5
Flue-gas temperature	[°C]	350
minimum outlet temperature	[°C]	120

Table 3.2: Definition of component parameters

Component	**parameter**	**Unit**	**Domain**	**Reference value**
Turbine	η_{is}	[-]	0.5 - 0.8	0.7
Shaft losses	η_{mech}	[-]	0.9 - 0.99	0.95
Generator	η_{gen}	[-]	0.9 - 0.99	0.94
Evaporator	$dp_{wf,in}$	[bar]	0 - 2	0
	$dp_{wf,out}$	[bar]	0 - 2	0
	dT_{pinch}	[K]	10 - 30	15
Recuperator	$dp_{wf,hot}$	[bar]	0 - 0.2	0
	$dp_{wf,cold}$	[bar]	0 - 1	0
	ϵ_{rec}	[-]	0.5 - 0.8	0.7
Condenser	$dp_{wf,in}$	[bar]	0 - 0.2	0
Pump	η_{is}	[-]	0.3 - 0.7	0.6

In tables 3.1 and 3.2 an overview is given of the model inputs and component parameters respectively.

3.4. OPTIMIZATION ALGORITHM

As described earlier the model is used to find some optimal combination of working fluid, cycle design and process parameters. For the first model the variable process parameters are only the evaporating pressure and the degree of superheat. Later extra variables will be added, in order to be able to vary the condensing temperature and the design of components. In some manner all these options will need to be simulated and for each working fluid one or more optima need to be found.

Instead of simulating all possible configurations, which would take too much computational time, an optimization algorithm will be used. In this chapter it is explained why a genetic algorithm is used, and how the algorithm works.

3.4.1. ALGORITHMS IN ORC LITERATURE

Optimization problems in Organic Rankine Cycle design, are often multivariable and sometimes multi-objective optimizations. In addition there is the possible presence of local optima. This yields the need for a rather ingenious optimization algorithm. Different algorithms are used in literature, most used for multivariable optimizations is the genetic algorithm. Xu et al. [9] use genetic algorithm to perform multivariable optimization for different ORC schemes and six variables and multiple single objective functions. Also Dai et al. [30] use a genetic algorithm for the optimization of an ORC for multiple variables and working fluids. Xi et al. [4] used a multi-objective genetic algorithm based on Pareto optimal solutions as optimizer. Instead of one optimal solution, the genetic algorithm here gives a sequence of optimal solutions in the cost-efficiency domain for each fluid, which they call the Pareto front.

3.4.2. GENETIC ALGORITHM THEORY

The Genetic Algorithm is especially suitable for multivariable problems with possible local optima, because it starts with an initial generation of points instead of optimizing from one point. The method is based on Darwin's theory of survival of the fittest. From each generation the individuals with the best genes (variables) leading to the best results, are most likely to produce offspring. In this work a genetic algorithm script written by Gustavo J. Otero for the purpose of turbine optimization is slightly adjusted and used for cycle optimization. The script produces an initial generation of solutions, which all lead to a positive work output by the cycle. After the successful formation of an individual, its variables are converted to binary numbers with a fixed length and these binary numbers are joined to form one binary code which defines the individual (the DNA). Then a number of steps is taken for the production of offspring.

1. Selection of individuals: Using multiple tournaments a number of parents is selected. All individuals from the last generation are distributed over the tournaments randomly. Of each tournament the best individual is selected. Pairs are formed from the best individuals which will be the parents for the next generation.

2. Crossover: Two random blocks of identical length and place in the genetic material are exchanged between the binary codes of the parents in order to create two new individuals (figure 3.3).

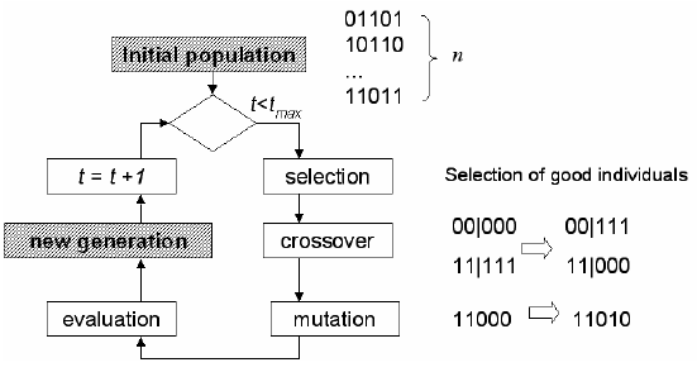

Figure 3.3: block scheme of the genetic algorithm

3. Mutation: After crossover there is a possibility of mutation of the binary code of each offspring, the probability of mutation is normally small and can be defined by the user. When there is a mutation, a random digit in the binary code is selected and changed

4. After this process the new individuals' binary codes are converted back to variable values, of which it is evaluated whether they are within the defined range, also it is evaluated whether this combination of variables leads to a sufficient result. If the variables are out of range or if the result is insufficient a new random individual is created.

5. The new generation is complemented with random new solution to reach the required population size.

Table 3.3 shows the genetic algorithm input parameters.

Table 3.3: Input parameters for adjustment of the genetic algorithm

Genetic algorithm	**input**
Number of generations	ca. 5-10
Generation size	ca. 10-50
Number of tournaments	ca. 4-24
Mutation probability	ca. 0.1

3.5. SENSITIVITY ANALYSIS

In this section the influence of the main components on the model accuracy is analyzed. This is done by examining the sensitivity of the total power output for varying parameter values, while all other parameter values remain constant, the reference values and the range in which they are varied are listed in table 3.2. This is done, in order to determine the necessary level of detail for the component models, also the total accuracy of the model can be estimated. Sensitivity for the predicted heat transfer coefficient is not taken into account here, as it only has an indirect influence on the power output as well as on the necessary heat transfer surface. In the next section the cost composition of the Triogen ORC is analyzed to estimate the influence of component geometry on the total cost of the cycle. As cost per kilowatt is the main criteria for the model, these two analyses have an important influence on the further development of the model.

Although it is preferred to give an accurate estimate of the total accuracy of the model, this is probably not possible. Most important reason for this is the accuracy of the component models which is uncertain, and the fact that although a model might be accurate, there might always be variation in the performance of a component because of small differences in the production or environment. Another problem is that the influence of inaccuracies on the total performance is often non linear and that it is influenced by other components as well. Last, the sensitivity of the power output for varying parameter values differs highly per fluid.

3.5.1. TURBINE

Most obvious might be the influence of turbine efficiency as well as mechanical and generator efficiency on the accuracy of the model. These efficiciencies influence the total power output almost one on one. Generator and mechanical losses are mostly dependent on the turbine frequency and are expected to vary within a rather small range, as for this application and for all fluids the turbines will be small and will rotate at high frequencies. The turbine efficiency is expected to show larger variations with changing fluid and process parameters, the accuracy of the efficiency prediction will therefore probably be a determining factor in the total accuracy of the model.

3.5.2. EVAPORATOR

From figure 3.4 it appears the influence of the pressure drop at the working fluid side of the evaporator on power output is negligible. Only for the high critical temperature fluids, which evaporate at relatively low pressures (around 10 bar), there is an effect due to the increased saturation temperature and increased pitch. The effect of increased pump power consumption is for all fluids very small, around 0.5 kW for a pressure drop of 2 bar. The pressure drop on the flue-gas side though is limited by the maximum back-pressure of the engines, that the ORC is applied with, which is a few kPa. From this it may be concluded that working fluid pressure drop may be neglected in the model. Also it can be concluded that the evaporator can be designed such that the heat transfer coefficient on the working fluid side is much higher than the heat transfer coefficient on the flue-gas side, as pressure drop closely relates to the heat transfer coefficient. And therefore the flue-gas heat transfer coefficient will be most determining for the total heat transfer coefficient and is desired to be predicted accurately, while working fluid heat transfer coefficient will have minor influence.

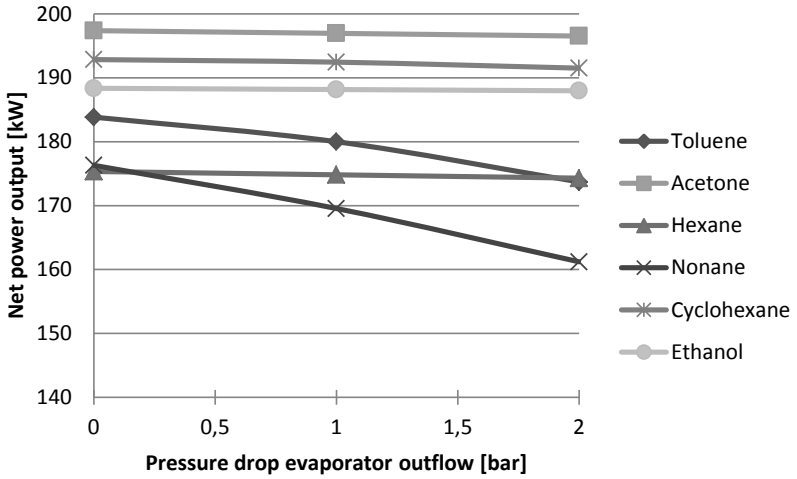

Figure 3.4: Influence of pressure drop in the evaporator on power output

3.5.3. CONDENSER AND RECUPERATOR

As already concluded in the last subsection, pressure drop at the high pressure liquid side has only negligible influence on the total performance of the cycle. The influence of pressure drop on the low pressure vapor side of the condenser and recuperator is shown in figure 3.5, this figure shows the influence of pressure drop at the inlet of the condenser, pressure drop on the vapor side of the recuperator shows same results. A deviation is shown in the effect of this pressure drop on the different working fluids, for heavier molecules with lower condensation pressures (Nonane, 0.03 bar) a higher impact is shown while light molecules (Hexane, 0.64 bar) are impacted only slightly. Therefore lower pressure drops and larger heat exchanger sizes are expected for the heavier molecules, while smaller heat exchangers with larger pressure drops may be used for the lighter molecules. In the development of recuperator and condenser models the heat transfer on the vapor side will probably be limiting, therefore both heat transfer and pressure drop on the vapor side must be predicted with high accuracy while less attention is needed on the liquid side.

The effectiveness of the recuperator was also varied, the results only show that some fluids, having an almost isentropic saturated vapor curve profit less from an effective recuperator compared to fluids with a negative saturated vapor curve.

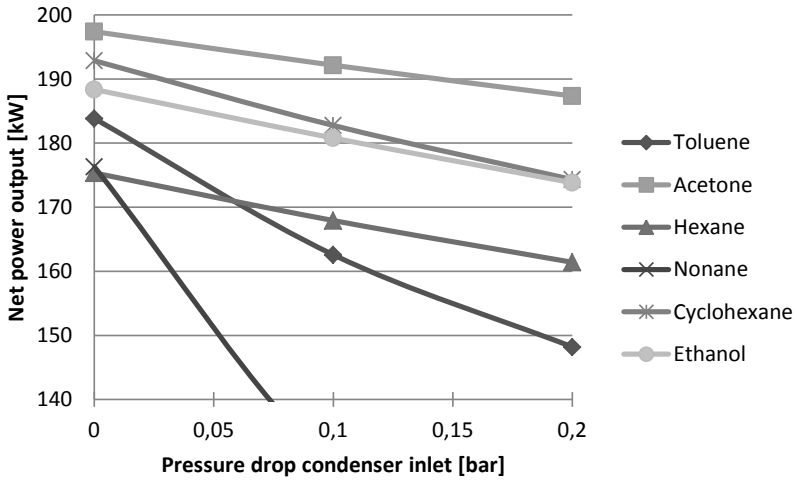

Figure 3.5: Influence of pressure drop in the condenser on power output

3.5.4. PUMP

Figure 3.6 shows the influence of pump efficiency on the total power output of the cycle. The figure shows that the fluids having higher evaporating or even supercritical pressures (Hexane, 40 bar) are influenced more by the pressure difference compared to the fluids having lower evaporating pressures (Nonane, 9 bar). The efficiency of the pump depends mainly on the type of pump used and how it is implemented in the cycle, while the process parameters will have minor influence on the achievable efficiencies. Therefore the pump efficiency is, although some variation is shown here, assumed constant in this work.

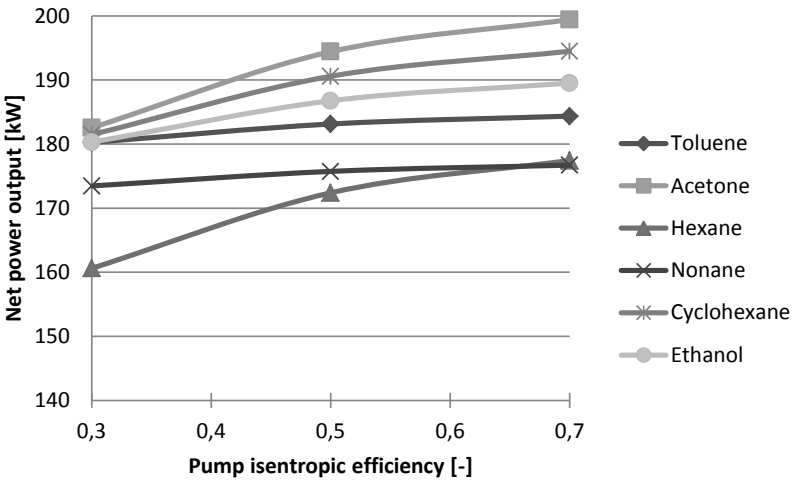

Figure 3.6: Influence of isentropic pump efficiency on power output

3.6. COST ANALYSIS

Although the focus in this research is on the condenser and recuperator, the cost of the whole ORC needs to be taken into account in order to calculate the total cost per kilowatt. In this section the cost composition of the current Triogen ORC is evaluated, and the significant costs which can be related to the design of the cycle are highlighted. The cost composition is not presented in full detail, as the composition of the fixed costs is not relevant for this work. The cost composition presented here is

based on the actual Triogen ORC cost composition.

Figure 3.7 shows the composition of the production cost for one ORC. The fixed costs cover the largest part of the total cost, these fixed cost include turbine, generator, pumps, piping, valves, control hardware, vacuum system, heat supply, auxiliary components, assembly, installation and testing.

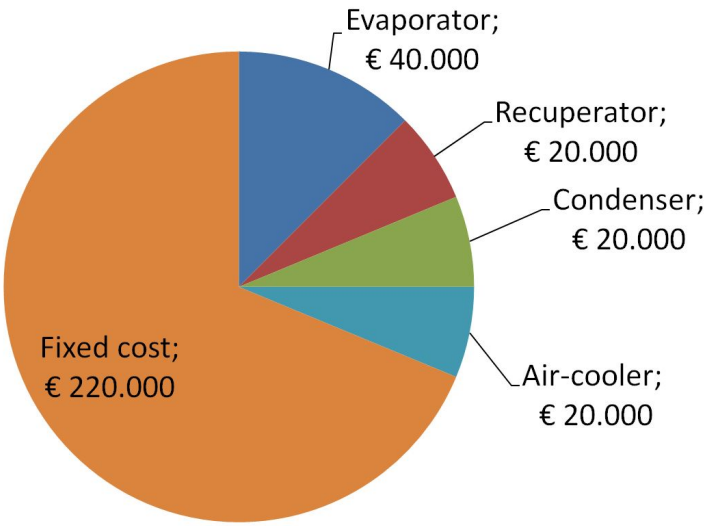

Figure 3.7: General cost composition of Triogen ORC system

4

COMPONENTS

In this chapter all main components are described. Per component first some attention will be given to the alternatives for the component design, then the alternative methods for the modeling of this component are described, and last the implementation in the model is described in more detail. Based on the sensitivity analysis in the former chapter an overview is made of the significance of the influence of component performance parameters in table 4.1. The parameters marked as not significant can be modeled roughly, more attention is needed for the parameters marked as significant and high accuracy is preferred for the parameters marked as critical. In addition to the component parameters assessed in the sensitivity analysis also the influence of parameters related to the cooling, water cycle and flue-gas are estimated in this table.

Table 4.1: significance of influence of component parameters on system performance

Component	**Parameter**	**Not significant**	**Significant**	**Critical**
Pump	$\eta_{is,pump}$		x	
Evaporator	ΔT_{pinch}			x
	Δp_{wf}	x		
	Δp_{fg}			x
Turbine	$\eta_{is,turbine}$			x
Recuperator	ϵ_{rec}			x
	Δp_{hot}			x
	Δp_{cold}	x		
Condenser	Δp_{wf}			x
	Δp_{aq}		x	
Air-cooler	$\Delta p_{aq,air-cooler}$		x	
	W_{fan}		x	
Water pump	w_{pump}	x	x	

In figure 4.1 an overview is given of the system design as modeled in this work. The recuperator is connected directly to the turbine and the condenser is connected directly to the recuperator to prevent pressure drop in the piping. In case there is no recuperator the condenser is connected directly to the turbine. The pressure drop in all other piping is neglected as it was found the influence of pressure drop in the high pressure section of the cycle is negligible. The influence of the storage vessel is not taken into account because pressure drop is expected to be low at this point. Although in practice a prefeed pump will be required, no prefeed pump is included in this work and the work of the prefeed pump is included in the main pump.

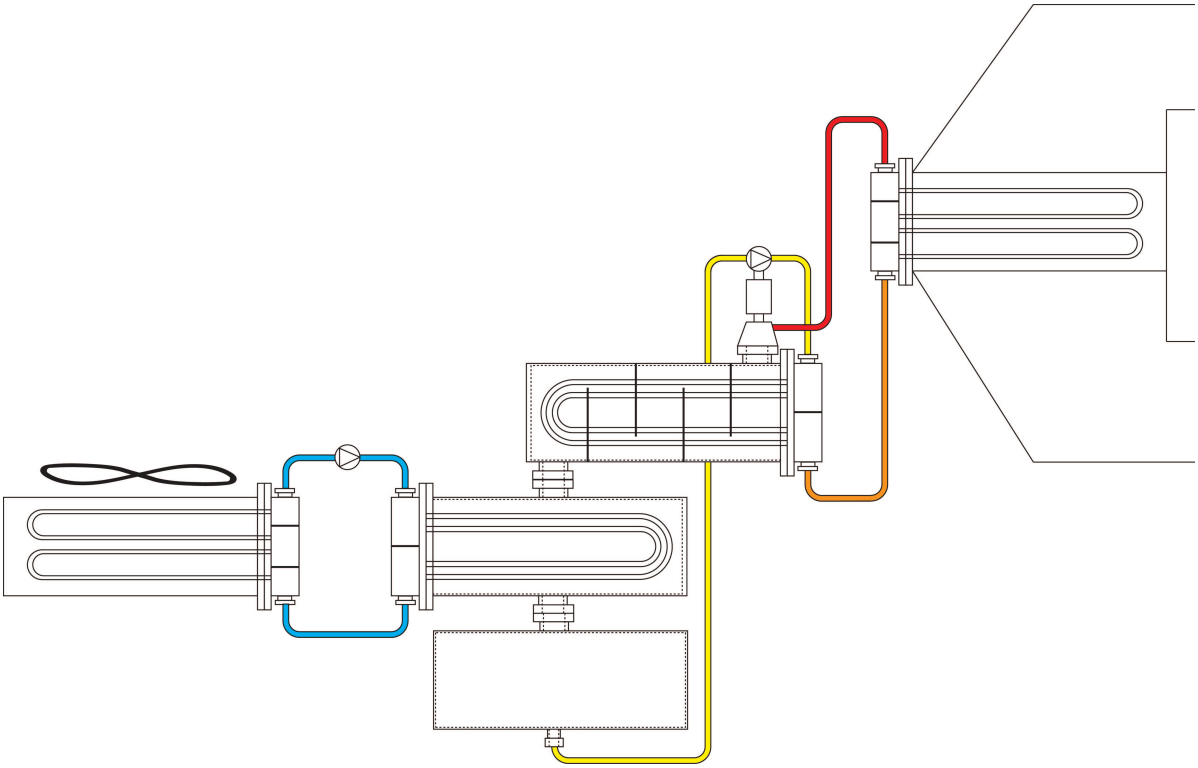

Figure 4.1: Graphical overview of cycle and component design

The components that are worked out in more detail, and which are therefore described in this chapter are the turbine, recuperator, condenser, air-cooler and evaporator. To conclude the cost calculation method is described in the last section.

4.1. CONDENSER AND RECUPERATOR

Recuperator and condenser are presented in one section because these two components have similar designs in the model. As these components are directly coupled on the vapor side, it is for reasons of supply and assembly decided to have equal types. Currently Triogen uses plate and shell heat exchangers, the recuperator is mounted on top of the condenser and a wide nozzle connects the two. For this new ORC Triogen is looking for a highly standardized low tech solution for these two components, of which the design is preferably Triogen property. Their preference is going to shell and tube heat exchangers though they are open for other solutions. It is briefly explained in this section why shell and tube heat exchangers are used, also the means of modeling these components and their place in the model framework are described.

4.1.1. TYPES OF HEAT EXCHANGERS

As already introduced Triogen is looking for highly standardized, low tech heat exchangers. It is preferred that multiple heat exchanger providers will be able to produce the standardized design. In addition for the sake of modeling it is preferred to use heat exchangers for which good heat transfer and pressure drop correlations are available in literature. Based on the results presented in section 3.5 it can also be said that pressure drop on the vapor side must be limited, while pressure drop on the liquid side may be relatively high. This, in combination with the fact that vapor has an orders of magnitude lower density compared to liquids, and mass-flows will have the same order of magnitude, it is probably best to have smaller flow areas for the liquid compared to the vapor flow areas. Last there is the desire to fit the ORC (apart from the air cooler and evaporator) in a standard 20 ft

container, this mainly limits the size of these two heat exchangers as they, together with the tank are the most voluminous components.

In this research shell and tube heat exchangers as well as plate heat exchangers have been studied. Good methods are available for calculating heat transfer and pressure drop in shell and tube heat exchangers, and many manufacturers are able to produce a tailor made design. Size is the main drawback of this design. The plate heat exchanger is the other alternative considered in this work, it is much more compact and offers the possibility to have pure counter flow, though does not give the freedom of design as prices rise to enormous heights when tailored plates need to be made. Also heat transfer and pressure drop correlations describe reality with less accuracy as each manufacturer uses its own plate designs. When using plate heat exchangers also some attention must be given to the applicability at high pressures and temperatures. After some considerations on the significance of the influence of alternative designs on total system performance, it is decided to only present the model and results for shell and tube heat exchangers. Reason for this is the inaccuracy of heat transfer, pressure drop and cost correlations, the relative errors in the estimation are expected to be in the same order of magnitude as the differences in cost and performance, and it will therefore be impossible to draw good conclusions on the design of the heat exchangers. And the heat exchanger model is used mainly to balance performance, pressure drop and cost.

4.1.2. APPLICATION AND BOUNDARIES

The practical design, the design decisions made, and the implications for the model are discussed in this subsection. Figure 4.2 gives an overview of the main parts and sections of the heat exchanger.

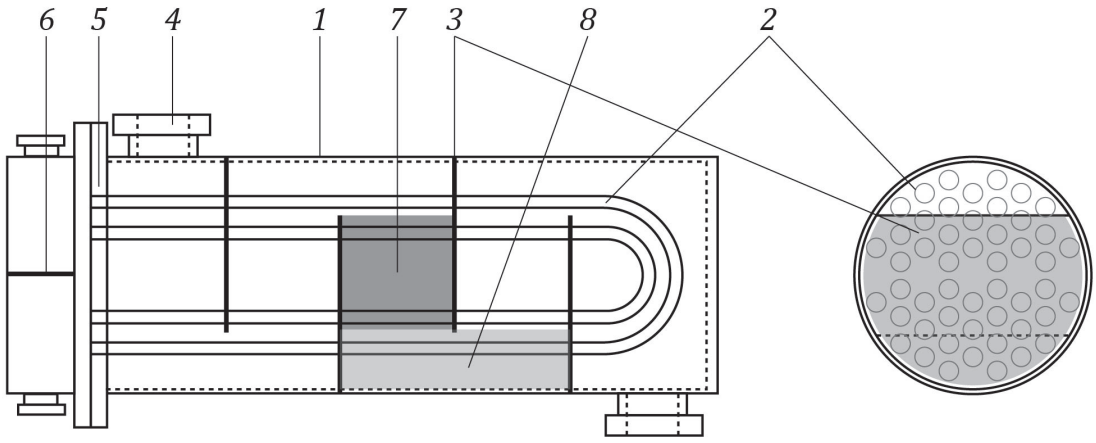

Figure 4.2: Nomenclature for shell and tube heat exchanger parts and sections. 1) shell, 2) tubes, 3) segmental baffle, 4) shell nozzle, 5) tube sheet, 6) pass partition plate, 7) cross flow section, 8) window section

The tubes are connected to the shell using tube sheets, which are the endplates of the shell, the most simple design is a fixed tube sheet on both ends of the shell. This may result in large thermal stresses, as there are temperature differences between the tube wall and the shell. Using a floating head or an expansion joint in the shell, thermal stresses can be reduced. Another option is the application of u-tubes, in this design only one tube sheet is used. This design can only be applied with an even number of tube passes. Having multiple tube passes has some effects on the design of a heat exchanger. First there is the thermal effect, with one tube pass and pure crossflow high effectivities and highest mean temperature difference is reached, having multiple tube passes reduces the thermal efficiency as is shown in figures 4.3 and 4.4 for 2 and 4 tube passes respectively. In this graphs the correction factor can be found for the log mean temperature difference over the full heat exchanger, using the relative temperature rise and drop of the hot and cold flow. The corrected temperature difference over the heat exchanger is given in equation 4.1 this equation is not used in the

model as the model calculates the local heat transfer and preasure drop instead of the global.

$$LMTD_{corrected} = F * LMTD \tag{4.1}$$

In the figures though, it is also seen that up to a correction factor for the log mean temperature difference of F=0.7 there is no significant difference between the two graphs, and it can therefore be concluded that for recuperators with a typical temperature difference, there is no difference in log mean temperature difference over the recuperator and a 4 pass heat exchanger could therefore be modeled as if it has only 2 passes. Secondly there is the effect of in tube velocity, a velocity in the range 1 to 2.5 m/s is preferred to prevent fouling and erosion. Also tube velocity enhances the heat transfer, and pressure drop, as tube side volume flows are expected to be small compared to the shell side volumetric flowrate, and that the influence of tubeside pressure drop on the cycle performance is small, it is assumed that multiple passes will yield to a better system design. The application of multiple tube passes also has a geometric effect, as pass partitions or tube bends cause some extra spacing between the tubes. This effect is dealt with in appendix A. In this work it is chosen to use two or four pass u-tubes.

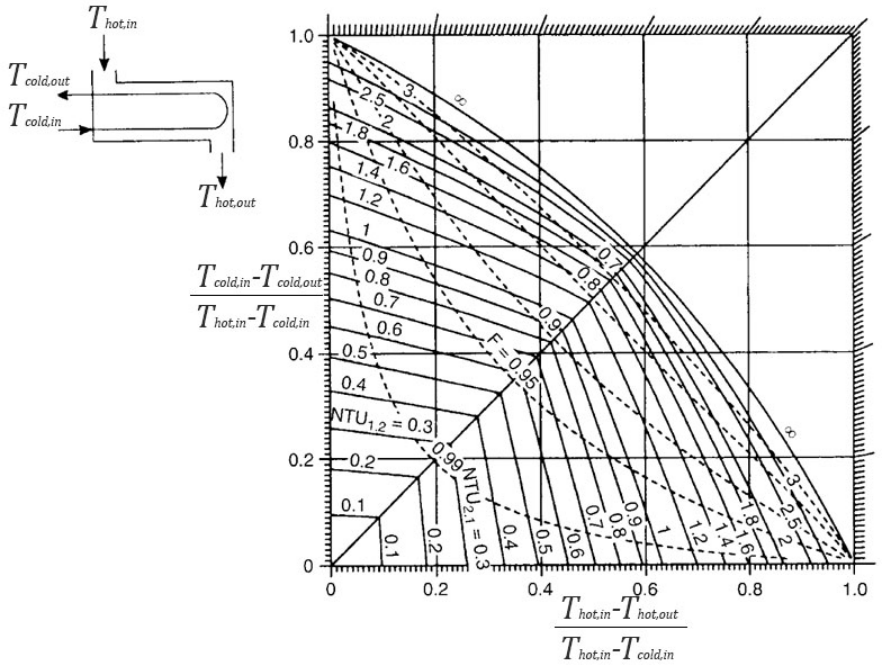

Figure 4.3: graphical representation of LMTD correction factor for 2 pass shell and tube heat exchangers[31]

The vapor velocity on the shell side is also limited to prevent vibration and erosion of the tubes. At atmospheric pressure this maximum velocity is around 20 m/s, at lower pressures velocities up to 70 m/s are allowed. It is assumed these velocities will be limited enough by the model, because of the limitation of the pressure drop, to prevent them from being too high. If entrance velocity is too high impingement plates may be applied, which leads to a higher pressure drop. The pressure drop caused by the impingement plates is not accounted for in the model. The tubes may have diameters according to the EN 10220 standard, having outer diameters of 16.0, 17.2, 18.0, 19.0 and 20.0 mm. In the model the diameter is therefore varied between 16.0 mm and 20.0 mm. For the calculation all tubes are assumed to have a wall thickness of 1 mm, in practice this wall thickness will depend on design pressure and temperature, and the diameter of the tube. Also the velocity and heat transfer coefficient on the tube side can be enhanced by the wall thickness. The tubes can be connected to

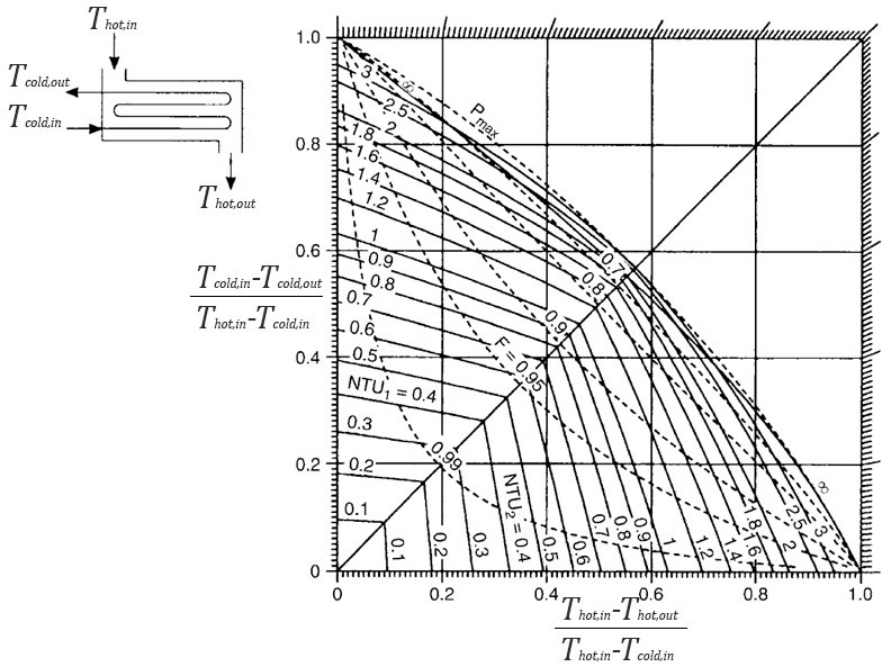

Figure 4.4: graphical representation of LMTD correction factor for and 4 pass shell and tube heat exchangers[31]

the tube sheet by rolling, which means the tube is expanded to fix it in the tube sheet, in some cases the connection is sealed with a small weld. Alternatively the tube can be connected to the tube sheet with a full strength weld, which is preferred for higher temperatures and pressures. The tube Pitch depends on the outer diameter, the tube material and the method of connection. Here a minimum tube pitch ratio of 1.25 and a minimum tube spacing of 5 mm are assumed.

4.1.3. ASSUMPTIONS

In this model the correlations presented in the VDI heat atlas[31] are used to predict the heat transfer coefficient and pressure drop. These correlations are based on cross-flow over a bundle of pipes. Using correction factors for leakages and uneven baffle spacings the local heat transfer coefficients can be calculated for each section. The pressure drop is calculated over these crossflow sections as well as over the in and outlet nozzles and the window sections. Allthough the window and crossflow pressure drops are more or less local. In this model these pressure drops are averaged over the length of one section as well as the temperature which is modeled as a function of the longtitudinal coordinate only.

In line with this assumption the baffle spacing which in actual heat exchangers is mostly a bit larger for the outer sections, is here assumed equal for all baffle spacings. The length of the heat exchanger though is not necessarily a multitude of the baffle spacing. Also the thickness of the baffles is neglected.

The only correction factors taken into account are the corrections for secondary flows associated with the spacing between baffle holes and tubes, between the baffle and the shell and the tubes in the window section. Other correction factors which are not taken into account are the correction for different fluid properties at the tube wall, which is defined in equation 4.2 in which the exponent n_p depends on the type of gas used and has a value of around 0 for cooling of air and around 0.12 for cooling of nitrogen. The influence is thus uncertain and negligibly small. The bypass correction is neglected as well under the assumption that enough sealing strips are applied to prevent the fluid from bypassing the tubes.

Last it is assumed that the pressure drop on the liquid side has negligible influence on the fluid properties and can therefore be subtracted from the pressure after calculating the heat transfer.

This set of assumptions makes it possible to calculate the surface, duty and pressure drop of the heat exchanger using just one iterative loop as is explained in the next section.

$$f_p = (\frac{T_b}{T_w})^{n_p} \tag{4.2}$$

4.1.4. MODEL LOGIC

The model for the shell and tube recuperator and condenser both start with calculating the duty over the whole heat exchanger. In both the vapor inlet enthalpy is known as well as the outlet pressure, on the cold side also the inlet enthalpy is known, and the pressure is assumed constant. For the recuperator the effectiveness is an optimization variable given by the model, with which the outlet enthalpy is calculated by equation 4.3. It is assumed for the use of this equation, that the heat capacity of the cold fluid is larger then the heat capacity of the hot fluid. This can have an effect on the reported value of the recuperator effectiveness, but does not have an effect on total system performance. For the condenser the degree of sub-cooling is assumed to be zero, and the outlet enthalpy is the enthalpy of saturated liquid at the outlet pressure. now duty and all in- and outflow enthalpies are known as given in equation 4.4

$$h_{hot,out} = h_{hot,in} - \epsilon_{rec} * (h_{hot,in} - h(p = p_{hot,out}, T = T_{cold,in})) \tag{4.3}$$

$$Q = \dot{m}_{hot} * (h_{hot,in} - h_{hot,out}) = -\dot{m}_{cold} * (h_{cold,in} - h_{cold,out}) \tag{4.4}$$

Now, using the assumption that pressure changes on the cold side have negligible influence on fluid parameters, all conditions are known at both the inlet and outlet of the U tube. For the recuperator, now a pressure drop is assumed to estimate the inlet pressure, the heat exchanger is split in sections of equal duty and the length of the heat exchanger and the pressure drop are calculated from the inlet to the outlet as shown in figure 4.5. The process of estimating the inlet pressure and calculating length and pressure drop is iterated until desired outlet pressure is reached, as is shown in figure 4.6. As will be explained in one of the next sections, in the condenser the conditions on the shell side are assumed constant, as free convection condensation drives the heat transfer and effects of desuperheating are neglected. The total surface and pressure drop on the cold side is calculated using the log mean temperature difference over the whole condenser as defined in equation 4.5.

$$LMTD_{cond} = \frac{\Delta T_{in} - \Delta T_{out}}{Ln(\frac{\Delta T_{in}}{\Delta T_{out}})},\ \Delta T_{in} = T_{hot,sat} - T_{cold,in},\ \Delta T_{out} = T_{hot,sat} - T_{cold,out} \tag{4.5}$$

4.1.5. SINGLE PHASE SHELL SIDE

The shell side heat transfer coefficients and pressure drop are calculated using the method given in the VDI heat atlas[31]. In this method the calculation of the heat transfer coefficient is based on heat transfer by flow across an ideal tube bundle. A correction is applied for the geometry, for the leakage through the holes in the baffles and for the arrangement of the pipes, using the Bell-Delaware method. This method is thought to be valid for Reynolds numbers: $10 < Re < 10^5$ and Prandtl numbers $0.6 < Pr < 10^3$.

The reynolds number for flow through an ideal tube bundle is given by equation 4.6 in which w is the velocity given by equation 4.8

$$Re = \frac{w d_o \pi / 2 \rho}{\mu \psi} \tag{4.6}$$

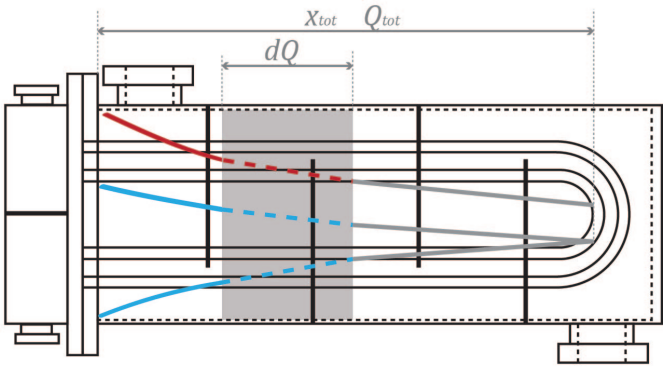

Figure 4.5: sections of equal duty (dQ) in the shell and tube heat exchanger, in which the blue and red lines indicate the temperature of the cold and hot flow respectively (solid = temperatures already calculated, striped = temperatures are being calculated, grey = temperatures not calculated yet).

$$Pr = \frac{\mu c_p}{\lambda} \tag{4.7}$$

$$w = \dot{V} / A_f \tag{4.8}$$

with

$$\psi = 1 - \frac{\pi}{4a} \; for \; b \geq 1 \tag{4.9}$$

$$\psi = 1 - \frac{\pi}{4ab} \; for \; b < 1 \tag{4.10}$$

The pitch ratio's a and b are defined as $a = X_t / d_o$ and $b = X_l / d_o$.

and the cross sectional area is calculated as

$$A_f = L_{b,c} * D_s \tag{4.11}$$

The Nusselt number is defined as

$$Nu_s = \frac{\alpha_S * d_o \pi / 2}{\lambda} \tag{4.12}$$

The shell side Nusselt number is calculated using equation 4.13, in which the Nusselt number for crossflow over an ideal tube bundle is calculated using equations 4.14, 4.15 and 4.16. The calculation of the correction factors is given in appendix B. f_A is a correction factor for the staggered tube arrangement, f_G is a correction factor for the geometry, accounting for the fact that there is a combination of cross-flow and co-flow due to the baffles and f_L is a factor correcting for the leakage through and past the baffles. Additional correction factors which are neglected here are f_P which corrects for the change of properties in the vicinity of the wall, the bypass correction factor f_B which is assumed to be one due to the application of sealing strips.

$$Nu_s = Nu_{s,av} f_G f_A f_L \tag{4.13}$$

The average Nusselt number for ideal crossflow is calculated using equation 4.14

$$Nu_{s,av} = 0.3 + (Nu^2_{s,lam} + Nu^2_{s,turb})^{1/2} \tag{4.14}$$

In which the laminar and turbulent Nusselt number are defined in equation 4.15 and 4.16 respectively.

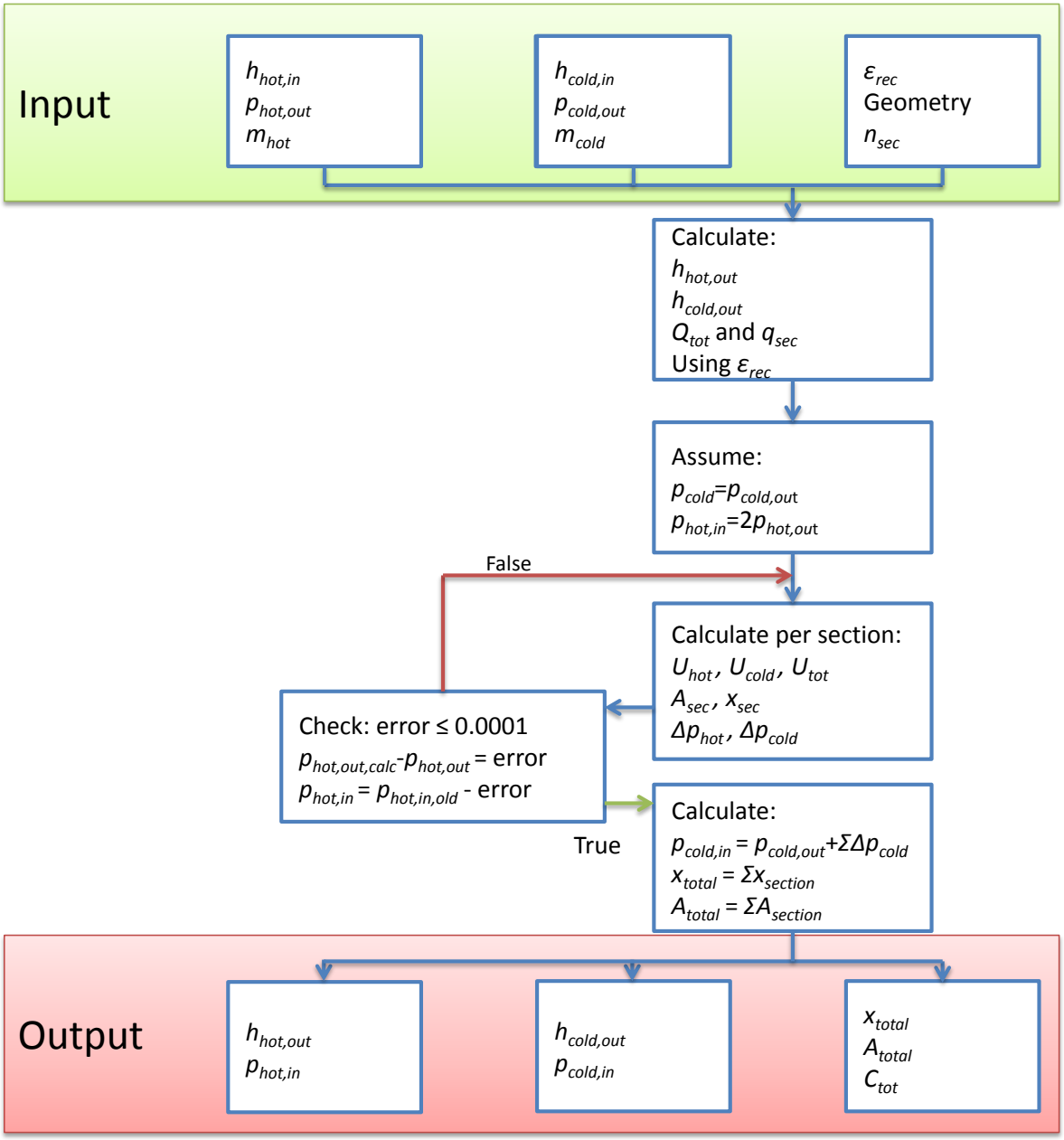

Figure 4.6: Block diagram of recuperator model, in which the blocks in the in and output blocks represent from left to right the hot flow parameters, cold flow parameters and additional/geometrical parameters.

$$Nu_{s,lam} = 0.644 * Re_s^{1/2} Pr^{1/3} \tag{4.15}$$

$$Nu_{s,turb} = \frac{0.037 * Re_s^{0.8} Pr}{1 + 2.443 Re_s^{-0.1} (Pr^{2/3} - 1)} \tag{4.16}$$

The shell side pressure drop consists of in- and outflow pressure drops and pressure drops due to the crossflow over the tube bundle corrected for leakage and geometry as well as a contribution from the window section. The pressure drop contributions of the crossflow and the window section are averaged over the length of each section using equation 4.17.

$$\frac{\delta p}{\delta L} = (\Delta p_c + \Delta p_w) J_L / L_{b,c} \tag{4.17}$$

In this equation Δp_c and Δp_w represent the pressure drop over one cross flow section and one window section respectively. The cross flow pressure drop is calculated using equation 4.18, in which ξ is a friction factor for one tube row multiplied by the number of main resistances n_{MR}, which is defined as the number of tube rows crossed in the cross flow section. Equation 4.19 gives the calculation of the window section pressure drop as a function of the laminar pressure drop and the turbulent pressure drop. The complete calculation of the pressure drops is given in appendix B.

$$\Delta p_c = \xi n_{MR} \frac{\rho w^2}{2} \tag{4.18}$$

$$\Delta p_w = \sqrt{\Delta p_{w,lam}^2 + \Delta p_{w,turb}^2} \tag{4.19}$$

In equation 4.17 J_L is the correction factor for the leakage flows:

$$J_L = exp(-1.33(1 + \frac{A_{o,sb}}{A_{o,tb} + A_{o,sb}})(\frac{A_{o,tb} + A_{o,sb}}{A_{o,cr}})^{-0.15(1+\frac{A_{o,sb}}{A_{o,tb}+A_{o,sb}})+0.8}) \tag{4.20}$$

4.1.6. SINGLE PHASE TUBE SIDE

The tube side heat transfer coefficient and pressure drop is calculated with the method explained in the VDI heat atlas [31] as well. Although the effects of thermal and hydrodynamic development of flow in pipes could be taken into account, these effects can be neglected here, as the pipe diameter is very small compared to the pipe length. These correlations are valid for Reynolds numbers: $Re < 10^6$ and Prandtl numbers $0.1 < Pr < 1000$. The used correlations are listed in appendix B.

4.1.7. CONDENSATION SHELL SIDE

In case of condensation on the shell side, a different geometry and different correlations are used. As already introduced, in this case a TEMA X shell is used, in this shell design in and outflow are in the center of the shell and the velocity through the pipes is negligible. Therefore pressure drop is only calculated at the inlet nozzle. The heat transfer is calculated as free convection condensation. free condensation on a single horizontal tube is described by the Nusselt condensation equation (equation 4.21) which is related to the heat transfer coefficient by equation 4.22.

$$\alpha_{Nu} = 0.728(\frac{\lambda_l^3 \rho_l^2 g h_{fg}}{\mu_l d_o \Delta T_{wo}})^{0.25} \tag{4.21}$$

$$\dot{q} = \alpha_{Nu} \Delta T_{wo} \tag{4.22}$$

In this equation, which is valid for low Reynolds numbers, it is shown that velocity does not influence the heat transfer coefficient. Also it can be noted that a smaller diameter leads to higher heat transfer coefficients. Higher ΔT_{wo} (which is the temperature difference between saturation and wall temperature) reduces the heat transfer coefficient, as a result of increasing boundary layer thickness, therefore the heat flux does not increase linearly with increasing temperature difference.

In addition to Nusselt's equation, there are two important phenomena which need attention here. First there is the desuperheating of the vapor, which is described elaborately in literature. As long as the pipe surface is below the saturation temperature of the vapor, condensation will occur, and heat transfer is therefore best described using correlations for condensation. Zhao et al. [32] use a correction factor with Nusselt's equation based on experiments with R134a. They relate the increase in heat transfer coefficient to the increase of dimensionless superheat ($\Delta T_{sup}/T_{sat}$). Another

method for accounting for the desuperheating is including the sensible heat of the superheated vapor in the latent heat term of Nusselt's equation. Both methods do not describe the process really accurately, the alternative though is describing the heat transfer using analytical methods, in which per pipe the two phase boundary layer is solved, which has a much too high level of detail. In this work, the degree of superheat is taken into account by including the sensible heat in the latent heat term of Nusselt's equation, this will result in a small increase of cost for the condensers with a large degree of superheat. Secondly there is the row effect, due to the condensate inundation by tubes situated above the lower tube rows, a larger condensate film forms at these lower tubes. This reduces the heat transfer according to equation 4.23, in which the m factor has a value of 1/4 to 1/6 [33]. Browne et al. also show the influence of the row effect has much less or even negligible effect on enhanced tube surfaces.

$$\frac{\alpha_{Nu,n}}{\alpha_{Nu}} = n^{-m} \tag{4.23}$$

The effect of inundation is accounted for by calculating an average row number correction factor:

$$f_{Nr} = \frac{N_{r,eff}^{-m} - m/N_{r,eff}}{1-m} \tag{4.24}$$

In which $N_{r,eff}$ is the effective number of rows estimated as

$$N_{r,eff} = \frac{D_{otl} * 0.9}{2X_l} \tag{4.25}$$

The average heat transfer coefficient is calculated using

$$\alpha_{Nu,av} = \alpha_{Nu} * f_{Nr} \tag{4.26}$$

4.1.8. VALIDATION

No real validation of the shell and tube heat exchanger model is possible, as there is no data available to validate the model with. Here Aspen is used to verify the order of magnitude of the parameters calculated by the heat exchanger model. First the results of Aspen and the model for two recuperator cases with toluene and two cases with pentane are compared, then the results for a condenser for toluene and a condenser for pentane are compared.

Table 4.2 shows the simulation results for the recuperator with toluene as working fluid. the geometry is kept constant in this simulation apart from the number of tube passes. The table shows that the number of tubes is predicted with only 1% difference between Aspen and the model, for four tube passes the model predicts somewhat less tubes then Aspen. Also for the shell side heat transfer coefficient in both cases there is only a small difference between the two predictions. Larger deviations are found on the tube side, for which a lower heat transfer coefficient is predicted for two passes, and a larger coefficient is predicted for four passes. It is found that for laminar flow the model predicts a bit lower compared to Aspen, and for more turbulent flows the model predicts slightly higher compared to Aspen. Most worrying are the differences in pressure drop predictions, although the overall pressure drop predictions differ only slightly, the pressure drop over the window sections is predicted around 1.5 times higher by the model, while the pressure drop over the cross flow sections is predicted to be around two times lower then the pressure drop predicted by Aspen.

For the recuperator with pentane as working fluid the baffle cut is varied while the number of tube passes is kept constant (table 4.3). Here again the number of tubes is predicted accurately and the tube side heat transfer coefficient is predicted a bit a higher by the model, as expected. The predictions for the shell side heat transfer coefficient are almost equal for a relative baffle cut of 0.3 while for a relative baffle cut of 0.2 the heat transfer coefficient as predicted by the model rises with

30% while the heat transfer coefficient as predicted by Aspen only rises a few percents. The pressure drop deviates more for pentane then it does for toluene.

Table 4.2: Comparison of the recuperator model with an Aspen model, for 2 and 4 tube pass heat exchangers and toluene as working fluid, $D_s = 0.55m$, $d_o = 0.016m$, $P_t = 0.032m$, $L_{b,c} = 0.55m$

		2 tube passes, length = 4.5 m			**4 tube passes, length = 3.5 m**		
		Model	**Aspen**	**error**	**Model**	**Aspen**	**error**
$T_{hot,in}$	[°C]	154.1	154.1		153.3	153.3	
$T_{hot,out}$	[°C]	103.6	100.28		103.2	101.5	
$T_{cold,in}$	[°C]	65.8	65.8		65.8	65.8	
$T_{cold,out}$	[°C]	106.2	108.44		105.9	107	
$p_{hot,in}$	[bar]	0.340	0.340		0.321	0.321	
$p_{hot,out}$	[bar]	0.233	0.225		0.233	0.243	
Δp_{hot}	[bar]	0.107	0.115	7.5%	0.088	0.078	-11.2%
$\Delta p_{hot,in}$	[bar]	0.0054	0.0076	39.2%	0.0056	0.0076	34.7%
$\Delta p_{hot,out}$	[bar]	0.0068	0.0023	-65.8%	0.0066	0.0021	-67.8%
$\Delta p_{hot,w}$	[bar]	0.0795	0.0714	-10.2%	0.0644	0.0438	-31.9%
$\Delta p_{hot,c}$	[bar]	0.0119	0.0328	174.9%	0.0098	0.0234	139.2%
N_t	[-]	229.7	232	1.0%	212.1	224	5.6%
l_c/D_s	[-]	0.3	0.305		0.3	0.320	
A_{tot}	$[m^2]$	51.99	54		37.21	40.8	
α_t	$[W/m^2/K]$	ca. 200	271.6		ca. 600	484.8	
α_s	$[W/m^2/K]$	ca. 140	145.8		ca. 140	145.8	

4.2. EVAPORATOR

In this work the design of the evaporator is as it is used currently for the Triogen ORC units. Triogen uses an flue-gas cooler type of evaporator with plain u-tubes. The working fluid flows in the tubes, the flue-gas flows in the shell. Triogen uses plain tubes mainly because it reduces fouling. As the design massflow and temperature of the heat source varies per heat source, Triogen designs a new evaporator for each application. For the design of the evaporator a model[34] is used which calculates, based on a fixed tube geometry, the number of tubes necessary to have enough heat transfer area, and the number of tubes per row that is needed to meet the pressure drop limitation on the flue-gas side.

The model splits the evaporator in three parts namely the preheater, boiler and superheater. Separate correlations are used for one phase heat transfer and boiling. Heat transfer is mainly limited on the flue-gas side, because the flue-gas is a low pressure gas flowing at low velocities which leads to very low heat transfer coefficients. The correlation used for heat transfer at the flue-gas side is the correlation by Zukauskas and Ulinkas (From Zukauskas "convective heat transfer in cross flow" Handbook of single-phase convective heat transfer). The model assumes a number of tubes per row, and then calculates per section of constant duty, the number of tube rows necessary for the heat transfer in that section. Then it calculates the pressure drop over that number of tube rows. After all sections have been evaluated, a total number of rows and a total pressure drop on the flue-gas side is calculated. Then the number of tube rows is iterated, in order to let the pressure drop meet the back-pressure limitation which is in all simulations set to 1 kPa. The model will try to have as few as possible tubes per row, while meeting this limitation, as this will increase the flue-gas velocity and the heat transfer coefficient and thus reduce the total number of tubes.

The evaporator model just described, is used as an add-on to the model described in section 3. The mass flow is still derived in the evaporator from the flue-gas massflow and temperature and

Table 4.3: Comparison of the recuperator model with an Aspen model, for shell and tube heat exchangers with a relative baffle cut of 0.2 and 0.3 respectively and pentane as working fluid, $D_s = 0.45m$, $d_o = 0.016m$, $P_t = 0.028m$, $L_{b,c} = 0.45m$

		l_c = 0.2, l = 2.44 m			l_c = 0.3, l = 3 m		
		Model	**Aspen**	**error**	**Model**	**Aspen**	**error**
$T_{hot,in}$	[°C]	197.1	197.1		197.05	197	
$T_{hot,out}$	[°C]	122	125.7		122	122.4	
$T_{cold,in}$	[°C]	65.6	65.6		65.6	65.6	
$T_{cold,out}$	[°C]	129.3	128.4		129.2	130.8	
$p_{hot,in}$	[bar]	2.45	2.45		2.44	2.44	
$p_{hot,out}$	[bar]	2.351	2.35		2.35	2.39	
Δp_{hot}	[bar]	0.099	0.1	1.0%	0.085	0.05	-41.2%
$\Delta p_{hot,in}$	[bar]	0.0014	0.0022	53.5%	0.0015	0.0022	53.3%
$\Delta p_{hot,out}$	[bar]	0.0012	0.0004	-71.0%	0.0012	0.0004	-71.8%
$\Delta p_{hot,w}$	[bar]	0.0560	0.0694	24.0%	0.0694	0.0281	-59.5%
$\Delta p_{hot,c}$	[bar]	0.0117	0.0290	147.1%	0.0146	0.0197	35.0%
N_t	[-]	177.1	180	1.6%	177.1	180	1.6%
l_c/D_s	[-]	0.2	0.195		0.3	0.303	
A_{tot}	[m^2]	21.7	23.1		26.4	27.9	
α_t	[$W/m^2/K$]	ca. 1050	815.3		ca. 1050	817.6	
α_s	[$W/m^2/K$]	ca. 490	377.8		ca. 370	369.8	

the pressure and the heating curve and pinch temperature difference of the working fluid. After the model has iterated the evaporator model is used only to determine the design and cost of the evaporator. A small error is introduced here, because the pressure drop at the toluene side of the evaporator is not taken into account. This pressure drop has a magnitude of 10 kPa. Which in combination with a typical massflow of around 2 kg/s leads to an error in the pump power estimation of ca. 20 Watt. In section 3.5 it was shown that even a pressure drop of 2 bar had negligible influence, which makes it acceptable to neglect this pressure drop here.

4.3. AIR-COOLER

To take into account the cost and the power consumption of the cooling, based on the water flow rate and temperatures, a model for the cooling should be taken into account. The water flow in Triogen ORC's is normally cooled using standard air-coolers which consist of finned tubes trough which the water flows. the cooling air is blown over the tubes using fans. The influence on the total system specific cost by the air-cooler can be split in three parts: The cost of the air cooler, the power consumption by the fans and the power consumption by the water pump due to the pressure drop over the tubes.

For the calculation of the geometry and pressure drops over the aircooler, again a model using correlations for the calculation of heat transfer coefficients and pressure drops could be used, similar to the evaporator model. Nevertheless it is chosen to fit the performance and cost of the air-cooler with quotations by Alfa Laval. This was chosen because the influence of the water cooling system on total performance and cost is expected to be relatively small and because adding extra variables to the optimization will add unnecessary complexity.

In order to be able to fit a correlation with the data from Aspen quotations, a few assumptions where made. First it was assumed the heat transfer coefficient is constant. Second it was assumed a constant number of tube-rows and a constant tube geometry was used, and that in order to maintain a constant heat transfer coefficient the fan power per surface area should be constant. Then it was assumed that pressure drop on the water side changes negligibly with the water mass flow and

surface area and may be assumed constant.

From the quotation and the assumptions it was concluded that the fan power consumption and air-cooler cost relate closely to the surface area. Because the heat transfer coefficient is unknown and assumed constant the UA value (heat transfer coefficient * surface area) is used instead, The UA value is calculated using equation 4.27:

$$UA_{air-cooler} = Q_{air-cooler} / LMTD_{eq} \tag{4.27}$$

In which $LMTD_eq$ is defined as:

$$LMTD_{eq} = \frac{\Delta T_{in} - \Delta T_{out}}{Ln(\frac{\Delta T_{in}}{\Delta T_{out}})},\ \Delta T_{in} = T_{aq,in} - T_{amb},\ \Delta T_{out} = T_{aq,out} - T_{amb} \tag{4.28}$$

The fan power was found to relate to the UA value as in equation 4.29:

$$W_{fan} = 0.1 * UA_{air-cooler} \tag{4.29}$$

The pressure drop over the water side of the air-cooler was found to be 0.5 bar. The work of the cooling water pump is calculated using the pressure drop over the air-cooler, piping and the condenser and a pump efficiency of 0.6.

Table 4.4: Quotation of Alfa Laval air coolers, supplemented with calculation of UA value and cost calculation according to cost correlation

Air temp [°C]	Cooler type	Duty [kW]	Engine power [W]	Cost price [€]	LMTD [K]	UA [kW/K]	€/UA [€/(kW/K)]	Engine power/UA [kW/(kW/K)]	Cost correlated [€]	Error [%]
15	805CT	757	2855	11829	28.9	26.2	451	0.109	11354	-4%
20	804BT	757	4568	14516	23.6	32.1	453	0.142	13603	-6%
25	804DT	753	4568	17350	18.2	41.4	419	0.110	17104	-1%
30	907C	761	2912	28844	12.4	61.2	471	0.047	24349	-16%
15	1003BT	461	1695	7587	28.9	16.0	475	0.106	7266	-4%
20	1002BT	452	2260	8966	23.6	19.1	468	0.118	8552	-5%
25	1004CT	456	2260	11022	18.2	25.0	440	0.090	10891	-1%
30	1004BT	449	3320	15962	12.4	36.1	442	0.092	15144	-5%

4.4. TURBINE

In literature several efficiency charts are available for estimating the achievable isentropic efficiency using the volumetric ratio (Vr equation 4.30) and the size parameter (SP equation 4.31) for both axial[35–37] and radial[38] inflow turbines. These charts are based on Craig and Cox loss correlations. Apart from the charts by Da Lio et al., where Refprop is used, the ideal gas law is used with a fixed heat capacity ratio assumed representative for ORC working fluids, in order to simulate the expanding vapor states. Unfortunately apart from the chart by Astolfi et al. [36] these charts show a limited range of volumetric ratios (up to 10) while volumetric ratios up to 50 are expected.

$$V_r = \dot{V}_{out,is} / \dot{V}_{in} \tag{4.30}$$

$$SP = \dot{V}^{0.5}_{out,is} / \Delta h^{0.25}_{is} \tag{4.31}$$

Figure 4.7 shows the heat capacity ratio γ has an increasing influence for increasing volume ratios. And although, a for ORC applications representative value of 1.1 and 1.05 is chosen respectively

by Macchi et al. and Astolfi et al., a relative estimation error for the fluids of a few percent is expected. According to Refprop the considered fluids have a heat capacity ratio varying from 1.05 to 1.4 at the inlet to 1 to 1.15 at the outlet. Da Lio et al.[37] say on this topic: "the efficiency is a function of five independent variables specific speed, specific diameter, Reynolds number, Mach number and specific heat ratio." "When dealing with a turbomachinery operating with a specific fluid in a fully developed turbulent flow regime the effects of the heat capacity ratio and the Reynolds number can be neglected." Considering the fact that these authors say the influence of specific heat ratio is negligible, and the lack of figures for the influence at higher volumetric ratios, the influence of heat capacity ratio is neglected.

Figure 4.8 shows lines of constant efficiency in the low volumetric ratio domain. A few things can be concluded on how the efficiency charts from different authors relate. First it can be concluded that the efficiency predicted for axial turbines using the ideal gas law (Macchi and Astolfi) are quite consistent with each-other, while Da Lio predicts slighlty lower efficiencies using the Refprop database. Secondly the lines for equal efficiencies show more or less the same trend, indicating that although there may be absolute differences between the charts, the relative errors of the predicted efficiencies are expected to be small. A last thing that does not appear very clear from this figure, though does deserve attention here, is the fact that radial inflow turbines perform better for higher volumetric ratios and low size parameters, while for low volumetric ratios and higher size parameters the axial turbine performs better. Therefore the chart by Astolfi et al. (figure 4.9[36]) for the efficiency of axial turbines is used only as an indication of the turbine performance for one fluid relative to the other. For designing the cycle more accurate predictions of radial inflow turbine performance will be necessary.

A correlation is fit on the graph in figure 4.9 in order to be able to calculate the turbine efficiency in the model. The correlation is given by equations 4.32 to 4.35. In converting the graph to a correlation, an additional estimated error of around 1 percentage point is made.

$$a = -17.335, b = -0.31176, c = -13.4053, d = 9.4899, e = 109.9875 \tag{4.32}$$

$$m = (1/SP * (SP - 0.002))^{0.5} \tag{4.33}$$

$$n = \frac{-1}{(SP * 68)^{1.4}} \tag{4.34}$$

$$\eta_{is,turb} = \frac{a * V_r^b + \frac{c * logV_r}{logd} + m * e + n * V_r}{100} \tag{4.35}$$

4.5. COST ESTIMATION METHOD

The cost for the recuperator and condenser is estimated using the same correlation. The cost is split in a fixed part of €10.000 which accounts for the cost of the heads and nozzles, a variable cost for the number of pipes of €40 per pipe which relates to the cost of manufacturing and a variable cost for the effective area of €100 per m^2, accounting for the material cost. This correlation for the cost estimation is fit on the cost estimation by Aspen. A few typical recuperators and condensers as they are proposed by the model, have been modeled in Aspen and the cost estimation by Aspen is used to fit the correlation on.

$$C_{recuperator/condenser}[€] = 10.000 + 40N_t + 100 * A_{tot} \tag{4.36}$$

The cost for the evaporator is calculated based on a fixed cost, plus a variable cost per tube, this is possible because the tubes in the evaporator have a fixed geometry. This cost estimation method

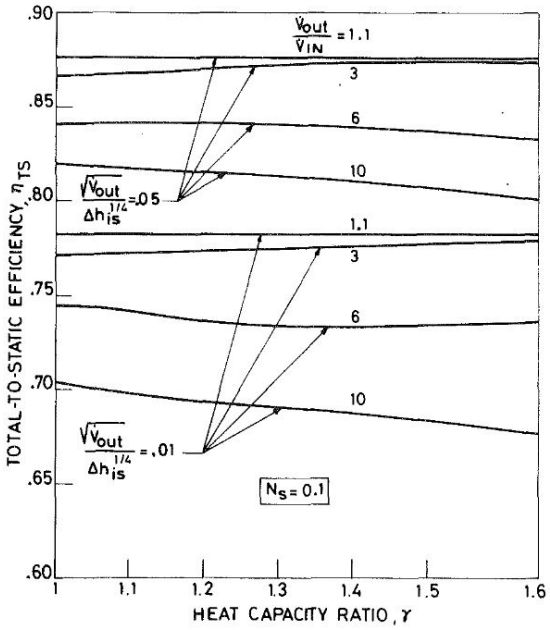

Figure 4.7: Influence of the heat capactity ratio γ of the working fluid on the efficiency of a turbine stage[35]

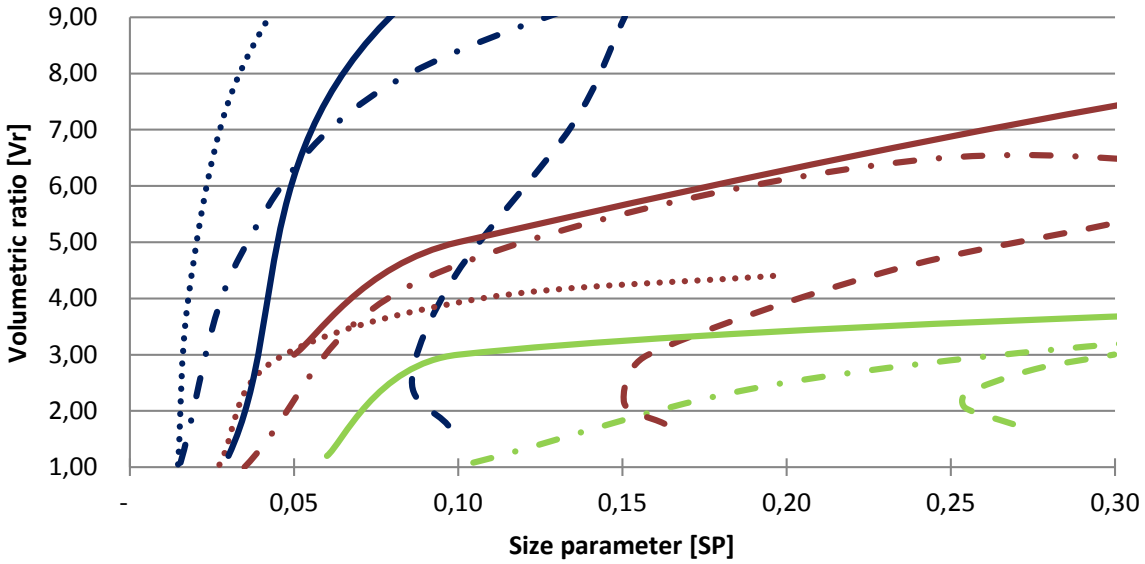

Figure 4.8: Lines of constant turbine efficiency, 0.85 = blue, 0.88 = red, 0.90 = green, as predicted for axial turbines and radial inflow turbines based on the size parameter and volumetric ratio. Astolfi[36] = solid, Macchi[35] = stripe and dotted, Da Lio[37] = striped, Perdichizzi[38] (Radial inflow) = dotted

is also part of the evaporator model used by Triogen for the design of the evaporator. The cost is €33 per tube, the fixed cost is €1000.

$$C_{evaporator}[€] = 1000 + 33N_t \tag{4.37}$$

The cost of the air-cooler is calculated using the UA value of the air-cooler, which is calculated using the total duty and equivalent mean temperature difference of the air-cooler as is explained in section 4.3. Using the quotation in table 4.4 the cost has been estimated and equation 4.38 is fit on the cost data. Because U is unknown and assumed constant, the cost is scaled with UA instead of

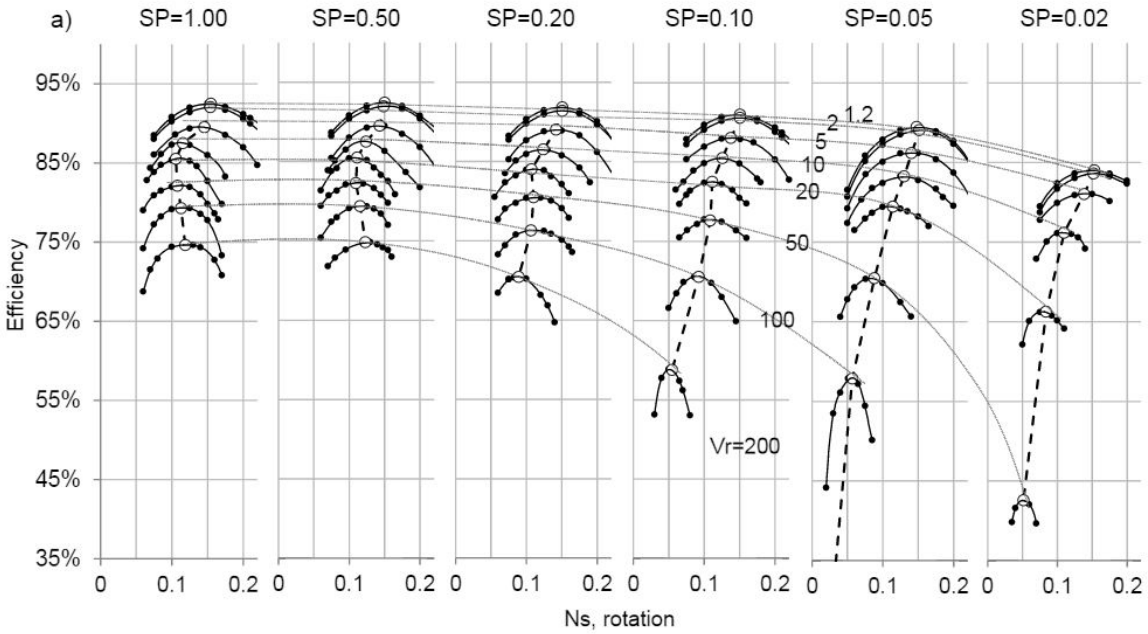

Figure 4.9: Efficiency chart for the prediction of turbine isentropic efficiency based on volumetric ratio, size parameter and specific speed [36]

the surface area.

$$C_{air-cooler}[€] = 600 * (UA)^{0.9}_{air-cooler} \tag{4.38}$$

In addition a fixed cost of €220.000 is assumed for the rest of the equipment. This cost includes the cost of the turbine, generator and pump, the piping and valves, the storage vessel, the flue-gas supply, the cooling water piping, assembly and installation, electronics and control, vacuum system and other auxiliary components.

The cost of these components will in practice not be constant and will off-course depend on the system design. For some of these components it is briefly discussed here why it's cost are assumed to be constant. The cost of the turbine for example consists for a large part of the milling of the blades which needs to be done very precise. This cost will probably depend on the size of the turbine, due to the lack of size calculations and good reference turbine costs no good estimates can be made of these cost. Also the cost of the turbine is quite low and is expected to vary only slightly. The cost of the flue-gas supply will vary highly per application as the length of the flue-gas channels and the number of heat sources connected to the ORC will vary per application. This is not within the scope of this research and therefore neglected. Last the piping and valves: on the vapor side of the system where there are large density differences per working fluid, there is no piping and components are connected to each other directly. On the liquid side the sizing of piping and valves will be approximately equal for each fluid as mass flows and densities are in the same order of magnitude.

5

RESULTS

In this chapter the results generated using the model are discussed. First the different optimization cases are introduced. Then a few typical results are discussed to get an impression of the order of magnitude of some typical numbers and where these numbers come from. Last the results are given per case.

5.1. SIMULATION CASES

In this chapter the results are presented from the simulation of the model. Six cases are simulated to test the performance of the selected fluids and the sensitivity for a few important parameters. In the first two cases all fluids are optimized, in the first case for the situation in which sulfuric acid condensation does not have a significant impact, the second case has a minimum wall temperature of 100°C in the evaporator. These two main cases are selected because it is unclear whether sulfuric acid condensation will have a significant impact or not. The subsequent cases are sensitivity analysis based on the first two cases.

1. The first optimization is the optimization without limitation at the outlet temperature, and an ambient temperature of 25 °C. This optimization represents the case in which the effect of flue-gas condensation is negligible.

2. The second case is the optimization with limitation at the wall temperature, and an ambient temperature of 25°C. This optimization represents the case in which sulfuric acid condensation is not negligible and is prevented.

3. The third case is a sensitivity analysis with the three best fluids only. To see the influence of the minimum wall temperature. Here the minimum wall temperature will be varied from 50°C to 150°C

4. The fourth case is an analysis meant as comparison with case 3. In this case the influence of flue-gas outlet temperature is tested, to see the difference in influence of minimum outflow temperature and minimum wall temperature. A minimum outlet temperature ranging from 50 to 160 degrees is tested.

5. The fifth case is a sensitivity analysis for the ambient temperature, to see whether a different model is necessary for different locations. The ambient temperature is varied from 5°C to 40°C. The minimum wall temperature is here assumed to be 100°C.

6. The sixth case is a sensitivity analysis for the magnitude of the fixed cost, her also the minimum wall temperature is here assumed to be 100°C.

In all cases the heat source is the exhaust gas of a diesel engine, with a mass flow of 5 kg/s and a temperature of 350°C. The cooling source is air cooled water, with a variable massflow and temperature. All pump isentropic efficiencies are set to 0.6, the mechanical and generator efficiencies are 0.95 and 0.94 respectively. All other components are implemented as described in chapter 4.

5.2. TYPICAL RESULTS

In this section two typical results are analyzed, the first is the optimum for toluene for case 1 and the second is the optimum for acetone for case 2. First typical plots are used to explain why these process parameters are the optimum process parameters, and to get an impression of what push these parameters. Then the composition of the power consumptions and losses as part of the turbine power are analyzed. Last the cost composition is analyzed.

5.2.1. TURBINE INLET PRESSURE

First of the process parameters analyzed in this section, is the turbine inlet pressure. The turbine inlet pressure determines for a large part the isentropic enthalpy difference over the turbine. A higher pressure, leads to a higher pressure ratio and a higher pressure ratio leads to a higher isentropic enthalpy difference and with that higher turbine power. This raises the expectation that the turbine inlet pressure would be as high as possible and would be near the critical point for all working fluids with a critical temperature below the flue-gas inflow temperature.

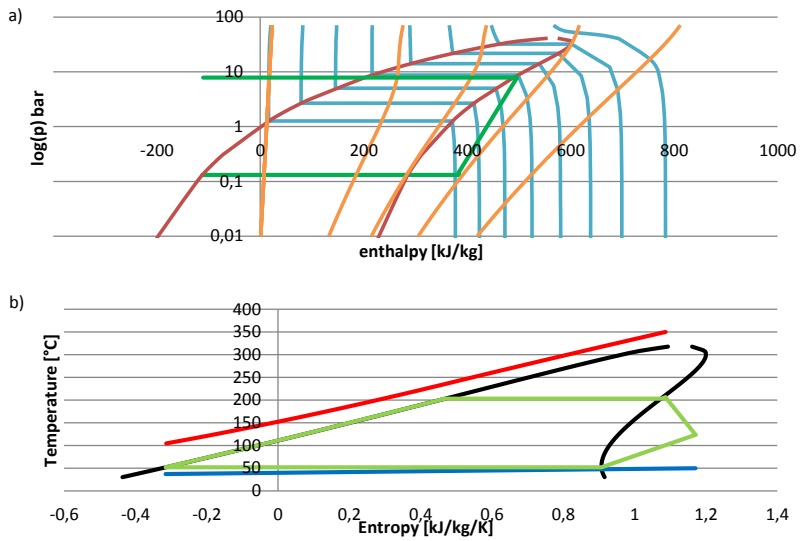

Figure 5.1: a) log(p)h diagram and b) Ts diagram showing the optimal cycle for toluene case 1

Figure 5.1 shows the log(p)-h and Ts diagram for the optimal cycle with Toluene in case 1. It is clear that saturation temperature could have been higher and that the isentropic enthalpy difference over the turbine would have been much larger without a large reduction of the massflow when the turbine inlet pressure would have been higher. The reason for the optimum turbine inflow pressure being this low is found in the turbine isentropic efficiency. It was explained that the turbine efficiency can be related to the size parameter and the volumetric ratio, and that high size parameters and low volumetric ratios lead to high turbine efficiency. While a higher turbine inlet pressure will increase the isentropic enthalpy difference over the turbine, it will also increase the pressure ratio and with that the volumetric ratio and will eventually decrease the turbine isentropic efficiency. The model now, looks for an optimal equilibrium between isentropic efficiency and isentropic enthalpy difference as is seen in figure 5.2. In comparison the results of an equivalent optimization

is shown with an assumed constant isentropic turbine efficiency of 0.78 in figure 5.3. This figure shows that indeed the turbine inlet pressure is much higher when the pressure does not affect the turbine efficiency.

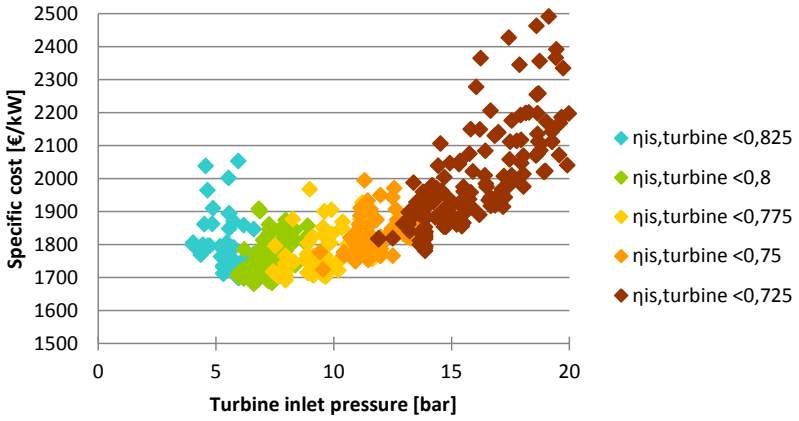

Figure 5.2: plot of optimization results for Toluene, case 1, showing the effect of turbine isentropic efficiency on the turbine inlet pressure

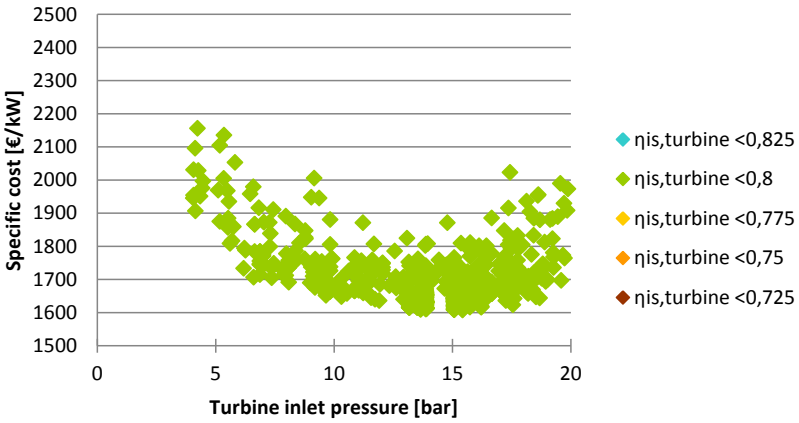

Figure 5.3: plot of optimization results for Toluene, case 1, with a constant isentropic turbine efficiency of 0.78

5.2.2. DEGREE OF SUPERHEAT

For case 1 the optimization with most working fluids shows a preference for low degrees of superheat. Increasing the degree of superheat has roughly two effects. The first effect is found in the log(p)-h diagrams. The isentropes in these diagram have a larger slope in the vicinity of the saturated vapor curve while the slope decreases when more superheat is added. When expanding the vapor, the isentropic enthalpy difference over the turbine is equal to the enthalpy difference between the points the isentrope crosses on the high and low pressure line. Therefore the more superheat, the larger is the isentropic enthalpy drop and therefore the power output per massflow of the working fluid. The other effect though, is the reduction of the massflow of the working fluid. For the working fluids that have a pinch temperature difference at the saturated liquid point, the effect of reduced massflow is so strong that no superheat is preferred. For the working fluids that have their pinch temperature difference at the evaporator inlet the optimum cycle does have superheat.

Another effect is related to the saturated vapor curve in the TS diagram. For the wet fluids (figure 2.3) some superheat is always necessary to prevent the formation of liquid in the turbine.

5.2.3. PINCH TEMPERATURE DIFFERENCE IN EVAPORATOR

The place and magnitude of the pinch temperature difference relates closely to the design of the evaporator. In accordance with the OHST theory explained in section 2.4.1 the results show the tendency to match the slope of the preheat temperature-duty curve with the flue-gas temperature curve in order to find a good equilibrium between the reduction of exergy destruction in the evaporator and size of the evaporator.

5.2.4. CONDENSER TEMPERATURE AND PRESSURE

The condenser temperature relates closely to the water temperature, a temperature difference of a few degrees at the water outflow is found to be optimal. The condenser temperature and pressure seem to be the result of an equilibrium mainly between the cooling system cost and auxiliary power consumption by water pump and fan and the turbine power. When the condenser pressure rises for example, the turbine power decreases, while when condenser temperature decreases the cooling water needs to be colder as well and cooling power consumption and cost rise. This effect is shown in figure 5.4

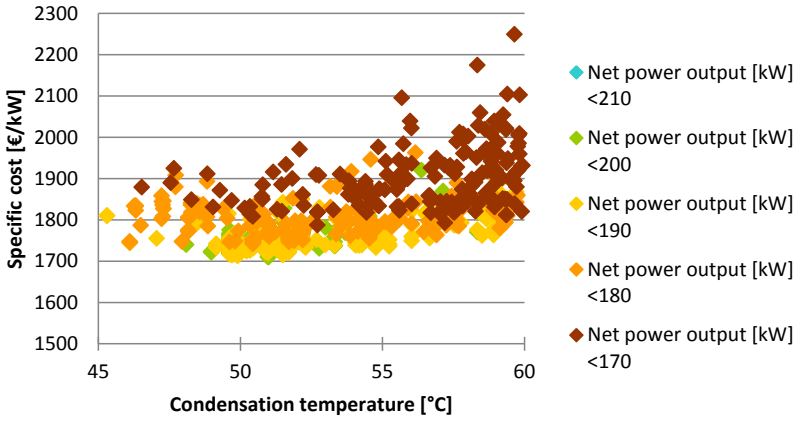

Figure 5.4: plot of optimization results for Acetone, case 2, showing the equilibrium between cooling power consumption and cost and turbine power output

5.2.5. RECUPERATOR EFFECTIVENESS

The application of the recuperator is dependent on a number of parameters. First there is the minimum outlet temperature, for almost all fluids in case 1 the optimal results are reached when no recuperator is used, while in case 2 a recuperator is necessary to reach the minimum wall temperature of 100°C. Figure 5.5 shows that, in order to reach the minimum wall temperature with low specific costs, an increasing recuperator effectiveness is necessary. Surprisingly the minimum wall temperature for case 2 is for some fluids above the 100°C, for ethanol for example it is more economical to have a bit extra recuperator effectiveness and reduce cost on evaporator and cooling. When the pinch temperature difference is at the working fluid inflow of the evaporator, which is the case mainly for low critical temperature working fluids, the application of a recuperator can increase the massflow of working fluid and with increasing the massflow the total power output is increased. For fluids with low condensing pressures such as toluene the application of a recuperator also causes a significant pressure drop which reduces the total power output. One of the secondary effects of the pressure drop over the recuperator for these fluids is an increase in condensing temperature.

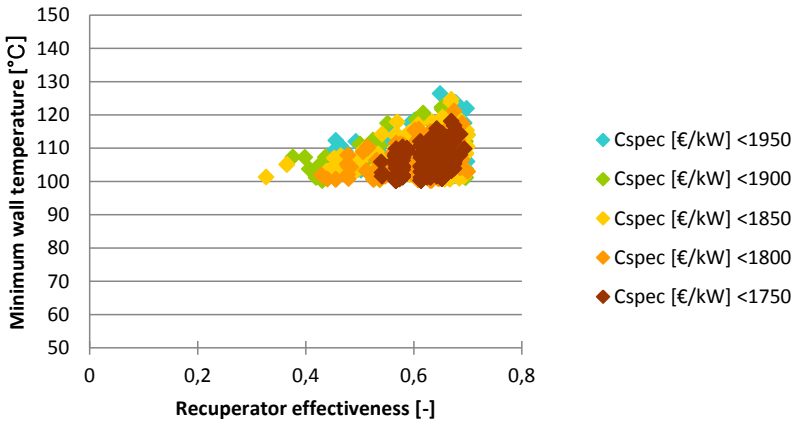

Figure 5.5: plot of optimization results for Acetone, case 2, showing the effect of minimum wall temperature on recuperator effectiveness and specific cost

5.2.6. COMPOSITION OF POWER OUTPUT

In this subsection the composition of the power output is analyzed. In next subsection the composition of the cost and the formation of the specific cost is presented. This is done to create some insight in the losses and the power consumption by pumps and fans. Due to the mechanical efficiency of 95% and the generator efficiency of 94%, 5% and 6% of the turbine power is lost respectively. The power consumption by the air-cooler fan is the next largest loss of power with approximately 2-3%, the water pump causes a power loss of around 1-2% of the total power. The power consumption by the working fluid pump is highly dependent on the pressure difference over the pump and mass flow of working fluid. In case of Toluene, the power consumption is only 1.5% while for acetone and other high pressure working fluids the pump power or back-work ratio can be over 3% and up to around 10%. The power production and consumption are given graphically in figure 5.6.

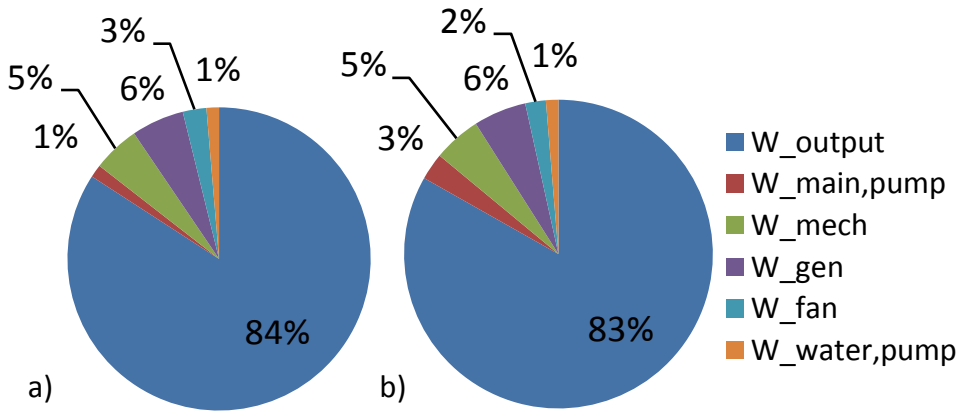

Figure 5.6: pie-chart of the net power production and component power consumption for the optimal cycle with a) Toluene, case 1, b) Acetone, case 2

5.2.7. COMPOSITION OF TOTAL COST

The total cost consists for a large part of fixed cost. These costs were assumed to be €220.000, including turbine, pumps, piping, casing and others. The total cost consists for a large part of these fixed cost. The variable cost consist of the evaporator, recuperator, condenser and air-cooler cost.

The cost composition for the optimal toluene and acetone cycle for case 1 and 2 respectively are shown in table 5.1 and figure 5.7.

Table 5.1: Cost composition for the optimal cycles with Toluene, case 1 and Acetone, case 2

		Toluene, case 1	**Acetone, case 2**
Total cost	[€]	315.000	330.000
Fixed cost	[€]	220.000	220.000
Evaporator	[€]	46.000	46.000
Recuperator	[€]	-	19.000
Condenser	[€]	27.000	25.000
Air-cooler	[€]	23.000	20.000

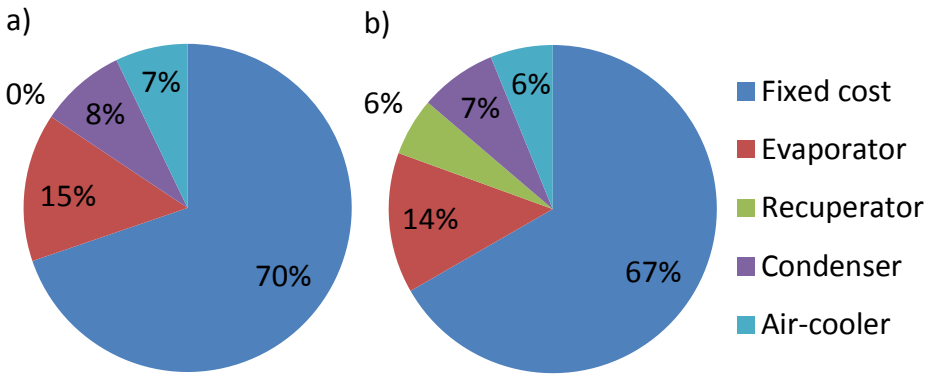

Figure 5.7: pie-chart of the cost composition for the optimal cycle with a) Toluene, case 1, b) Acetone, case 2

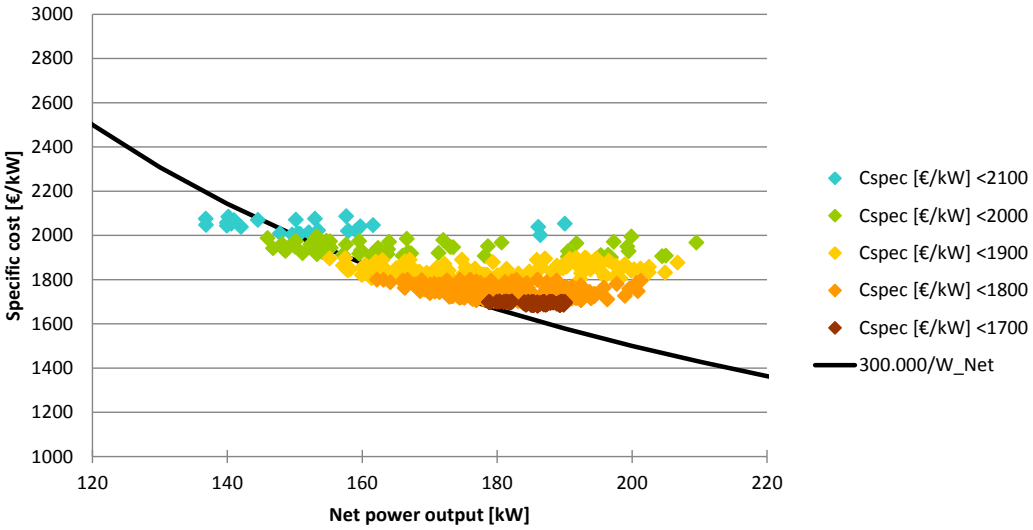

Figure 5.8: plot of optimization results for Toluene case 1, showing the relation between net power output and specific cost

Due to this large part of fixed costs optimizing for specific cost is almost the same as optimizing for maximum total power output. Figure 5.8 and 5.9 show the specific cost versus power out-

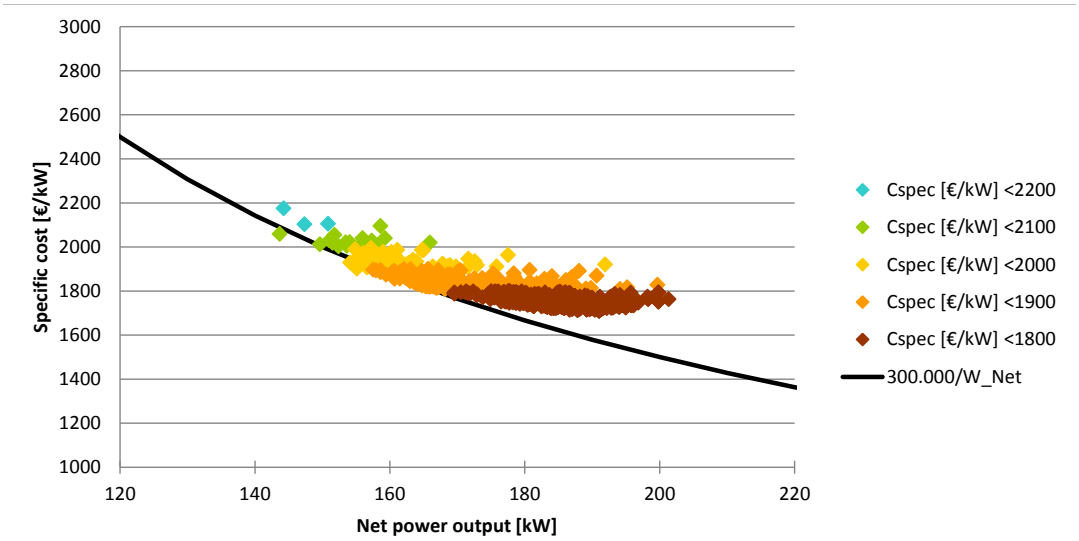

Figure 5.9: plot of optimization results for Acetone case 2, showing the relation between net power output and specific cost

put curves for the optimization of Toluene case 1 and Acetone case 2. It shows that both have the same trend as the curve from equation 5.1. Due to the large fixed costs and the necessity to have a evaporator, condenser, air-cooler and in some cases a recuperator, the total cost is always around €300.000. Only at high power output and at the optimal cost to power output ratio the total system cost start to increase and the specific cost start to deviate from equation 5.1. Another thing that is pictured in figures 5.8 and 5.9 is that the specific cost slope flattens around the optimum which means there is actually a range of good process parameters. Also it can be concluded from this, that although the optimal specific costs for Toluene is €1682 with a power output of 189 kW, it could also be chosen to have a power output of 200 kW with slightly higher specific costs.

$$C_{spec} = €300.000/W_{net} \tag{5.1}$$

5.3. CASE 1

In the first case an optimization is performed for all fluids without limits on the flue-gas or wall temperature. In table 5.2 for each working fluid the optimal cycle is given by the total power output, the specific cost and a few important process parameters. A full overview of the cycles for acetone, ethanol and toluene is given in appendix C. In addition the power output and specific cost are shown in figure 5.10.

Table 5.2: main input and output parameters for optimal specific cost in case 1

Working fluid	p_{crit} **[bar]**	T_{crit} **[°C]**	C_{spec} **[€/kW]**	W_{tot} **[kW]**	p_{high} **[bar]**	ΔT_{sup} **[K]**	T_{cond} **[°C]**	ϵ_{rec} **[-]**	m_{wf} **[kg/s]**	$\eta_{turbine}$ **[-]**
Toluene	41.3	318.6	1682	188.9	7.9	3.3	51.6	0.00	2.0	0.78
Cyclohexane	40.8	280.5	1737	184.3	11.8	0.4	51.7	0.00	2.2	0.79
Heptane	27.4	267.0	1923	166.0	7.5	1.6	51.0	0.00	2.2	0.79
Ethanol	62.7	241.6	1744	182.0	18.1	61.8	50.9	0.00	1.0	0.75
Acetone	47.0	235.0	1647	195.6	23.0	32.5	48.8	0.00	1.7	0.77
Hexane	30.3	234.7	1907	165.7	12.0	1.7	51.2	0.00	2.3	0.80
R113	33.9	214.1	1860	172.5	25.1	10.9	52.7	0.00	5.7	0.79
R141b	42.1	204.4	1759	184.7	36.6	30.0	48.3	0.00	3.8	0.78
R11	44.1	198.0	1697	188.1	37.9	55.3	49.2	0.00	4.6	0.80
Pentane	33.7	196.6	1956	168.6	24.1	31.0	46.7	0.59	2.2	0.79

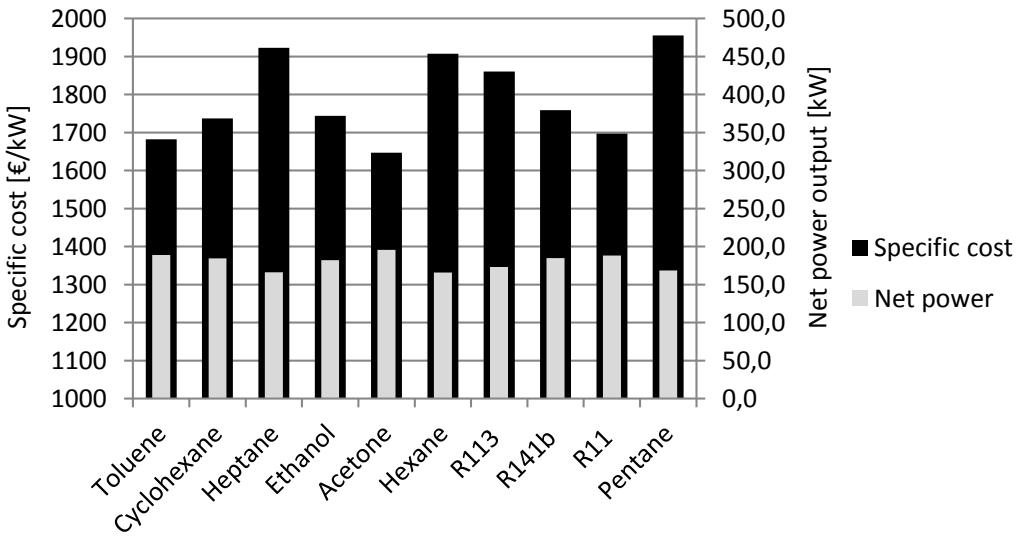

Figure 5.10: plot of optimization results for case 1, showing the specific cost on the left axis and total power on the right axis

Acetone, Toluene and R11 perform best followed closely by cyclohexane, ethanol and R141b. Also a relation can be found between the optimal power output and the specific costs. In figure 5.11 all optima from case 1 are pointed in the net power-specific cost domain. From this figure it can be found that the total cost of the cycle is almost constant at €320.000. As can be expected there is one exception, which is pentane, as pentane uses a recuperator and is therefore more expensive.

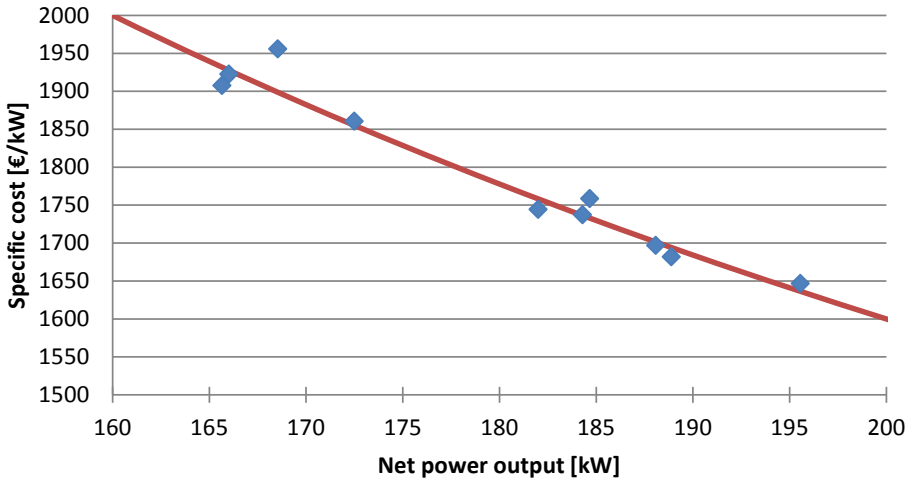

Figure 5.11: plot of optimization results for case 1 (blue dots), and a trend line specific cost = 320.000/net power (red line)

5.4. CASE 2

In the second case the cycle is optimized identical to case 1 but now with a minimum wall temperature in the evaporator of 100°C. This case is representive for the case where a diesel fuel with moderately high sulfur content is used and sulfuric acid condensation at the walls needs to be prevented. Table 5.3 and figure 5.12 show the results for case 2 in the same format as the results for case 1 were presented.

Table 5.3: main input and output parameters for optimal specific cost in case 2

Working fluid	p_{crit} **[bar]**	T_{crit} **[°C]**	C_{spec} **[€/kW]**	W_{tot} **[kW]**	p_{high} **[bar]**	ΔT_{sup} **[K]**	T_{cond} **[°C]**	ϵ_{rec} **[-]**	m_{wf} **[kg/s]**	$\eta_{turbine}$ **[-]**
Toluene	41.3	318.6	1900	171.7	11.9	2.0	56.9	0.46	1.8	0.76
Cyclohexane	40.8	280.5	1855	181.0	14.8	5.1	55.4	0.60	2.1	0.78
Heptane	27.4	267.0	2038	156.6	11.4	1.0	59.4	0.53	2.1	0.78
Ethanol	62.7	241.6	1810	178.4	16.6	129.3	51.5	0.52	0.9	0.76
Acetone	47.0	235.0	1709	193.0	20.5	76.0	50.0	0.59	1.5	0.79
Hexane	30.3	234.7	1950	166.8	17.3	17.3	53.3	0.58	2.1	0.77
R113	33.9	214.1	1888	176.4	30.0	33.5	49.9	0.58	5.0	0.78
R141b	42.1	204.4	1843	176.7	24.8	56.3	53.7	0.67	3.8	0.82
R11	44.1	198.0	1705	199.6	39.2	82.8	47.6	0.63	4.4	0.80
Pentane	33.7	196.6	1956	168.6	24.1	31.0	46.7	0.59	2.2	0.79

As expected, the specific cost is higher for each fluid compared to what it was in case 1, apart from pentane, which was already using a recuperator in case 1. In contrast with expectations some fluids produce actually more power in the second case compared to the first case, these fluids are R113 and R11. This can be explained by the fact that these fluids both have the pinch temperature difference at the working fluid inflow of the evaporator. when maintaining the process parameters constant and increasing the recuperator effectivity, the total massflow could be increased leading to higher powers. In this case though the total superheat is increased as well as the evaporator pressure, which also increases the power.

Another interesting thing is the condensation temperature. For the working fluids condensing at low pressure the condensation temperature appears to increase while the other remain more or less constant. This increase of pressure can be explained using the pressure drop over the recuperator,

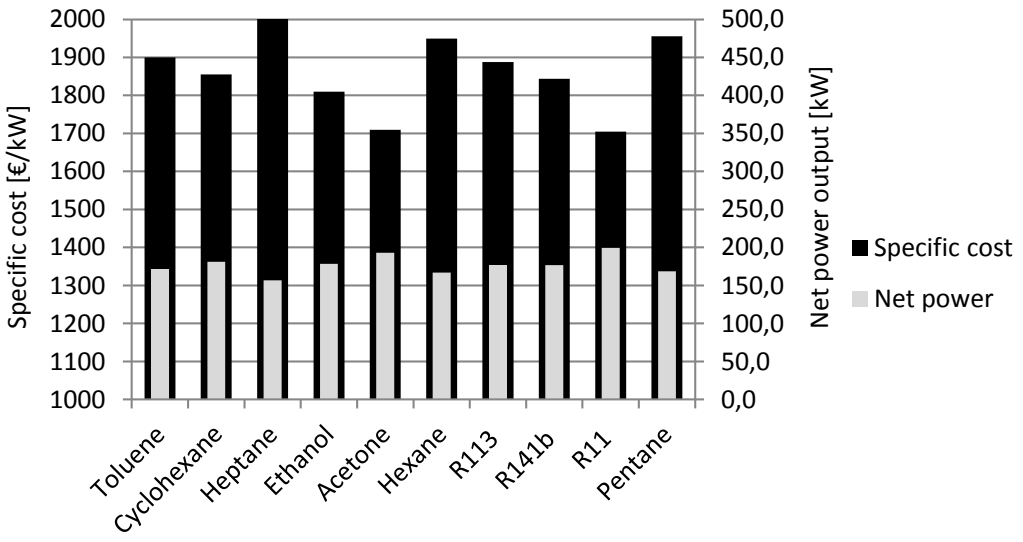

Figure 5.12: plot of optimization results for case 2, showing the specific cost on the left axis and net power on the right axis

because the recuperator adds a significant pressure drop the added power output from the turbine is enhanced less by having a low condensation temperature. Therefore the equilibrium between turbine output power and cooling system power consumption finds a new optimum, at a higher condensation temperature.

From the results of case 1 and 2 now a selection of 3 working fluids is made. As well as in case 1 R11 and acetone perform best. Though, because the use of R11 is restricted because of its ozone depletion potential, it will not be further analyzed in the next cases. Acetone is followed by ethanol, R141b, cyclohexane and toluene. From these fluids ethanol and toluene are chosen to analyze further in the coming cases. R141b is not chosen because it has a too low thermal stability limit (ca. 90°C). Toluene was chosen because it performs really well at case 1 and because it is most interesting for Triogen. Ethanol was chosen instead of cyclohexane as it adds more variety to the set of 3 fluids. The structure and thermophysical properties of cyclohexane are a bit similar to toluene, while ethanol is completely different, it has for example a wet vapor saturation curve, while toluene and acetone, have a dry and isentropic one respectively, see figure 2.3.

5.5. CASE 3, MINIMUM WALL OUTLET TEMPERATURE

In this case, for the selected three fluids, the minimum wall temperature in the evaporator is varied from 50°C to 130°C to get an impression of the sensitivity of these fluids for the minimum wall temperature and to see which fluid is most suitable at different minimum wall temperatures. In case 1 and 2 it was already shown that some fluids are influenced more by the minimum wall temperature compared to others. In this section the exact influence on these best fluids is discussed.

Figure 5.13 shows the optimal specific cost taking into account a minimal evaporator wall temperature of 50°C to 130°C for acetone, ethanol and toluene. The curves for all three fluids show a kink in the curve at the point where it becomes more economical to use a recuperator instead of having no recuperator. As for all fluids the minimum wall temperature in the optimal solution of case 1 is already above 50°C, the curves start flat. When the minimum wall temperature is increased, the optimal specific costs for a non-recuperated cycle start to increase a lot. This is caused by the close relation between evaporator inflow temperature of the working fluid and the minimum wall temperature. A higher minimum wall temperature will immediately force the condensing temperature

to be higher. Also the optimal solutions for case 1 with recuperator have a minimum wall temperature, which is around 100°C therefore the curves are flat again after the kink. Only for toluene this minimum wall temperature is around 80°C, therefore the curve for toluene is not flat after the kink.

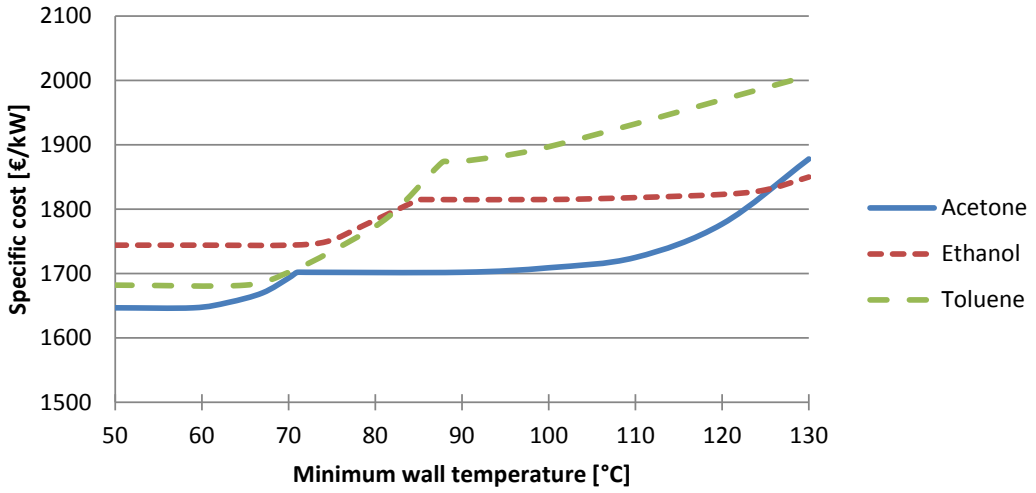

Figure 5.13: plot of optimization results for case 3, showing the effect of the minimum evaporator wall temperature on the specific cost

From the figure it can be concluded that acetone is the best working fluid for most minimum wall temperatures. Only around 70°C toluene performs slightly better and above 130°C ethanol performs better. Acetone is rather sensitive for the minimum wall temperature. This is caused mainly by the maximum temperature of 276.85°C of the acetone model in Refprop, which limits the turbine inlet temperature and the amount of superheat. Therefore the recuperator has a limited ability to preheat the liquid before entering the evaporator. Ethanol on the other hand is effected only slightly by this limitation, this was not expected, as it has a wet saturated vapor curve, and the vapor leaves the turbine in case 1 with only a slight bit of superheat. To have enough heat available in the recuperator more superheat needs to be added in the evaporator, which in principle reduces the mass flow. For ethanol though the effect of reduced massflow is effectively compensated by the effect of increasing isentropic enthalpy difference over the turbine as was described in section 5.2.2. Last there is Toluene, which shows to be very sensitive for the increase in minimum wall temperature mainly due to the application of the recuperator, which causes a relatively large pressure drop. The influence of the pressure drop was already shown in section 3.5

5.6. CASE 4, MINIMUM FLUE-GAS OUTFLOW TEMPERATURE

In contrast with case 3, in this case the in literature more common definition of the minimum outflow temperature is used to prevent sulfuric acid condensation. The main purpose of this case is analyzing the difference between the two definitions. The limitation of the flue-gas outflow temperature is normally used in literature, because in most studies there is no model used, describing the heat transfer in the evaporator. Only the stream properties are known, so when condensation of flue-gases must be taken into account limiting the outflow temperature seems the best option.

Figure 5.14 shows the optimal specific cost taking into account a minimal flue-gas outflow temperature of 50°C to 160°C for acetone, ethanol and toluene. The figure is highly different compared to figure 5.13, most striking is the difference in temperature at which it is more economic to use a recuperator instead of not using it. In case 3 it was shown that the increase of wall temperature caused a huge decrease in power production and increase of cost for the cycles without recuperator, as the condensation temperature needed to be increased to meet the minimum wall temperature.

Now when only the flue-gas outflow temperature is limited the cycles without recuperator perform reasonably good up to much higher temperatures. For toluene it is even more efficient to have no recuperator up to the upper limit of 160°C.

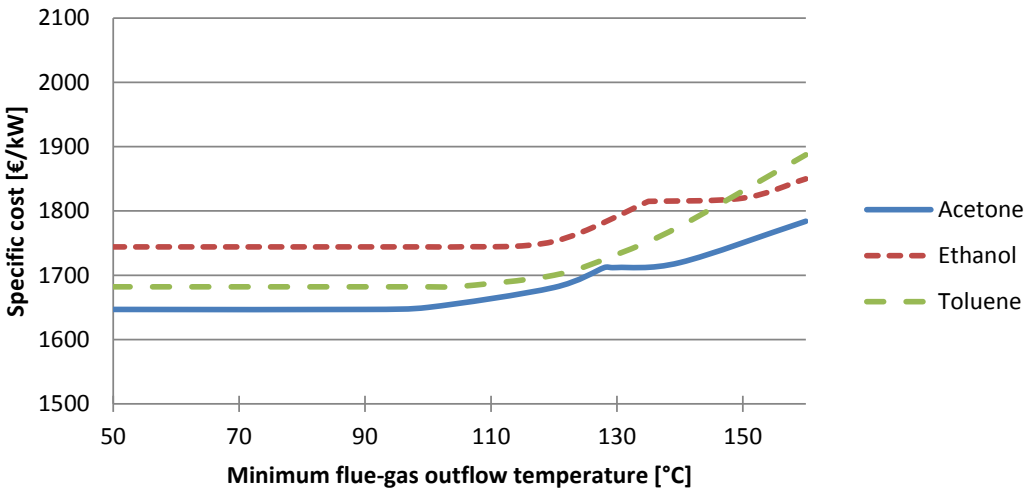

Figure 5.14: plot of optimization results for case 4, showing the effect of the flue-gas minimum outflow temperature on the specific cost

As appeared from case 3, the wall temperature is closely related to the working fluid inflow temperature. Harmful acids are expected to condense already on the wall when the wall temperature is below the sulpuric acid dew point and/or water dew point while the flue-gas temperature is still far above these temperatures. Therefore it is recommended to use the working fluid temperature at the inlet of the evaporator as limiting variable when no detailed evaporator model is used and condensation of acids must be prevented.

5.7. CASE 5, AMBIENT TEMPERATURE

In this case the sensitivity of the results for a the ambient temperature is tested, the ambient temperature is varied from 0°C to 40°C, case 2 is used as basis. This is done to evaluate whether it is useful to have different modules for different climates. In addition the sensitivity may be different per fluid, from which it may be concluded that some fluids are more suitable for colder climates, while others fit better in warmer climates.

In figures 5.15 and 5.16 the optimization results are shown, both the specific cost as well as the net power output are given. The figure shows a remarkable difference between the optima for toluene and acetone. Acetone shows a large decrease of specific costs and increase of net power for lower ambient temperatures. This can be easily explained by the reduced condensation pressure that can be reached due to the lower ambient temperature. The specific cost decrease for toluene at low ambient temperatures on the other hand, is much smaller, also the cost increase at higher ambient temperatures is rather small. This is caused by the low condensation pressure of toluene in combination with the pressure drop over the recuperator. Already in case 2 it was shown that toluene suffers from a large pressure drop over the recuperator which decreased the total turbine output power. Now when the condensation pressure is decreased the density decreases, and pressure drop increases. Which effectively causes only a small increase of turbine power. Therefore the results for Toluene at ambient temperatures below 30°C show a constant condensation temperature of around 57°C, the only reduction in specific cost is caused by the reduction of cooling power consumption and cost.

Ethanol suffers slightly from the same effect at low ambient temperatures. The curves in the two

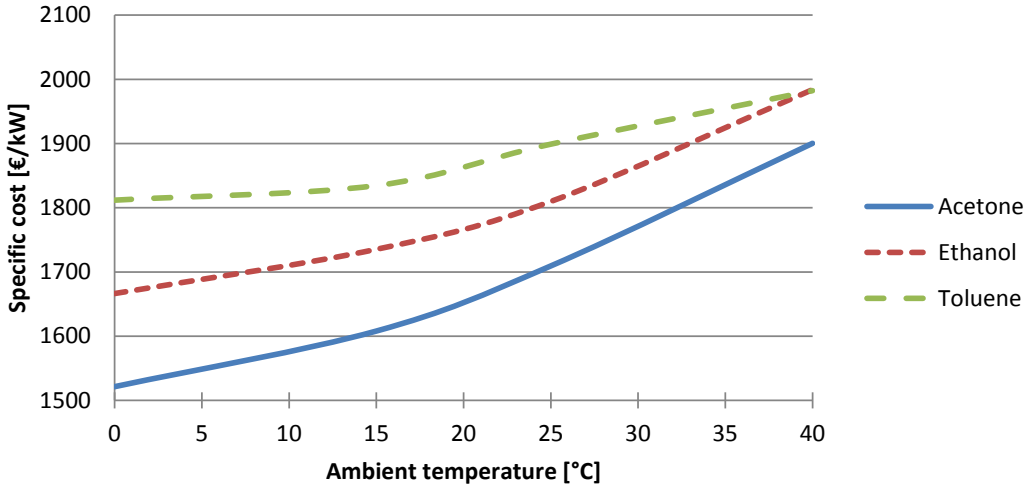

Figure 5.15: plot of optimization results for case 5, showing the effect of the ambient temperature on the specific cost

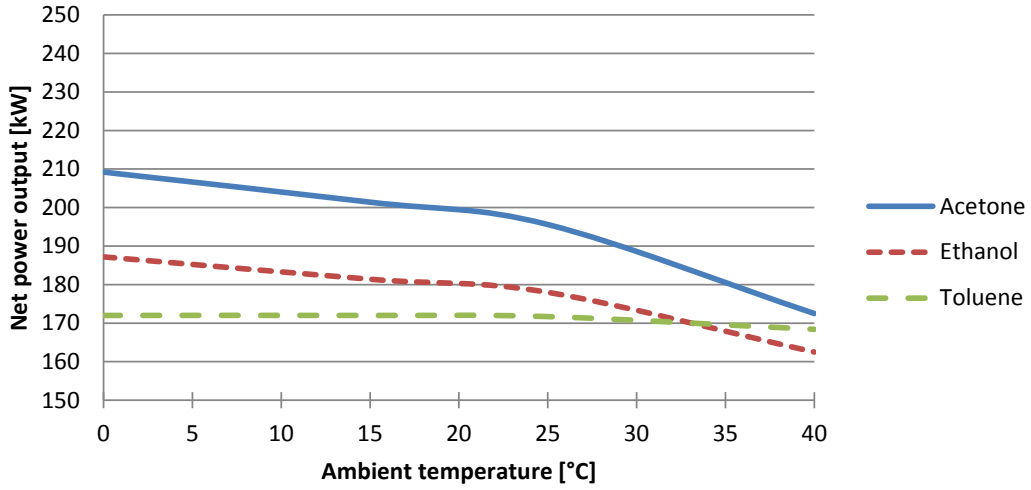

Figure 5.16: plot of optimization results for case 5, showing the effect of the ambient temperature on the net power output

figures flatten a bit for these lower temperatures as at condensation temperatures below 50°C the pressure drop becomes significant for ethanol also.

This results would be highly different when case 1 would have been used as the reference case and when there would not have been a limit on the wall temperature. Because when the application of a recuperator is not necessary the influence of pressure drop for toluene would be smaller, and the condensation temperature would be lower for toluene also. On the other hand, to prevent water condensation in the evaporator, the minimum wall temperature in the evaporator would need to be around 50-60°C which would limit the condensation temperature or raise the need for a recuperator again.

From these results it can be concluded that toluene is more suitable as working fluid in warmer climates than it is for colder climates. Also it can be concluded for toluene that there is no use in a specified module for colder climates. Because even the optimized results show that only the cooling system needs to be adapted to the ambient temperature. For acetone and ethanol on the other hand the effect of ambient temperature is much larger, also the results indicate that when a specified design is made for colder climates acetone or ethanol would be preferred.

5.8. CASE 6, MAGNITUDE OF FIXED COST

In case 6 the magnitude of the fixed cost is varied to analyze the effect of the fixed cost on the optimal process parameters. It is expected that for lower fixed cost a less efficient cycle is preferred in which there are larger temperature differences over the heat exchangers, in order to further reduce the cost of the total cycle and make a more optimal cost to power ratio. For the sake of clarity of the solutions it is chosen to simulate all cycles with recuperator, even though the optimal solution for the cycles with low fixed costs would be without recuperator. This is chosen in order to have clearer trends in the figures, which makes the explanation easier to understand. In addition the fixed cost will never decrease to values this low in practice.

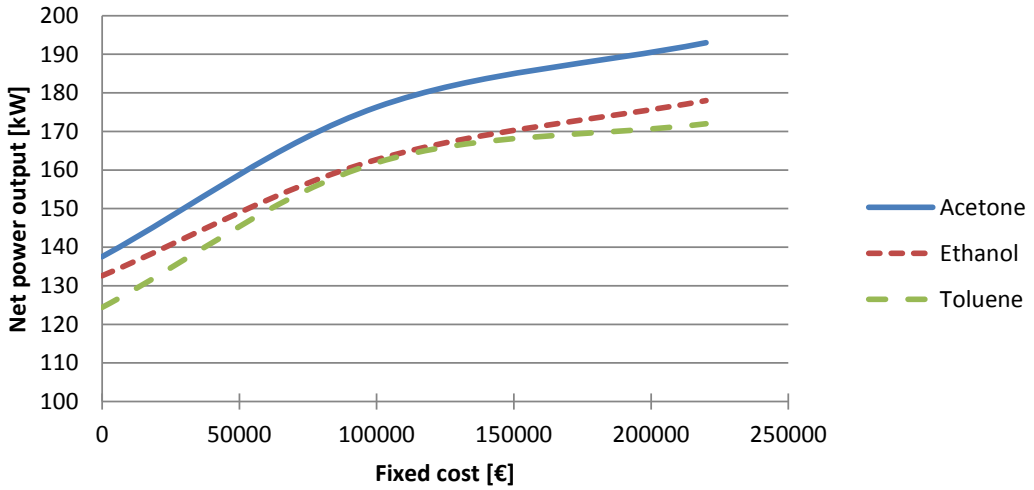

Figure 5.17: plot of optimization results for case 6, showing the effect fixed cost on the net power output

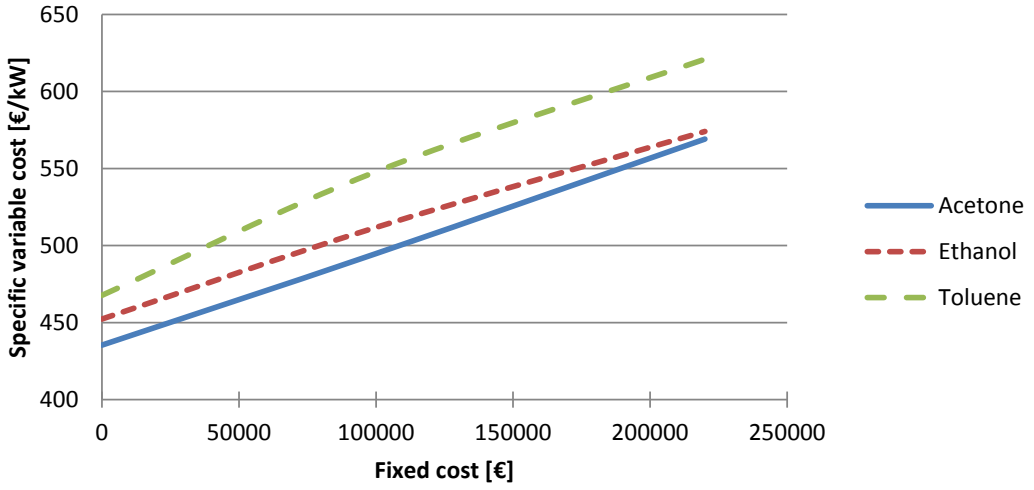

Figure 5.18: plot of optimization results for case 6, showing the effect of fixed cost on the optimal specific variable cost

In figure 5.17 the net power production of the optimal solutions is shown for a range of fixed costs from €0 to €220.000. The figure shows as already expected an increase of power production with increasing fixed cost. When the fixed cost would be infinitely large the net power production would approach the maximum achievable power production as component cost is becoming less significant with respect to the fixed cost. Therefore the curves approach a horizontal asymptote.

The increase of the specific variable cost is shown in figure 5.18, from this figure it can be concluded that indeed the specific variable cost is increasing with increasing fixed cost. Figure 5.19 shows there is a nearly linear relation between fixed cost and variable cost. This indicates that the cost reduction due to reduction in fixed cost is much larger compared to the reduction in specific variable cost.

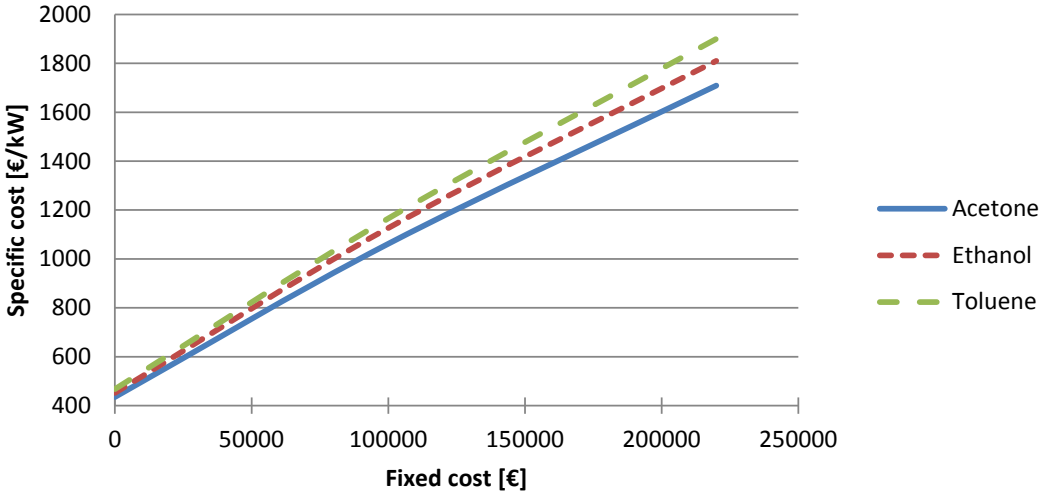

Figure 5.19: plot of optimization results for case 6, showing the effect of fixed cost on the optimal specific cost

If power output and specific variable cost are changing some process parameters and geometry must change as well. From the results it is found that most parameters remain more or less constant, most influenced are the evaporator pinch temperature difference (figure 5.20), the condensation temperature (figure 5.21) and the shell diameter. With the condensation temperature obviously also the water temperature and mass flow change. The turbine inlet pressure, the degree of superheat and the effectiveness of the recuperator where found to remain more or less constant, as these determine largely the performance of the cycle and because the recuperator effectiveness is necessary to meet the boundary conditions. These parameters on the other hand have only small influence on the cost.

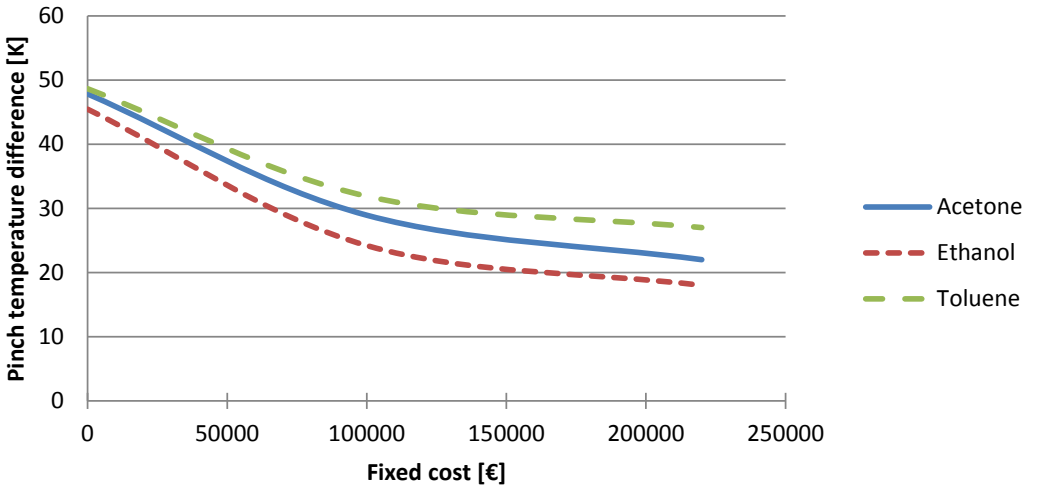

Figure 5.20: plot of optimization results for case 6, showing the effect of fixed cost on the optimal pinch temperature difference in the evaporator

From these results it can be concluded that the magnitude of the fixed cost has an influence

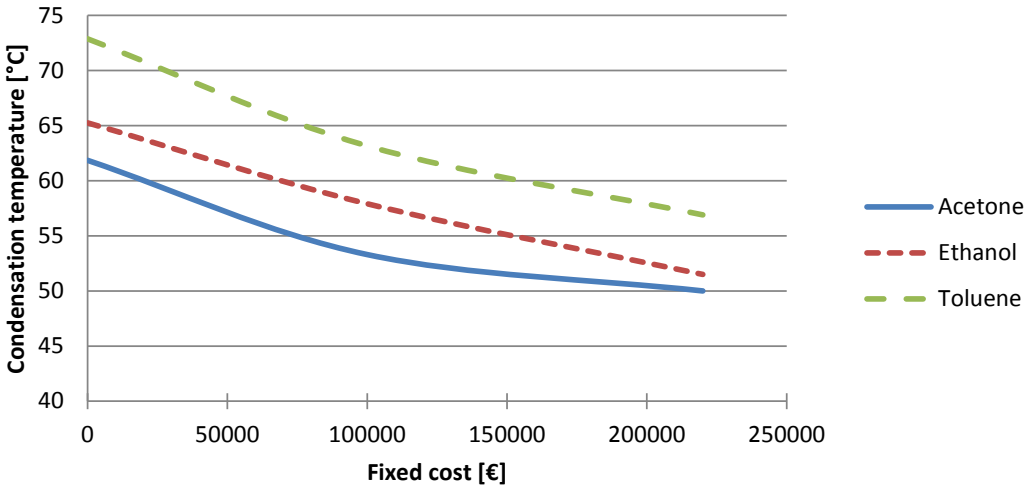

Figure 5.21: plot of optimization results for case 6, showing the effect of fixed cost on the optimal condensation temperature

on the optimal process parameters and system design. And that in case of significantly reduced fixed cost, a less efficient and less expensive cycle design would be favored. Therefore when a new system is designed and effort is done to decrease the fixed cost, this reduction in cost may be taken into account already when selecting the process parameters in order to achieve minimal specific cost. Also it can be concluded that in fluid selection and system optimization the total system cost must be taken into account, not only the cost of the main components.

6

CONCLUSIONS AND RECOMMENDATIONS

In this work the Organic Rankine Cycle (ORC) is optimized to minimum specific cost, for application with a 350 °C heat source and a mass flow rate of 5 kg/s. It is found that under all tested circumstances lowest specific cost is reached using acetone as working fluid. If clean flue-gases are used and outflow temperatures are not limited, a cycle without recuperator can reach a minimum specific cost of around €1650,- per kW, toluene as well performs good under these circumstances with slightly higher specific costs of €1680,- per kW. When flue-gases or regulations yield limitations on outflow temperature or minimum wall temperature, specific cost increases. In the case of a minimum evaporator wall temperature of 100°C the specific cost increases to around €1700 and €1900 per kW respectively. Main cause of the small increase of specific cost for acetone relative to the increase of the specific cost for toluene, is the application of the recuperator and the impact of the pressure drop associated with the recuperator. The impact of this pressure drop is much smaller for acetone as it has a relatively high condensation pressure at 50°C of 0.8 bar, in contrast with the low condensation pressure of toluene, which is 0.1 bar.

For selecting a working fluid, for an ORC applied with high temperature gaseous waste heat, a number of guidelines are given here. This first set of guidelines is found useful for the preselection of working fluids.

1. For heat sources with a relatively high temperature, above 250°C, the sub-critical cycle was found to be the best option. At lower heat source temperatures the exergy destruction in the evaporator is relatively large which makes it relevant to reduce the average temperature difference in the evaporator. The transcritical cycle and the sub-critical cycle with a mixture as working fluid have a better matching temperature profile in the evaporator which increases the cycle efficiency at low temperatures with about 10%. The efficiency increase at higher temperatures was found to be only a few percent, which can not compensate for the increased pressure and complexity.

2. The temperature slope of the flue-gas needs to be more or less parallel to the slope of the working fluid temperature in the preheater. This is necessary to make sure there is no unnecessary exergy destruction and to make sure the evaporator size is limited. Based on the average heat capacity during preheat it can be assessed whether a working fluid fits a heat source temperature or not, using the optimal heat source temperature (OHST) theory.

3. Condensation pressure is preferred to be around 1 bar. This reduces the impact of pressure drop on system performance with respect to lower condensation pressures, and enables the application of more compact heat exchangers. Whether the condensation pressure is chosen

to be higher or lower then 1 bar depends on the preference for leakage of air into or working fluid out of the system

4. A highly important parameter for the design of a Rankine cycle for a high temperature heat source, is the thermal stability of the working fluid. Unfortunately literature on thermal stability of working fluids is limited.

To asses the cycle performance and compare the performance of different working-fluids a thermodynamic model of the cycle may be used. To find the optimal process parameters an optimization algorithm is necessary, no rule of thumb is found to select for example the optimal turbine inlet pressure. For the design of an optimization model for a gaseous waste heat recovery ORC the following set of considerations can be taken into account.

1. When condensation of sulfuric acid in flue-gases is expected to limit the cooling of the flue-gases, this can be accounted for by applying a minimum wall temperature to the used evaporator model. If the used evaporator is not detailed enough, the inflow temperature of the working fluid in the evaporator can be limited as well. Highly different results where found when this limitation was modeled as a limitation on the flue-gas outflow temperature instead.

2. In literature, and from the sensitivity analysis it is found that a good estimation of the turbine efficiency is necessary in order to be able to compare process parameters and working fluids. A better model for radial turbines is preferred, on the other hand, the simplicity of the currently used model fits in a cycle optimization model.

3. To make an estimation of the pressure drop and cost of the heat exchangers simpler models can be applied compared to those applied in this work. At this stage of system design the precise design of the heat exchangers is not yet relevant and is hard to optimize as it depends on many aspects. For example the Kern correlations can be used for estimation of heat transfer in shell and tube heat exchangers.

4. Including water loop and flue-gas in the analysis, is useful for determining specific cost. Also it gives good insight in the influence of flue-gas pressure drop limitations and ambient temperature. An interesting addition to the currently performed analysis would be assessing the influence on cooling cost when the process parameters are fixed and only the water flow, water temperature and ambient temperature are varied. In order to asses the applicability of the module in different climates.

The optimal working fluid is found to be acetone. Due to its isentropic saturated vapor curve it performs well thermodynamically and due to the relatively high condensation pressure, the cost of the recuperator and condenser as well as the pressure drop in these components is low. Condenser and recuperator models where used in this work to balance performance, pressure drop and cost. It was found that for the comparison of different heat exchanger designs, highly accurate validated models must be used in order to have a significant comparison. In addition the influence of pressure, fouling, sealing and size on total system cost and applicability of a heat exchanger type with process conditions should be evaluated as well. Therefore it is thought that it is better to select a heat exchanger design when working fluid and process parameters are roughly known.

Although toluene is not the optimal working fluid a set of conclusions is drawn here which are related to the use of toluene with heat source temperatures of around 350°C. This is done because the application of toluene performs well under certain circumstances and will probably be a more economical alternative for Triogen as they are already experienced with toluene.

1. The main cause for the relatively high specific cost for toluene, is the decrease of turbine power due to the pressure drop in the recuperator. Under circumstances where the application of the recuperator is not necessary or the pressure drop over the recuperator is less significant, toluene shows to be more competitive to acetone. First of these circumstances is no limitation on the evaporator wall temperature or clean fuel, in this case no recuperator is necessary. Second is high ambient temperatures, at high ambient temperatures toluene condensates at a higher pressure and pressure drop over the recuperator is less significant. Last toluene performs slightly better, relative to other working fluids, when fixed costs are low. Because also under these circumstances condensation pressure is increased and the influence of recuperator pressure drop is reduced.

2. In order to have good thermodynamic performance using toluene in combination with low specific cost it is advised to have a relatively low turbine inlet pressure of around 10 bar. It was observed that an increase of turbine inlet pressure leads to an increase of isentropic enthalpy difference over the turbine, though also to a reduction in isentropic turbine efficiency and mass flow. In addition pressure requirements for the recuperator and evaporator are milder possibly leading to cost reduction in these components. Last benefit of a low evaporation temperature is the applicability with even lower heat source temperatures, due to the low evaporation temperature.

Based on former considerations, it is recommended for Triogen to develop a new module, using again toluene as working fluid. The turbine inlet pressure of this cycle should be reduced to around 10 to 15 bar in order to increase turbine and ultimately cycle efficiency and to ensure better applicability with lower temperature heat sources. A condensation temperature of around 55-60 °C is recommended to ensure applicability in warmer climates, and because performance increase with lower condensation temperatures was found to be small.

To conclude there are two additional recommendations for Triogen. First it is concluded that in order to dramatically reduce specific cost, either system size must be increased or fixed cost must be decreased. It is expected, more cost reduction can be reached by evaluating and redesigning the rest of the system compared to redesigning the main components and selecting an alternative working fluid. Secondly it was found that when there is no limitation of outflow temperature the specific costs can be decreased by around 10% by removing the recuperator. It is recommended to evaluate for what types of flue-gases it is necessary to use a recuperator to prevent excessive corrosion in the evaporator, and in what cases the recuperator is not necessary. In addition a new system design must be made without a recuperator.

A

SHELL AND TUBE GEOMETRY

The geometry is defined using the correlations by Shah and Sekulic [39], all equations are given here as they are used in the recuperator and condenser model. The heat exchanger geometry can be defined by the user or optimization algorithm using the parameters given in table A.1. For the condenser baffle spacing and baffle cut are irrelevant.

Table A.1: Definition of shell and tube heat exchanger geometry

	Parameter	**Unit**	**Used range**
Shell diameter	D_s	[m]	0.5
Tube outside diameter	d_o	[m]	0.16-0.20
Relative tube pitch	P_t/d_o	[-]	1.2-2.0
Relative baffle spacing	$L_{b,c}/D_s$	[-]	0.2-1.0
Relative baffle cut	l_c/D_s	[-]	0.3
Tube wall thickness	δ_{tw}	[m]	0.001
Nozzle diameter	D_N	[m]	$0.5 * D_s$

For the recuperator a 30°triangular tube staggering is used which makes $C_t = 0.866$. with a longitudinal pitch $X_l = (3/2)^{1/2} P_T$ and a transverse tube pitch $X_t = P_t$. The pitch ratio's a and b are defined as $a = X_t/d_o$ and $b = X_l/d_o$.

The number of tubes is calculated using equation A.1

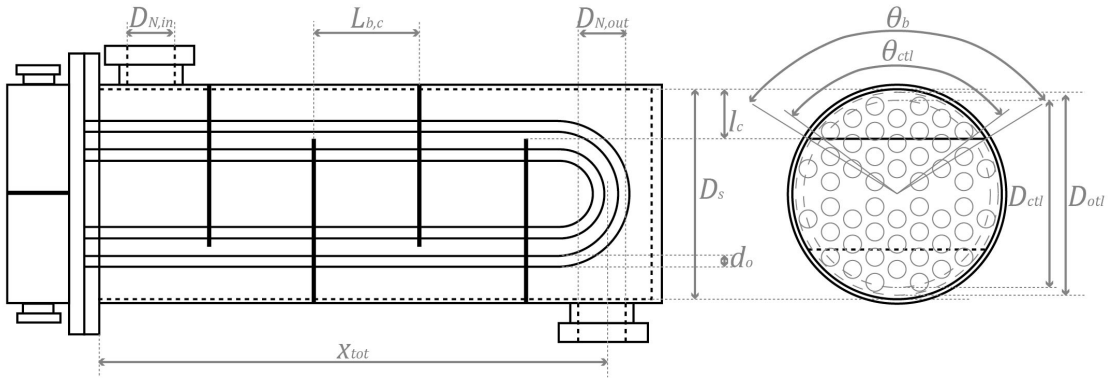

Figure A.1: Nomenclature for basic shell and tube heat exchanger geometry

$$N_t = \frac{(\pi/4)D_{ctl}^2}{C_t * P_t^2}(1-\psi_t) \tag{A.1}$$

In which $D_{ctl} = D_{otl} - d_o$ is the central tube limit which is represented graphically in figure A.1, the outer tube limit is defined in equation A.2, ψ_t is a correction factor for the number of passes given in equation A.3 for two tube passes.

$$D_{otl} = D_s - (0.017 * D_s + 0.0265) \tag{A.2}$$

$$\psi_t = 19.985 * D_{ctl}^{-0,975} \tag{A.3}$$

A.1. WINDOW SECTION

The area of the window section is calculated using equation A.4.

$$A_{fr,w} = \frac{\pi}{4}D_s^2(\frac{\theta_b}{2\pi} - \frac{sin\theta_b}{2\pi}) \tag{A.4}$$

where θ_b is the baffle cut angle, which is represented in figure A.1 graphically and given in equation A.5.

$$\theta_b = 2cos^{-1}(1-2l_c/D_s) \tag{A.5}$$

And the fraction of tubes in the window section is

$$F_w = \frac{\theta_{ctl}}{2\pi} - \frac{sin\theta_{ctl}}{2\pi} \tag{A.6}$$

in which θ_{ctl} is

$$\theta_{ctl} = 2cos^{-1}(\frac{D_s - 2l_c}{D_{ctl}}) \tag{A.7}$$

Now the number of tubes in the window section can be calculated from the fraction of tubes in the window section and the window area occupied by tubes is

$$A_{fr,t} = \frac{\pi}{4}d_o^2 F_w N_t \tag{A.8}$$

The net flow area in the window section is $A_{o,w} = A_{fr,w} - A_{fr,t}$ and the hydraulic diameter of the window section is

$$d_{h,w} = \frac{4 * A_{o,w}}{P} \tag{A.9}$$

in which P is the wetted perimeter of the shell and the tubes in the window region. A last geometrical parameter for the window section is the number of effective tube rows in crossflow in the window section:

$$N_{r,cw} = \frac{0.8}{X_l}[l_c - 1/2(D_s - D_{ctl}] \tag{A.10}$$

A.2. CROSS FLOW SECTION

The fraction of the tubes in the crossflow section is $F_c = 1 - 2F_w$. The number of tube rows crossed during flow through one crossflow section is estimated using equation A.11.

$$N_{r,cc} = \frac{D_s - 2l_c}{X_l} \tag{A.11}$$

The crossflow A_f is defined as

$$A_f = D_s * L_{b,c} \tag{A.12}$$

A.3. BYPASS AND LEAKAGE FLOW AREAS

Tube to baffle and shell to baffle leakage area's are given in equations A.13 and A.14 respectively. In which $\delta_{sb} = 0.0031 + 0.004 * D_s$ mm and $\delta_{tb} = 0.0004$ mm.

$$A_{o,tb} = \frac{\pi}{4}[(d_o + \delta_{tb})^2 - d_o^2]N_t(1 - F_w) \tag{A.13}$$

$$A_{o,sb} = \pi D_s \frac{\delta_{sb}}{2}(1 - \frac{\theta_b}{2\pi}) \tag{A.14}$$

B

SHELL AND TUBE CORRELATIONS

B.1. SINGLE PHASE SHELL SIDE

B.1.1. HEAT TRANSFER

The average Nusselt number for ideal crossflow is calculated using equation B.1

$$Nu_{s,av} = 0.3 + (Nu_{s,lam}^2 + Nu_{s,turb}^2)^{1/2} \tag{B.1}$$

In which the laminar and turbulent Nusselt number are defined in equation B.2 and B.3 respectively.

$$Nu_{s,lam} = 0.644 * Re_s^{1/2} Pr^{1/3} \tag{B.2}$$

$$Nu_{s,turb} = \frac{0.037 * Re_s^{0.8} Pr}{1 + 2.443 Re_s^{-0.1} (Pr^{2/3} - 1)} \tag{B.3}$$

$$Nu_s = Nu_{s,av} f_G f_A f_L \tag{B.4}$$

$$f_G = 1 - (2F_w) + 0.524(2F_w)^{0.32} \tag{B.5}$$

$$f_A = 1 + \frac{2}{3 * X_l / d_o} \tag{B.6}$$

$$f_L = 0.4 \frac{A_{o,tb}}{A_{o,tb} + A_{o,sb}} + (1 - 0.4 \frac{A_{o,tb}}{A_{o,tb} + A_{o,sb}}) exp(-1.5 \frac{A_{o,tb} + A_{o,sb}}{A_{o,cr}}) \tag{B.7}$$

B.1.2. PRESSURE DROP

$$\Delta p_c = \xi n_{MR} \frac{\rho w^2}{2} \tag{B.8}$$

For staggered tube arrangement the moody friction factor is given by

$$\xi = \xi_{lam} f_{z,l} + \xi_{turb} f_{z,t} [1 - exp(-\frac{Re + 200}{1000})] \tag{B.9}$$

In this equation the correction factors for viscosity changes near the wall ($f_{z,l}$ and $f_{z,l}$) are neglected as they are small and add a large amount of computational time. the friction factor for laminar flow is calculated using equation B.10.

$$\xi_{lam} = \frac{f_{a,l,v}}{Re} \tag{B.10}$$

In which $f_{a,l,v}$ is given by

$$f_{a,l,v} = \frac{280\pi[(b^{0.5}-0.6)^2+0.75]}{(4ab-\pi)a^{1.6}} \; for \; b \geq 0.5\sqrt{2a+1} \tag{B.11}$$

and

$$f_{a,l,v} = \frac{280\pi[(b^{0.5}-0.6)^2+0.75]}{(4ab-\pi)a^{1.6}} \; for \; b < 0.5\sqrt{2a+1} \tag{B.12}$$

The friction factor for turbulent flow is given by

$$\xi_{turb} = \frac{f_{a,t,v}}{Re^{0.25}} \tag{B.13}$$

with

$$f_{a,t,v} = 2.5 + \frac{1.2}{(a-0.85)^{1.08}} + 0.4(b/a-1)^3 - 0.01*(a/b-1)^3 \tag{B.14}$$

In this correlations Reynolds number is calculated differently compared to the heat transfer correlations as

$$Re = \frac{w d_o \rho}{\mu} \tag{B.15}$$

Additionally there is the pressure drop in the window sections which is calculated using

$$\Delta p_W = \sqrt{\Delta p_{W,lam}^2 + \Delta p_{W,turb}^2} \tag{B.16}$$

where

$$\Delta p_{W,lam} = \sqrt{\Delta p_{W,lam}^2 + \Delta p_{W,turb}^2} \tag{B.17}$$

$$\Delta p_{W,lam} = [\frac{56}{\frac{e w_z \rho}{\mu}} N_{r,cw} + \frac{52}{\frac{D_{h,w} w_z \rho}{\mu}} (\frac{L_{b,c}}{D_{h,w}}) + 2](\frac{\rho w_z^2}{2}) \tag{B.18}$$

$$\Delta p_{W,turb} = (0.6 n_{r,cw} + 2)(\frac{\rho w_z^2}{2}) \tag{B.19}$$

In which w_z is a function of the crossflow and window velocity

$$w_z = \sqrt{w * w_W} \tag{B.20}$$

with

$$w_W = \frac{\dot{V}}{A_{fr,w} - A_{fr,t}} \tag{B.21}$$

B.1.3. NOZZLES

The pressure drop in the nozzles i scalculated as

$$\Delta p_N = \xi_N(\frac{\rho w_N^2}{2}) \tag{B.22}$$

$$\xi_{N,in} = 3.308(\frac{A_N}{A_f})^{1.14}(\frac{d_N}{D_i})(\frac{D_{otl}}{d_N}) \tag{B.23}$$

and

$$\xi_{N,out} = 2.482(\frac{A_N}{A_f})^{1.14}(\frac{d_N}{D_i})(\frac{D_{otl}}{d_N}) \tag{B.24}$$

with

$$(\frac{A_N}{A_f}) = \frac{\pi/4 d_N^2}{\pi/4(D_i^2 - n_T d_o^2)} \tag{B.25}$$

B.2. SINGLE PHASE TUBE SIDE

For the heat transfer on the tube side of the shell and tube heat exchanger correlations for both the laminar and turbulent flow regime are used. The flow is assumed laminar for Reynolds numbers $Re < 2300$ and turbulent at $Re > 10^4$ in between there is a transition region. In this section first the heat transfer relations for laminar and turbulent flow are given, later the heat transfer for the transition region is given based on these correlations. All used correlations assume fully developed flow, which can be used because d_i/L will be small.

The Reynolds numbers for tube flow is given as

$$Re = \frac{w\rho d_i}{\mu} \tag{B.26}$$

The nusselt number for the laminar flow regime is given as

$$Nu_{lam} = 3.66 \tag{B.27}$$

The nusselt number for the turbulent flow regime is given as

$$Nu_{turb} = \frac{(\xi/8)RePr}{1 + 12.7\sqrt{\xi/8}(Pr^{2/3} - 1} [1 + 1/3(d_i/x)^2/3] \tag{B.28}$$

In which the latter term is neglected, the friction factor is given in equation B.32. The Nusselt number in the transition region is calculated by interpolating between the Reynolds number in the range $2300 < Re < 10^4$, as is shown in equation B.29.

$$Nu_{trans} = (1-\gamma)Nu_{lam,Re=2300} + \gamma Nu_{turb,Re=10^4} \tag{B.29}$$

where γ is given by

$$\gamma = \frac{Re - 2300}{10^4 - 2300}, \; 0 \leq \gamma \leq 1 \tag{B.30}$$

The pressure drop is calculated using

$$\Delta p = \xi \frac{l}{d_i} \frac{\rho w^2}{2} \tag{B.31}$$

with for turbulent flow

$$\xi = (1.8log_{10}(Re) - 1.5)^{-2} \; for \; Re \geq 2300 \tag{B.32}$$

and for laminar Hagen poiseuille flow

$$\xi = 64/Re \; for \; Re < 2300 \tag{B.33}$$

In addition friction factors for tube in and outflow are $xi_{in} = 1$ and $\xi_{out} = 0.64$

C

DATA SHEETS CASE 1 AND 2

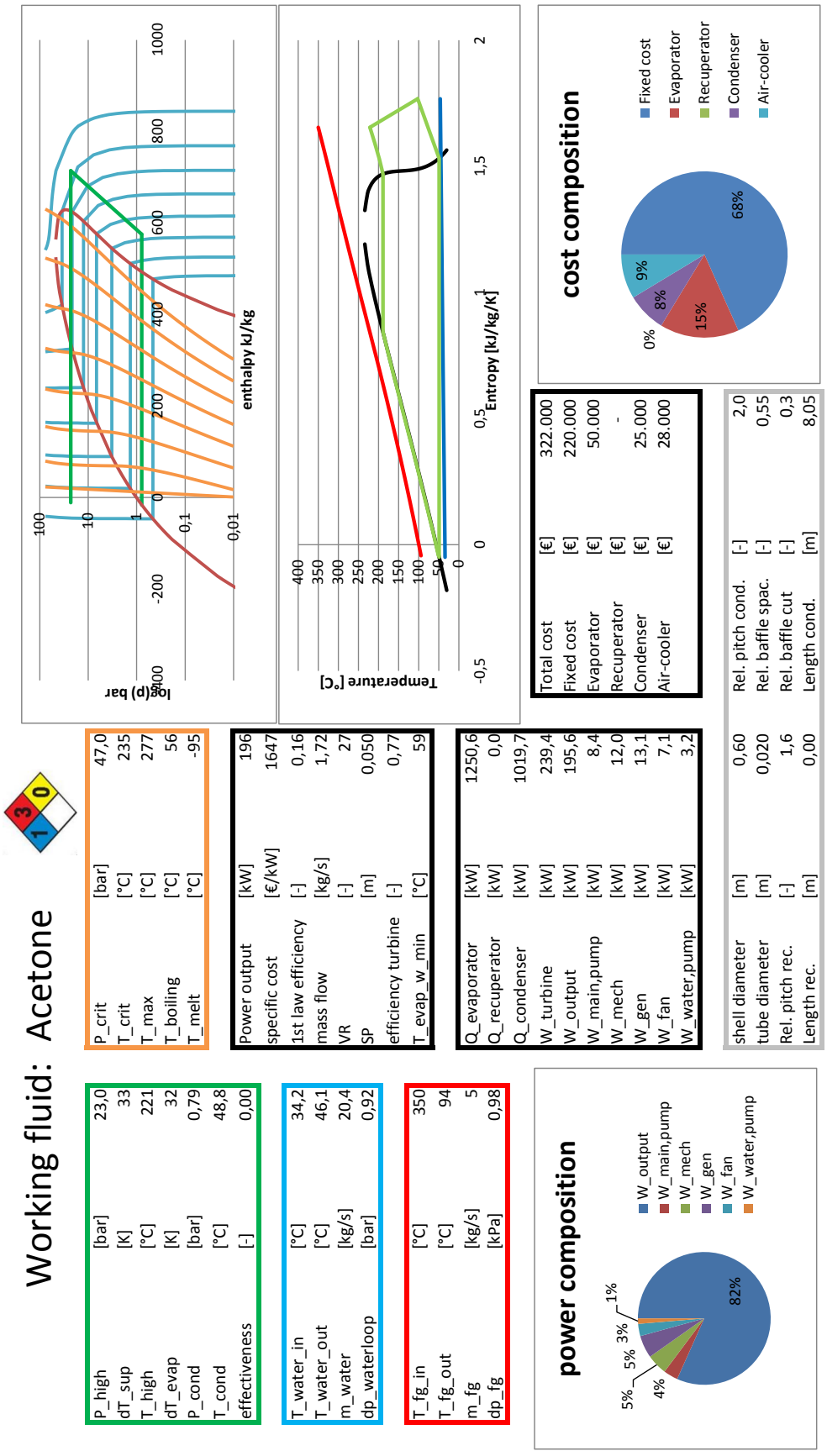

Figure C.1: Data sheet of optimal result for Acetone in case 1

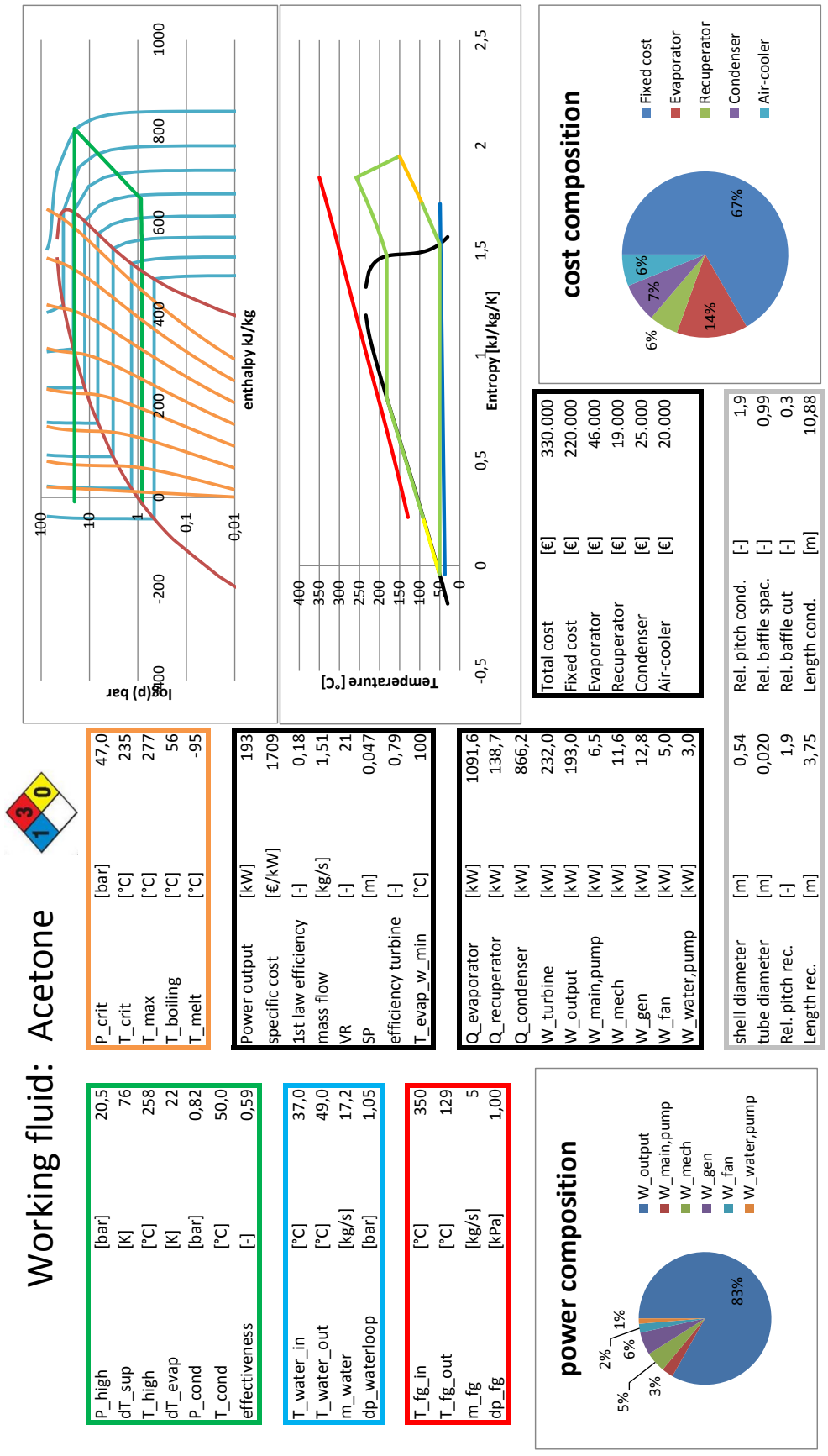

Figure C.2: Data sheet of optimal result for Acetone in case 2

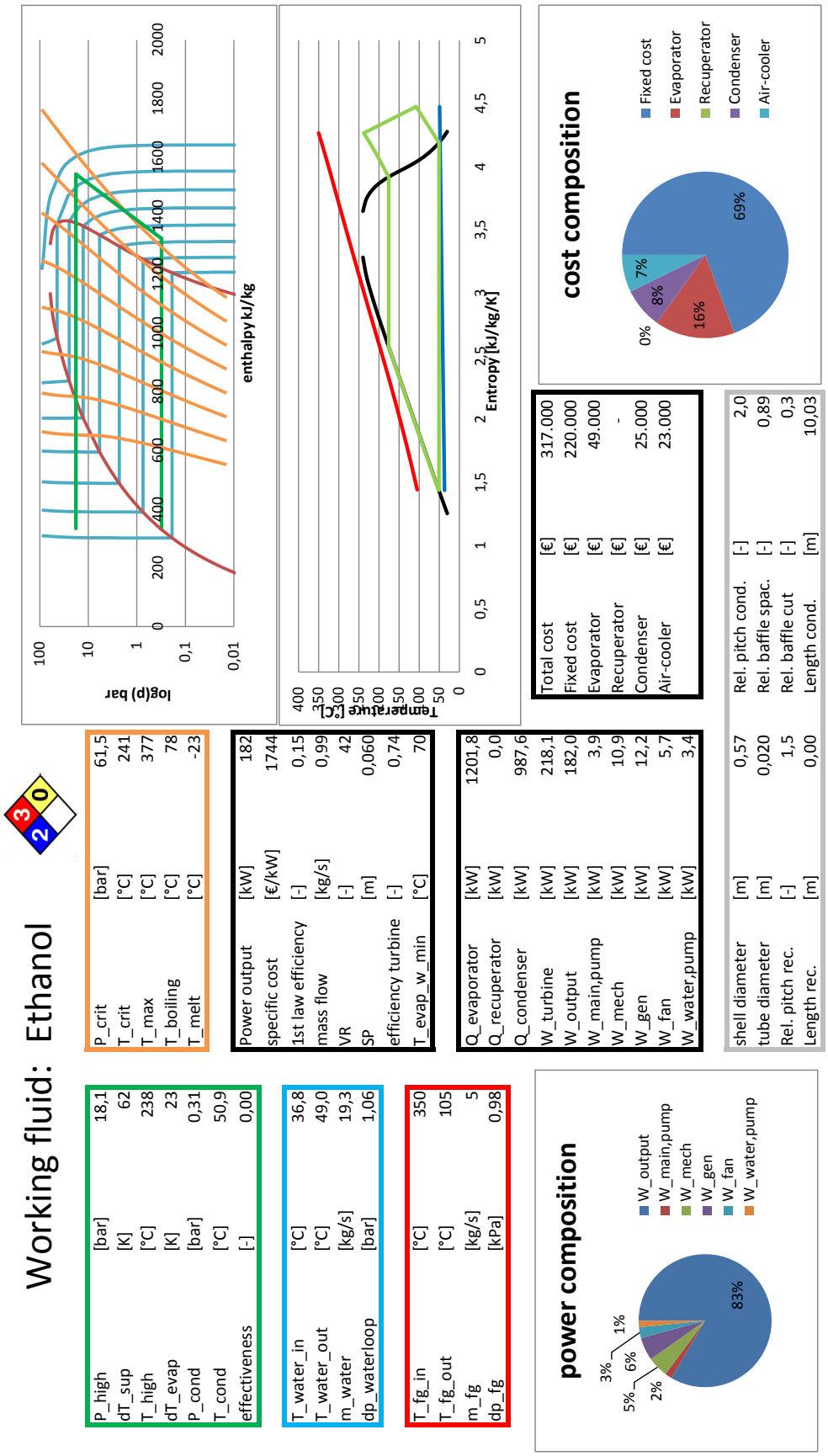

Figure C.3: Data sheet of optimal result for Ethanol in case 1

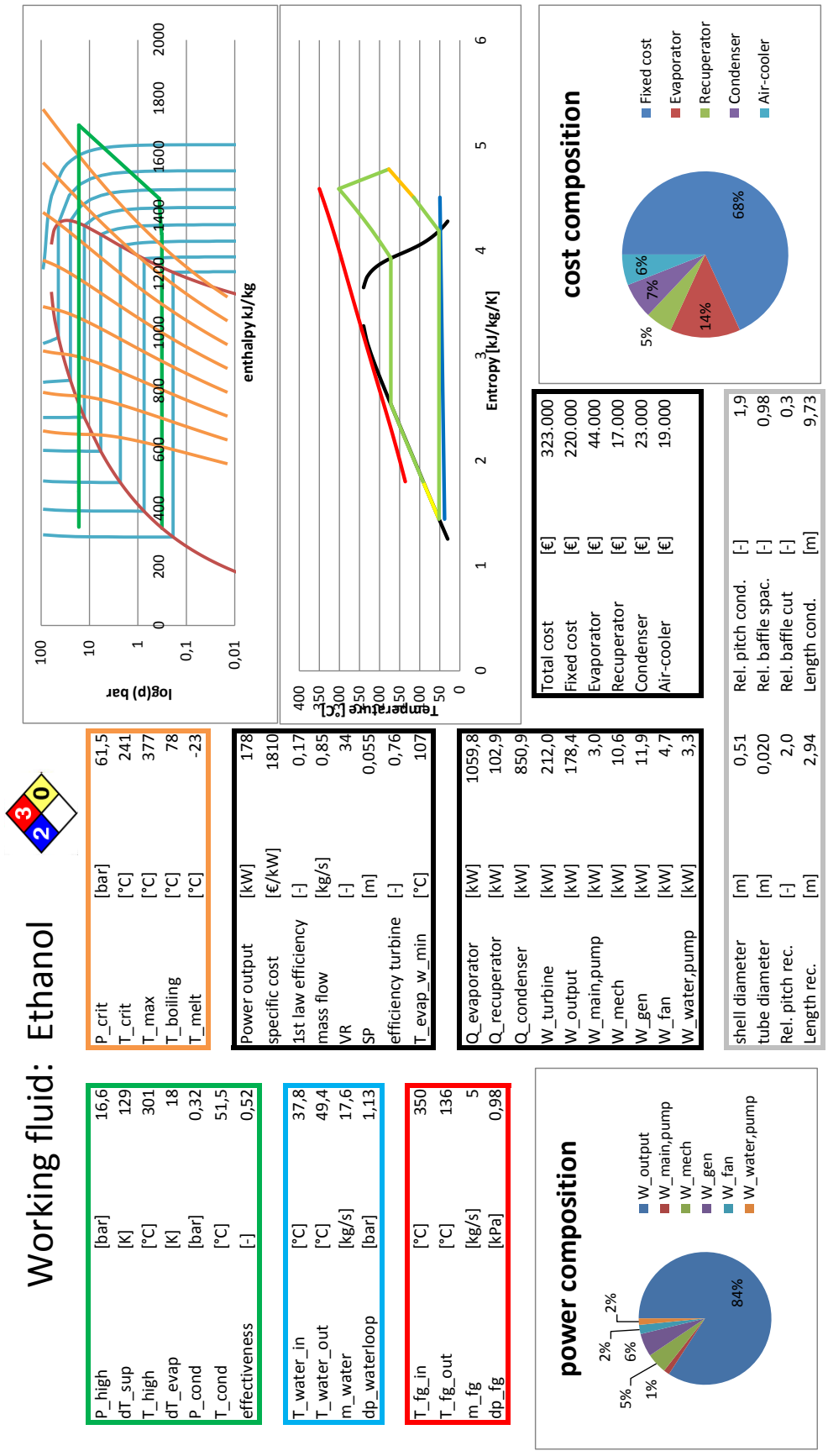

Figure C.4: Data sheet of optimal result for Ethanol in case 2

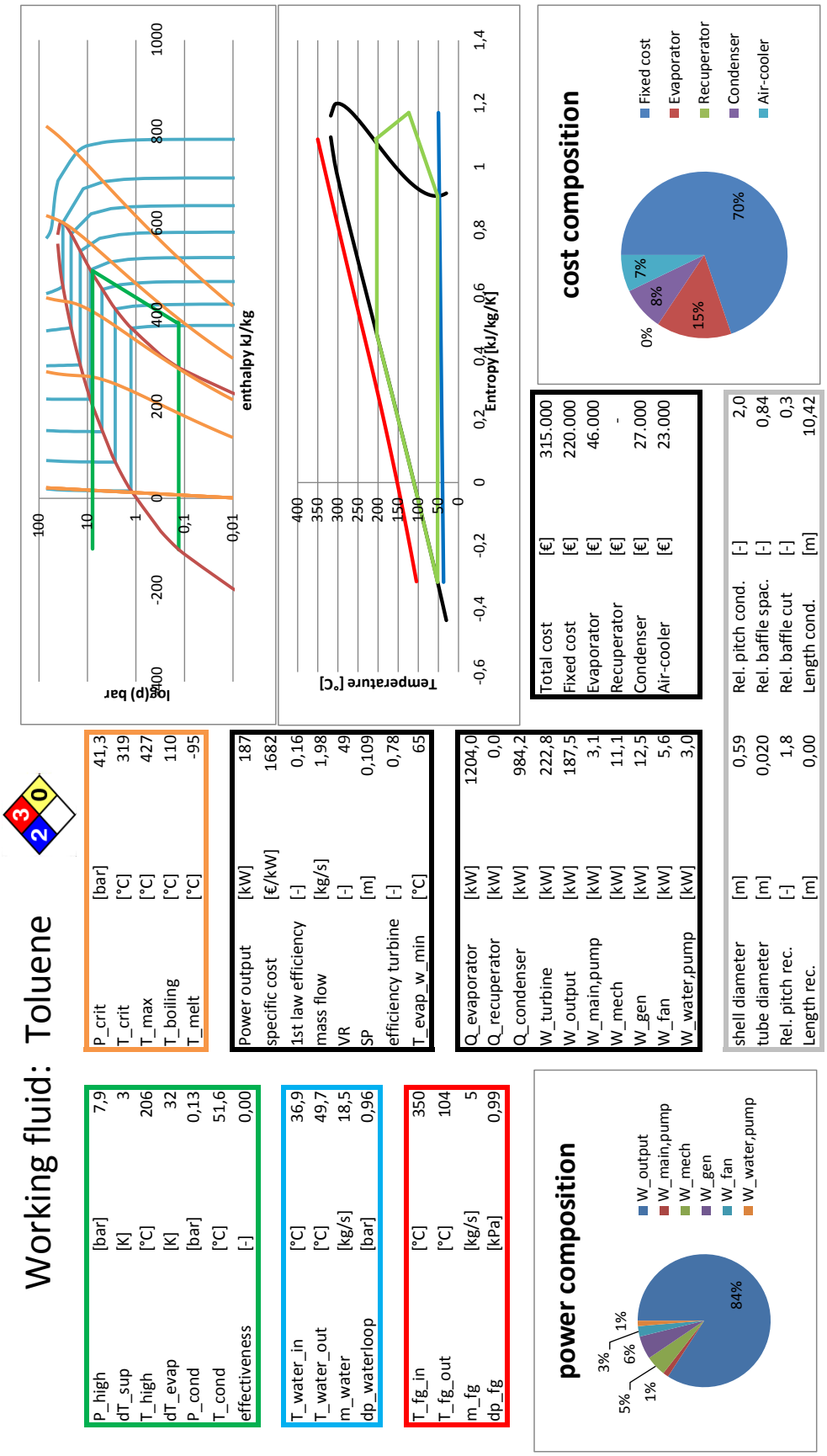

Figure C.5: Data sheet of optimal result for Toluene in case 1

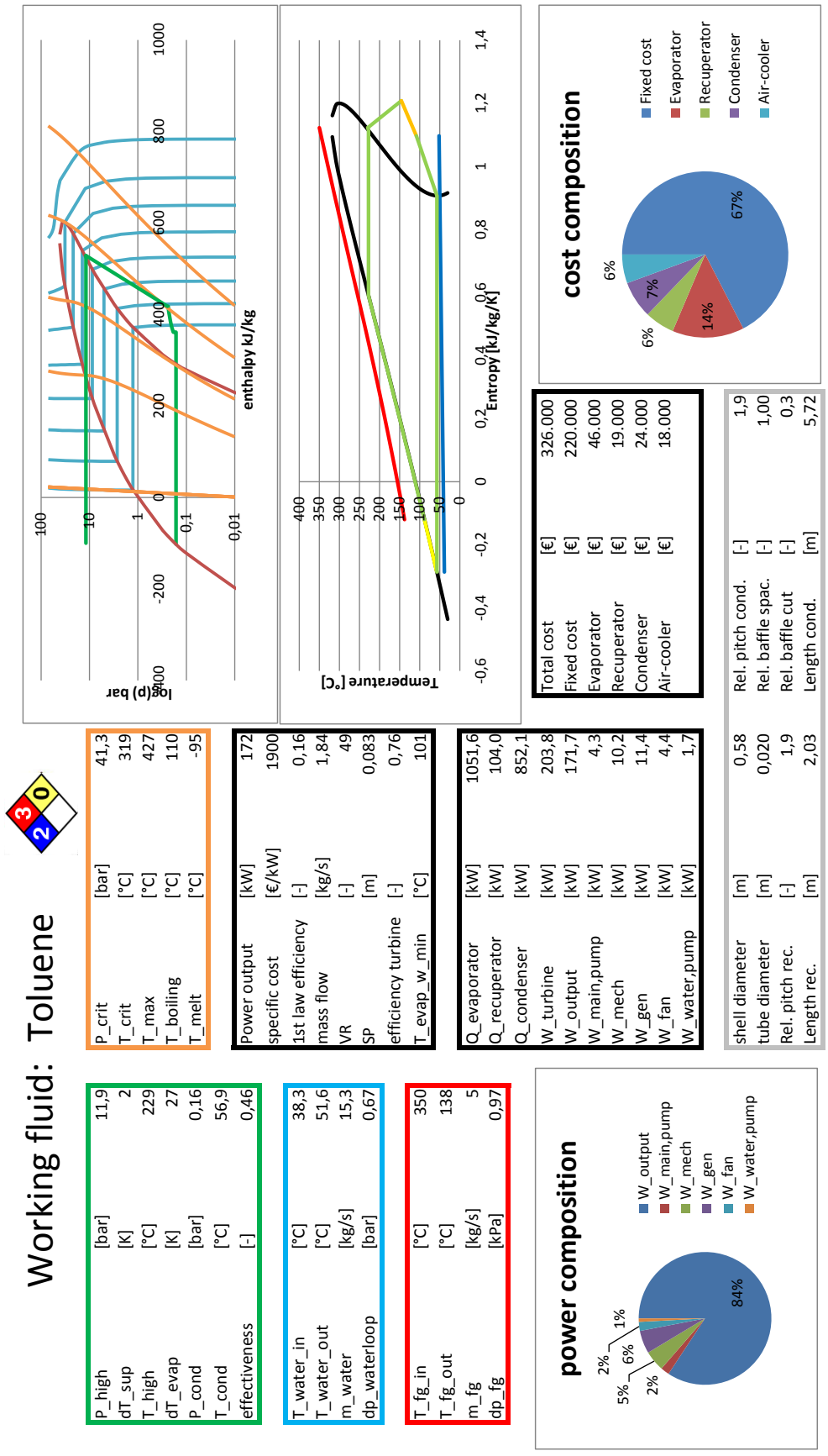

Figure C.6: Data sheet of optimal result for Toluene in case 2

BIBLIOGRAPHY

[1] P. Colonna, E. Casati, C. Trapp, T. Mathijssen, J. Larjola, T. Turunen-Saaresti, and A. Uusitalo, *Organic Rankine Cycle Power Systems: From the Concept to Current Technology, Applications, and an Outlook to the Future,* Journal of Engineering for Gas Turbines and Power **137**, 100801 (2015).

[2] B. T. Liu, K. H. Chien, and C. C. Wang, *Effect of working fluids on organic Rankine cycle for waste heat recovery,* Energy **29**, 1207 (2004).

[3] G. Shu, X. Li, H. Tian, X. Liang, H. Wei, and X. Wang, *Alkanes as working fluids for high-temperature exhaust heat recovery of diesel engine using organic Rankine cycle,* Applied Energy **119**, 204 (2014).

[4] H. Xi, M.-J. Li, Y.-L. He, and W.-Q. Tao, *A graphical criterion for working fluid selection and thermodynamic system comparison in waste heat recovery,* Applied Thermal Engineering **89**, 772 (2015).

[5] A. I. Papadopoulos, M. Stijepovic, and P. Linke, *On the systematic design and selection of optimal working fluids for Organic Rankine Cycles,* Applied Thermal Engineering **30**, 760 (2010).

[6] M. Lampe, M. Stavrou, H. M. Bucker, J. Gross, and a. Bardow, *Simultaneous optimization of working fluid and process for organic rankine cycles using PC-SAFT,* Industrial and Engineering Chemistry Research **53**, 8821 (2014).

[7] M. E. Mondejar, M. Thern, and M. Genrup, *Aerodynamic Considerations in the Thermodynamic Analysis of Organic Rankine Cycles,* ASME 2014 Power Conference , V002T09A016 (2014).

[8] F. Ahlgren, M. E. Mondejar, M. Genrup, and M. Thern, *Waste heat recovery in a cruise vessel in the Baltic Sea by using an organic Rankine cycle: a case study,* Journal of Engineering for Gas Turbines and Power **138**, 1 (2015).

[9] J. Xu, X. Luo, Y. Chen, and S. Mo, *Multi-criteria Design Optimization and Screening of Heat Exchangers for a Subcritical ORC,* Energy Procedia **75**, 1639 (2015).

[10] D. Maraver, J. Royo, V. Lemort, and S. Quoilin, *Systematic optimization of subcritical and transcritical organic Rankine cycles (ORCs) constrained by technical parameters in multiple applications,* Applied Energy **117**, 11 (2014).

[11] S. Lemmens, *A perspective on costs and cost estimation techniques for organic Rankine cycle systems,* in *ASME ORC 2015* (Brussels, 2015) pp. 1–10.

[12] J. Vivian, G. Manente, and A. Lazzaretto, *A general framework to select working fluid and configuration of ORCs for low-to-medium temperature heat sources,* Applied Energy **156**, 727 (2015).

[13] S. Lecompte, H. Huisseune, M. van den Broek, and M. De Paepe, *Methodical thermodynamic analysis and regression models of organic Rankine cycle architectures for waste heat recovery,* Energy **87**, 60 (2015).

[14] M. Chys, M. V. D. Broek, B. Vanslambrouck, and M. D. Paepe, *Potential of zeotropic mixtures as working fl uids in organic Rankine cycles,* EGY **44**, 623 (2012).

[15] M. Lampe, P. Edel, J. Schilling, J. Gross, and A. Bardow, *Integrated design of working fluid mixtures and organic Rankine cycles (ORC) in the continuous-molecular targeting (COMT) framework,* in *ASME ORC 2015* (Brussels, 2015) pp. 1–9.

[16] R. Radermacher, *Thermodynamic and heat transfer implications of working fluid mixtures in Rankine cycles,* International Journal of Heat and Fluid Flow **10**, 90 (1989).

[17] J. G. Andreasen, L. Pierobon, U. Larsen, F. Haglind, and C. Author, *Multi-objective optimization of organic Rankine cycle power plants using pure and mixed working fluids,* in *ASME ORC 2015* (Brussels, 2015) pp. 1–11.

[18] S. Quoilin, M. V. D. Broek, S. Declaye, P. Dewallef, and V. Lemort, *Techno-economic survey of organic rankine cycle (ORC) systems,* Renewable and Sustainable Energy Reviews **22**, 168 (2013).

[19] B.-R. Fu, Y.-R. Lee, and J.-C. Hsieh, *Design, construction, and preliminary results of a 250-kW organic Rankine cycle system,* Applied Thermal Engineering **80**, 339 (2015).

[20] Y. Zhu, Z. Hu, Y. Zhou, L. Jiang, and L. Yu, *Discussion of the internal heat exchanger's effect on the Organic Rankine Cycle,* Applied Thermal Engineering **75**, 334 (2015).

[21] D. Walraven, B. Laenen, and W. D'haeseleer, *Comparison of shell-and-tube with plate heat exchangers for the use in low-temperature organic Rankine cycles,* Energy Conversion and Management **87**, 227 (2014).

[22] I. H. Aljundi, *Effect of dry hydrocarbons and critical point temperature on the efficiencies of organic Rankine cycle,* Renewable Energy **36**, 1196 (2011).

[23] W. Liu, D. Meinel, M. Gleinser, C. Wieland, and H. Spliethoff, *Optimal Heat Source Temperature for thermodynamic optimization of sub-critical Organic Rankine Cycles,* Energy **88**, 897 (2015).

[24] L. Calderazzi and P. C. di Paliano, *Thermal stability of R-134a, R-141b, R-13I1, R-7146, R-125 associated with stainless steel as a containing material,* International Journal of Refrigeration **20**, 381 (1997).

[25] M. A. Fabuss, A. S. Borsanyi, B. M. Fabuss, and J. O. Smith, *Thermal Stability Studies of Pure Hydrocarbons in a High Pressure Isoteniscope,* Journal of Chemical and Engineering Data **8**, 64 (1963).

[26] I. B. Johns, E. A. McElhill, and J. O. Smith, *Thermal stability of some organic compounds,* Journal of Chemical & Engineering Data **7**, 277 (1962).

[27] M. Pasetti, C. M. Invernizzi, and P. Iora, *Thermal stability of working fluids for organic Rankine cycles: An improved survey method and experimental results for cyclopentane, isopentane and n-butane,* Applied Thermal Engineering **73**, 764 (2014).

[28] A. Bahadori, *Estimation of combustion flue gas acid dew point during heat recovery and efficiency gain,* Applied Thermal Engineering **31**, 1457 (2011).

[29] M. Mosburger, J. Fuschetto, D. Assanis, and Z. Filipi, *Effect of high sulfur military JP-8 fuel on heavy duty diesel engine emissions and EGR cooler condensate,* SAE International Jorunal of Commercial Vehicles **1**, 100 (2009).

[30] Y. Dai, J. Wang, and L. Gao, *Parametric optimization and comparative study of organic Rankine cycle (ORC) for low grade waste heat recovery,* Energy Conversion and Management **50**, 576 (2009).

[31] V. Gesellschaft, *VDI Heat Atlas*, VDI-Buch (Springer Berlin Heidelberg, 2010).

[32] Z. Zhao, Y. Li, L. Wang, K. Zhu, and F. Xie, *Experimental study on film condensation of superheated vapour on a horizontal tube,* Experimental Thermal and Fluid Science **61**, 153 (2015).

[33] M. Browne and P. Bansal, *An overview of condensation heat transfer on horizontal tube bundles,* Applied Thermal Engineering **19**, 565 (1999).

[34] A. Hiemstra, *A steady state evaporator model,* Master's thesis, Universiteit Twente, the Netherlands (2011).

[35] E. Macchi and a. Perdichizzi, *Efficiency Prediction for Axial-Flow Turbines Operating with Nonconventional Fluids,* Journal of Engineering for Power **103**, 718 (1981).

[36] M. Astolfi and E. Macchi, *EFFICIENCY CORRELATIONS FOR AXIAL FLOW TURBINES WORKING WITH NON-CONVENTIONAL FLUIDS,* in *ASME ORC 2015* (Brussels, 2015) pp. 1–12.

[37] L. Da Lio, G. Manente, and A. Lazzaretto, *New efficiency charts for the optimum design of axial flow turbines for organic Rankine cycles,* Energy **77**, 447 (2014).

[38] a. Perdichizzi and G. Lozza, *Design Criteria and Efficiency Prediction for Radial Inflow Turbines,* Gas Turbine Conference and Exhibition (1987).

[39] R. Shah and D. Sekulic, *Fundamentals of Heat Exchanger Design* (Wiley, 2003).